TU

Technische Universität Wien

DIPLOMARBEIT

Incorporation of Thermoresponsive Hydrogels into Lamellar Nanocomposite Thin Films

ausgeführt am

Department of Chemistry and Chemical and Nuclear Engineering
University of New Mexico, Albuquerque, U.S.A.

und am

Institut für Materialchemie
Technische Universität Wien

unter der Anleitung von

Prof. C. Jeffrey Brinker, Dr. Bernd Smarsly (University of New Mexico)

Prof. Ulrich Schubert, Dr. Nicola Hüsing (Technische Universität Wien)

durch

Georg Garnweitner

Tigergasse 3/10
1080 Wien

TU

Vienna University of Technology

DIPLOMA THESIS

Incorporation of Thermoresponsive Hydrogels into Lamellar Nanocomposite Thin Films

Department of Chemistry and Chemical and Nuclear Engineering
University of New Mexico, Albuquerque, U.S.A.

and

Institut of Materials Chemistry
Vienna University of Technology

supervised by

Prof. C. Jeffrey Brinker, Dr. Bernd Smarsly (University of New Mexico)

Prof. Ulrich Schubert, Dr. Nicola Hüsing (Vienna University of Technology)

by

Georg Garnweitner

Tigergasse 3/10
1080 Vienna/Austria

Illustrations

Superscript Arabic numbers refer to the Bibliography Section.

The following abbreviations are used throughout text and graphics.

Table of Abbreviations:

CMC	critical micelle concentration
CP	cross-polarization
2-D / 3-D	2-dimensional / 3-dimensional
DSC	differential scanning calorimetry
EISA	evaporation-induced self-assembly
Fig.	figure
FT	fourier-transformation
IEP	iso-electric point
IR	infra-red spectroscopy
LCST	lower critical solution temperature
MAS	magic-angle spinning
NMR	nuclear magnetic resonance
SAXS	small-angle X-ray spectroscopy
2 θ	scattered angle in SAXS measurements
TEM	transmission electron microscopy
TGA	thermo-gravimetric analysis
UV	ultra-violet light
VIS	visible light
XRD	X-ray diffractometry

Index of Chemicals:

A2**	acidic silica sol, prepared by hydrolysis of TEOS
ACHN	1,1'-azobis(1-cyclohexanecarbonitrile)
AIBN	azobis(isobutyronitrile)
APS	ammoniumperoxodisulfate
BIS	*N*,*N'*-methylenebisacrylamide
BME	benzoin dimethyl ether
n-BuOH	n-butanol
CTAB	cetyltrimethylammonium bromide
DM	dodecyl methacrylate
EtOH	ethanol
HCl	hydrochloric acid
HDM	1,6-hexanediol dimethacrylate
MPS	3-(trimethoxysilyl)propyl methacrylate
NH_3	ammonia (30% solution in water)
NIPAAM	*N*-isopropylacrylamide
PATMS	3-(trimethoxysilyl)propyl acrylate
7-OTS	trimethoxy(7-octen-1-yl)silane
TEMED	*N*,*N*,*N'*,*N'*-tetramethyl ethylenediamine
TEOS	tetraethyl orthosilicate, tetraethoxysilane
THF	tetrahydrofurane

Table of Contents

1 Introduction

1.1 Evaporation-Induced Self-Assembly

Since the first synthesis of surfactant-templated mesoscopically ordered silica,[1,2] the preparation of nanoscopic mesostructures such as 2-dimensional hexagonal cylinders or cubic lattices via sol-gel processing has attracted much attention. Many groups focused on the synthesis and analysis of mesostructured thin films, for two major reasons: First, a variety of potential applications is expected for these films, e.g. in catalysis, molecular separation or as sensors.[3] Also, by removal of the structure-directing agent, films with high porosity can be obtained, which appear suitable as insulators in integrated circuit devices because of their low dielectric constant.[4] The second advantage of these films is their very simple and straightforward preparation, in particular after the development of Evaporation-Induced Self-Assembly (EISA).[5,6,7]

The preparation of mesostructured materials relies on the fast formation of a stable 3-dimensional inorganic network – this can be achieved by sol-gel chemistry. Gels based on silica, SiO_2, are the most prominent examples, due to the availability of inexpensive precursors showing moderate reactivity, allowing for a simple preparation process. Typically, silicate salts or alkoxysilanes are used as precursors; most common are tetraethyl orthosilicate (TEOS), $Si(OCH_2CH_3)_4$, and tetramethyl orthosilicate, $Si(OCH_3)_4$. The formation of the SiO_2 network is actually a complex process and can be divided into two types of reactions: the hydrolysis of the precursor, generating a reactive silanol species, and the subsequent condensation by formation of Si-O-Si bonds. The reaction sequence is shown in Scheme 1.1.

Hydrolysis

$$Si(OR)_4 + x\ H_2O \xrightarrow{H^+ / OH^-} Si(OH)_x(OR)_{4-x} + x\ ROH$$

Condensation

Dehydration

$$2\ Si(OH)_x(OR)_{4-x} \longrightarrow (RO)_{4-x}(HO)_{x-1}Si\text{-}O\text{-}Si(OH)_{x-1}(OR)_{4-x} + H_2O$$

Dealcoholation

$$2\ Si(OH)_x(OR)_{4-x} \longrightarrow (RO)_{3-x}(HO)_xSi\text{-}O\text{-}Si(OH)_{x-1}(OR)_{4-x} + ROH$$

$$\longrightarrow\longrightarrow SiO_2$$

Scheme 1.1: Sol-gel processes of alkoxysilanes

The hydrolysis of alkoxysilanes is catalyzed by acids and bases, such as (dilute) hydrochloric acid. The resulting species, from partly hydrolyzed $(RO)_3Si(OH)$ to silicic acid, $Si(OH)_4$, are highly reactive but can be stabilized at the isoelectric point (IEP), which equals a pH value of about 4.0 for the stated species. Otherwise, condensation (gelation) takes place, causing the formation of a three-dimensional network of SiO_4-tetrahedrons. Bulk gels are obtained which still contain a significant amount of solvent (EtOH). They can be dried in an oven, which leads to glass-like xerogels, or extracted with solvents under super-critical conditions to yield highly porous aerogels.[8] After complete solvent removal, these gels consist of pure silica (SiO_2).

The preparation of mesostructured silica thin films emanates from a solution containing the alkoxysilane. To facilitate the formation of the silica network, the precursor is usually pre-hydrolyzed in an organic solvent, e.g. ethanol, but can then be kept stable for months by storing at -20°C and setting the pH value to the IEP (for TEOS, this has been optimized in the so-called A2** stock solution).[9] The film is created by either dipping a substrate into this solution ("dip-coating") or applying some solution onto a surface ("casting"); the latter, however, leads to a higher (and practically uncontrollable) film thickness. A more sophisticated method is "spin-coating", where some solution is applied onto a substrate which is then spun at high speed to obtain a homogeneous film.

The key step for the formation of mesostructured films is the addition of a surfactant to the precursor solution to function as structure-directing agent. Surfactants are organic molecules consisting of a hydrophilic head group and a hydrophobic tail, typically an apolar hydrocarbon chain. In polar, protic solvents such as water or EtOH, these molecules tend to aggregate above a critical concentration (denoted as critical micelle concentration, CMC), forming spherical micelles or even more complex arrangements such as 2-D hexagonal rods, cubic phases or lamellae at higher concentrations.[10] A variety of structures is formed in surfactant systems consisting of more than 2 components. The schematic phase diagram for a surfactant-oil-water system is presented in Figure 1.1. It shows the diversity of structures which can be obtained.

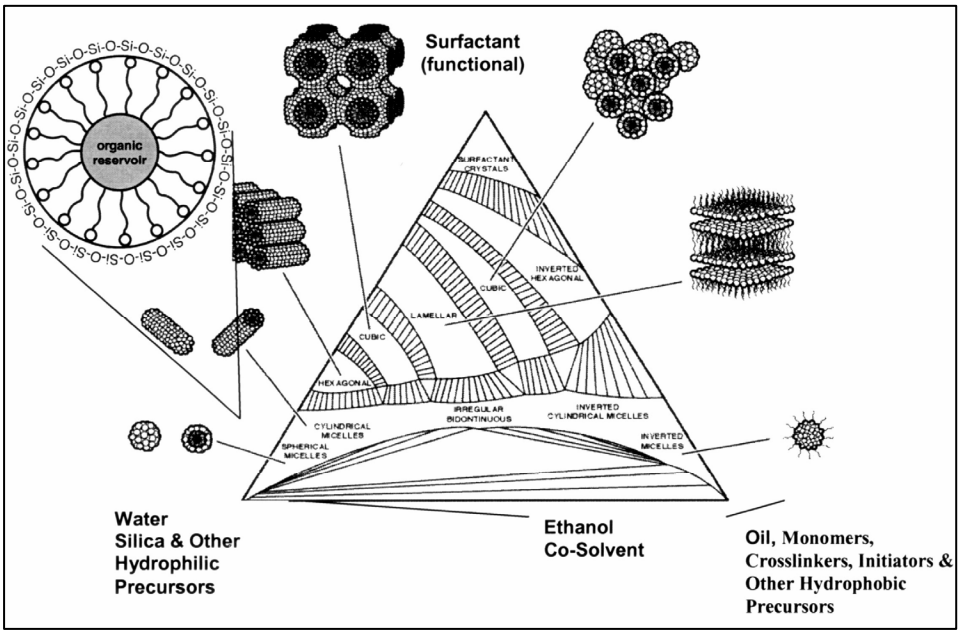

Figure 1.1: Phase diagram of a water-oil-surfactant system.[5]

According to the EISA method, however, the chosen concentration of the surfactant does not exceed the CMC in the precursor solution. Therefore, it is homogeneously distributed within the solvent (typically, ethanol), as are the silica precursors. Upon dip-coating, at first a homogeneous film is formed on the substrate as it is removed from the solution. Over time, the volatile solvent steadily evaporates, simultaneously increasing the concentration of the surfactant. Once the CMC is reached, micelles and, at higher concentrations, more complex structures are formed. The silica precursor remains distributed in the solvent in the hydrophilic moieties. The hydrophobic phases contain the alkyl chains of the surfactant molecules; their hydrophilic head groups are situated at the interface of the phases. After film formation, condensation of the silica precursors is enhanced, creating a stable SiO_2 matrix which only forms in the hydrophilic domain of the supramolecular surfactant structure and therefore conservates the mesostructure. Usually, the sample is then heated to 350-550°C to remove the surfactant (calcination); there are also other possible methods such as solvent extraction or photocalcination by exposure to vacuum UV irradiation.[11] Calcination of 2D-hexagonal or cubic structures leaves complex pore systems within the silica,[12] whereas lamellar systems collapse, resulting in almost nonporous amorphous silica.

The structure-formation upon removal of the substrate from the solution is illustrated in Figure 1.2. The decrease in film thickness and increase in surfactant concentration over time above the reservoir (proportional to the distance above reservoir) are plotted against each other. Instantly after removing the observed substrate from the solution, the film is very thick as it still contains a large amount of solvent, resulting in a low surfactant concentration. As the solvent evaporates, the film thickness decreases and the surfactant concentration slowly increases, at a certain point reaching the CMC, which leads to the formation of micelles or/and more complex structures such as hexagonal rods or lamellae. The last remaining amount of solvent evaporates fast (due to a high surface-to-volume ratio), resulting in a strong increase in surfactant concentration. At the "drying line", all free EtOH has evaporated (though there can be significant amounts trapped within the silica species).

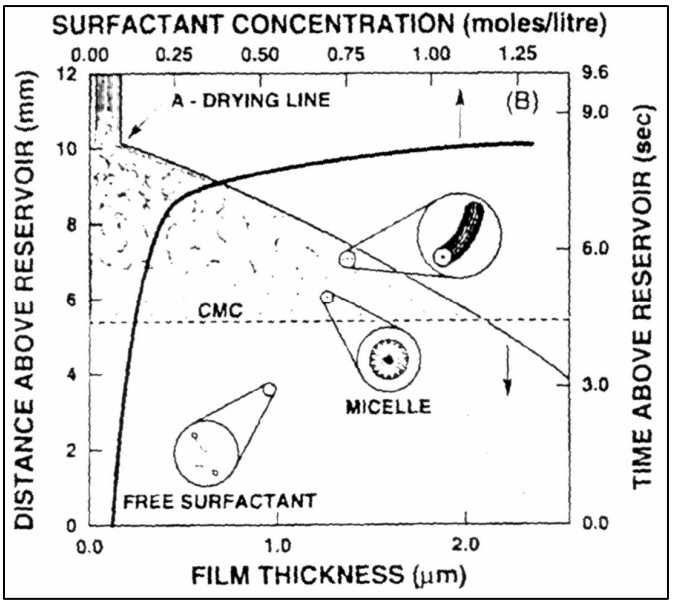

Fig. 1.2: Illustration of the processes occurring upon dip-coating.[5]

There are several types of surfactants. The formation of mesostructured films using alkyltrimethyl ammonium chlorides and bromides has been studied extensively.[13] Other common surfactants are amphiphilic block co-polymers of ethylene oxide and propylene oxide (Pluronics), but also a variety of other surfactant types have been explored.[14,15,16] In this work, a well-known surfactant of the former type was used, CTAB (cetyltrimethylammonium bromide, also known as hexadecyltrimethylammonium bromide), as it is convenient to handle and several types of structures can easily be obtained. Its structure is illustrated in Figure 1.3.

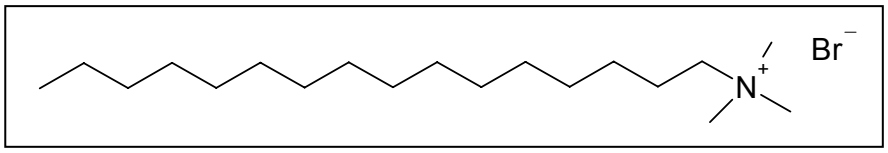

Fig. 1.3: Structure of cetyltrimethylammonium bromide (CTAB).

In the form of a lyotropic phase, CTAB can lead to a variety of structures; the formation of lamellar, cubic and 2-D as well as 3-D hexagonal structures has been reported.[17] Recent publications indicate that the final mesostructure is a function of various parameters such as the TEOS:CTAB ratio, pH value, the rate of evaporation, or humidity.[18,19,20] Detailed studies show that, under specific conditions, 2-D hexagonal structures develop from lamellar ordering upon growth of a mesoporous silica film at an air/liquid interface.[21] In-situ time-resolved small-angle X-ray scattering (SAXS) measurements also revealed that the formation process of cubic mesostructured films occurs via lamellar and hexagonal intermediate structures.[22]

The phase diagram CTAB-water-ethanol is presented in Figure 1.4. This diagram, however, is only accurate for EtOH/H_2O/CTAB systems, implying that no other species are present. Other structures, such as lamellae, can easily be achieved in the presence of hydrophobic species such as monomers or coupling agents.

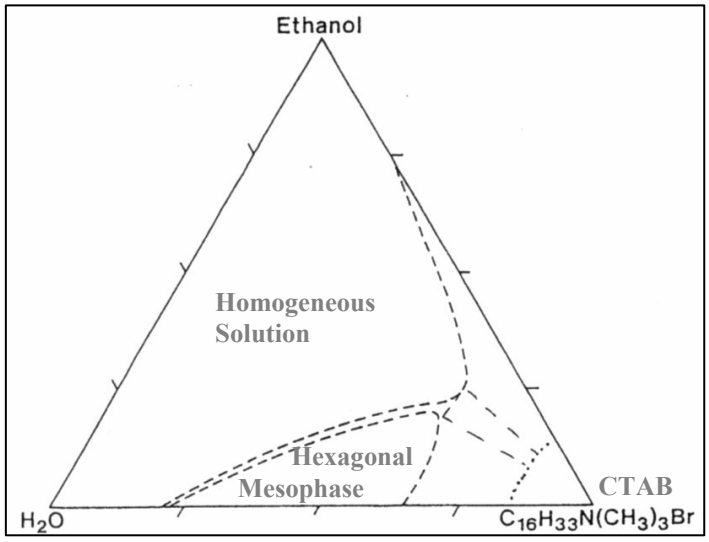

Fig. 1.4: Phase diagram of CTAB-EtOH-H_2O, adapted from [23].

The condensation process of the silica matrix is greatly accelerated and practically completed by calcination, but this also leads to a large shrinkage of the structure.[24] Exposure to ammonia vapor after preliminary drying of the films leads to base-catalyzed silica condensation, enhancing the stability of the network whilst minimizing its shrinkage. The surfactant can then be removed by extraction methods.[25]

1.2 Organic-Inorganic Hybrid Nanocomposite Films

In the last years, not only the preparation of mesoporous silica was studied extensively, but a second field of research in the area of mesostructured systems emerged: it was found that hybrid materials, consisting of an inorganic network similar to the silica structures discussed above, but also of an organic polymer, which is situated in the "pores" of the system, show outstanding properties. Many biological systems, such as the nacre of abalone shell, are also made up of such mesostructures. Especially lamellar ordering is found in these systems, formed by alternating layers of inorganic species (such as $CaCO_3$, silica or hydroxyapatite) and organic, functional polymers.[26] Whilst retaining its functionality, the delicate organic species is protected by the inorganic matrix, showing greatly enhanced mechanical stability. Also, the inorganic framework provides the geometric platform for the alignment and attachment of the organic matter. Therefore, the artificial synthesis of these hybrid systems constitutes a very promising and exciting field in the search for novel materials with unique properties.

The preparation of inorganic/polymer hybrid coatings is described in a variety of recent studies, mostly using silica as the inorganic part.[27,28,29,30] For example, the hardness of a conducting polymer was drastically increased by its incorporation into a composite film, using sol-gel processing.[30] The mild characteristics offered by the sol-gel process allow the combination of inorganic and organic components in virtually any ratio. These hybrids are outstandingly versatile in their composition, processing as well as optical and mechanical properties.[31]

There are several strategies for the preparation of mesostructured organic/inorganic nanocomposites. The key problem is to establish a firm connection between the organic moiety and the inorganic framework of the mesostructured thin film. Many approaches emanate from an already existing inorganic structure. For example, a layered nanocomposite consisting of silicate and polyimide was obtained emanating from a layered silicate (Na-kenyaite). The silicate was swollen in an aqueous solution, inducing simultaneous incorporation of a coupling agent, which is bound to the silica by condensation. This chemically modified silicate was then added to a solution of poly(amic acid); the polymer is tethered onto the organic end groups of the coupling agent, hence forming a stable nanocomposite.[32]

A second route is the self-assembly approach. The organic compound can be covalently linked to a silica precursor before the preparation of the film, which leads to incorporation of the organic constituents directly into the framework but requires the synthesis of the hybrid precursor.[33,34] A more straightforward method is to embed the organic compound between the siliceous walls during the self-assembly process.[5] Starting from a homogeneous solution containing both inorganic precursors and organic monomers, the formation of the mesostructure simultaneously causes the hydrophobic organic species to migrate into the hydrophobic domains formed by the alkyl chains of surfactant molecules. This imposes some restrictions on the organic monomer: it must be soluble in the precursor solution but exhibit enough hydrophobicity to separate from the silica species upon structure formation. In a second step, the organic species are polymerized, but also the inorganic matrix has to be stabilized by enhancing the silica condensation. In some cases, the structure-directing agent itself can act as the polymerizable organic monomer, as has been shown for amphiphilic diacetylene species – ordered poly(diacetylene)/silica nanocomposite films were rapidly formed.[35]

The incorporation of organic matter via self-assembly is an interesting route to nanocomposites, as a great variety of monomers can be used. Using the EISA approach, a lamellar nanocomposite consisting of alternating layers of poly(dodecyl methacrylate) and silica was synthesized. This was achieved by adding dodecyl methacrylate (DM) monomers to the precursor solution and then performing dip-coating. Evaporation of the solvent (EtOH) led to instant structure formation, creating inorganic layers of the silica precursor and remaining solvent, alternating with organic layers containing DM monomer, the hydrophobic part of the surfactant, a coupling agent and an initiator. The interface between the layers was formed by the hydrophilic head groups of surfactant molecules. In a separate step, a free radical polymerization was conducted to obtain poly(dodecyl methacrylate) confined in the organic layers. To stabilize the system, the samples were exposed to ammonia vapor to enhance the condensation of the silica matrix.[36]

This approach constitutes a promising pathway to create layered structures containing organic polymers and a supporting inorganic framework. The general procedure is shown in Fig. 1.5.

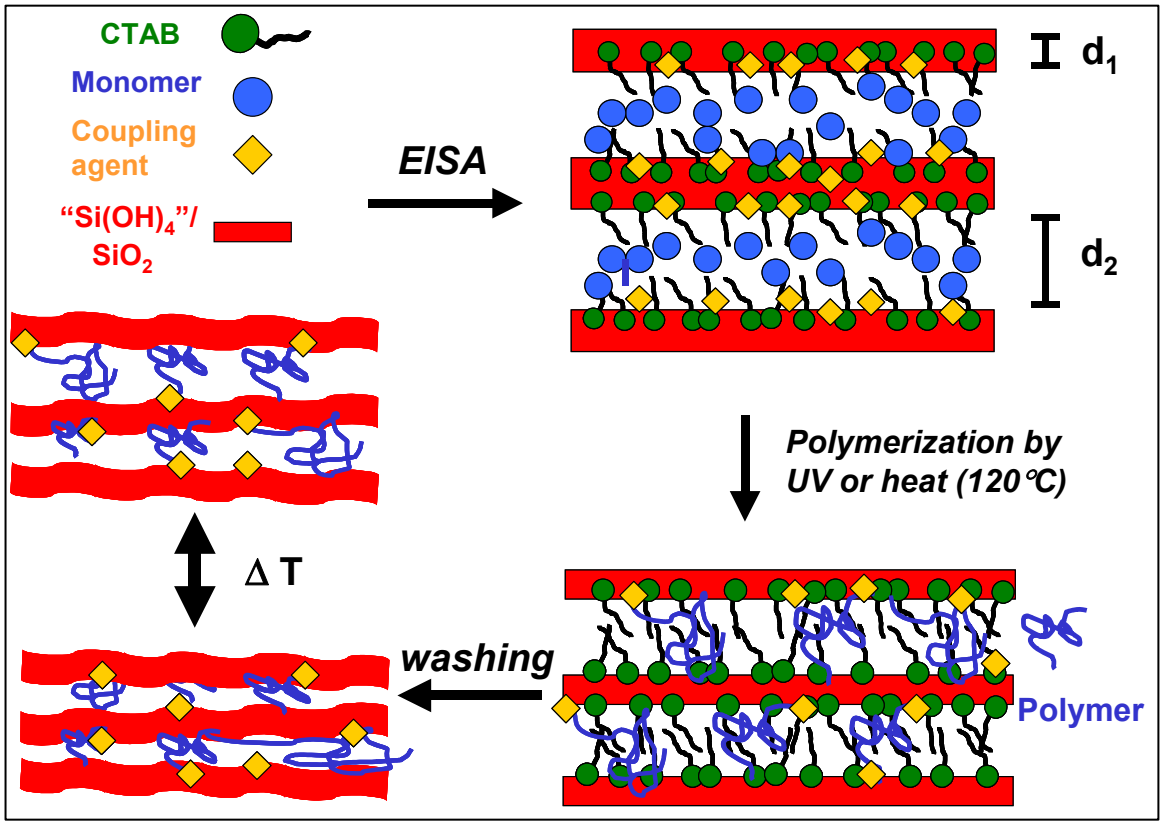

Fig. 1.5: Scheme of the synthesis of layered nanocomposites via EISA.

Although this represents a straightforward and promising approach for the incorporation of a variety of polymers into nanostructured films, there are still a number of problems which have to be solved. Not the actual structure formation process constitutes the key difficulty, but the necessary treatments to obtain a mechanically and chemically stabilized system. In particular, it is crucial to retain a high degree of ordering of the film while performing polymerization of the organic species as well as the treatment to enhance condensation of the silica precursors.

The main problems hereby are:

- Polymers generally undergo substantial changes in their hydrophobic/hydrophilic behavior compared to the monomers. This could even induce phase separation after the polymerization, causing damage to the mesostructure. Also, in the initial precursor solution, the addition of rather hydrophobic monomers and initiators could disturb the fragile silica/surfactant balance and may hinder the self-assembly process, leading to structures with significantly lower ordering or even the formation of a film only structured in limited domains.

- The monomers used must exhibit relatively high reactivity to allow fast and complete polymerization at not too harsh conditions. In a classical free radical polymerization, the degree of polymerization strongly depends on various parameters such as the general initiation method, the chosen initiator, the initiator concentration or the monomer concentration. The optimum synthesis conditions for polymers incorporated in mesostructured thin films may be greatly different from bulk systems.

- Free radical polymerization processes can be quite exothermic. As the silica network is rather fragile at this stage, the mesostructural order could become significantly distorted due to a locally violent reaction. Another problem is the temperature dependence of self-assembly, which could induce the formation of altered structures in local domains.

As reported above, the removal of the surfactant from lamellar silica structures results in the collapse of the structure, forming amorphous silica. This is not only the case for a calcination treatment – the structure-directing agent can also be removed by extraction methods or, simply, washing with organic solvents. In order to explore the functionality of the organic polymer, it is necessary to remove the surfactant; calcination, however, would lead to instant decomposition of all organic material. Therefore, washing is the only possibility; it is easy to imagine, though, that also the polymer is removed by this procedure unless there is a firm connection between the polymer and the silica layers. A coupling agent is used to create such a firm, covalent linkage between the layers.

Some examples of commonly used coupling agents (which will be further explored and discussed in this work) are shown below in Figure 1.6.

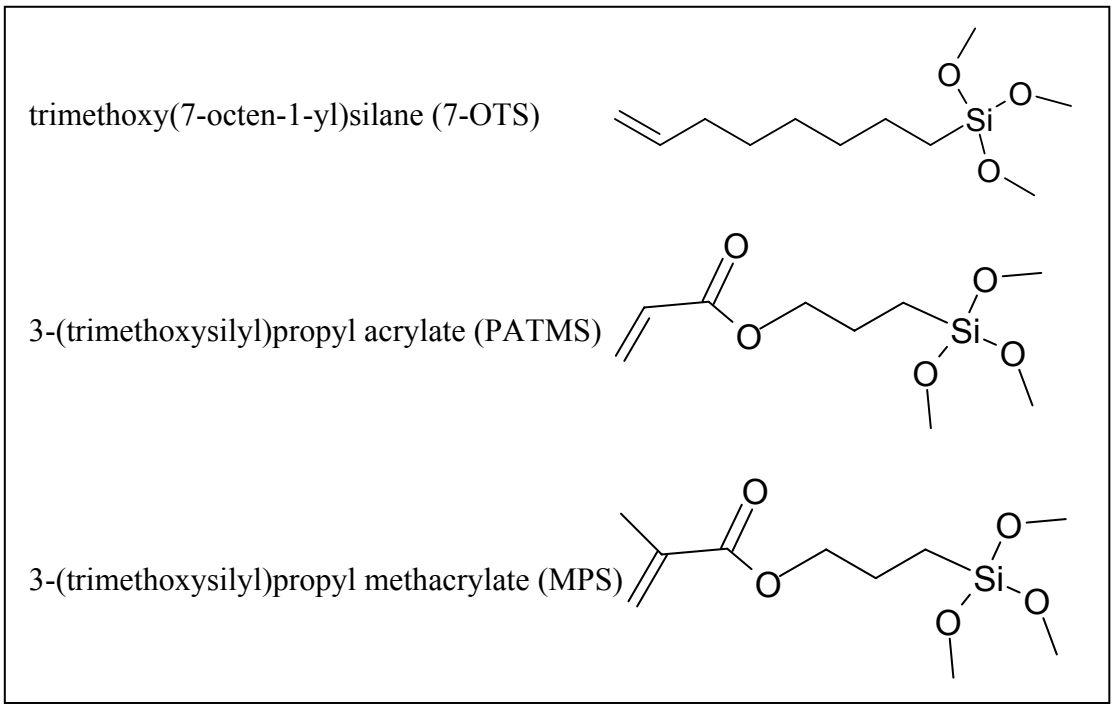

Fig. 1.6: Structure of various coupling agents.

Both structures nicely illustrate the functionality of a coupling agent: the siloxane head group is chemically similar to the precursor species for the silica matrix and reacts analogously. It is intended to establish a connection to the silica matrix by hydrolysis and condensation. The organic chain features a polymerizable double bond to react with other monomers and create a link to the polymer. Depending on the chemical environment, this double bond is more or less reactive. It is obvious that an activated double bond as in MPS and PATMS is much more reactive than the one in 7-OTS, the other shown example. However, not a high reactivity is desired, but the coupling agent is expected to provide a stable connection between the layers – on the other hand, this linkage actually should not be too rigid to avoid high mechanical stress within the film upon processes such as condensation of the silica.

The molecular structure of interconnected layers for the example of a poly(dodecyl methacrylate) nanocomposite is illustrated in Figure 1.7.

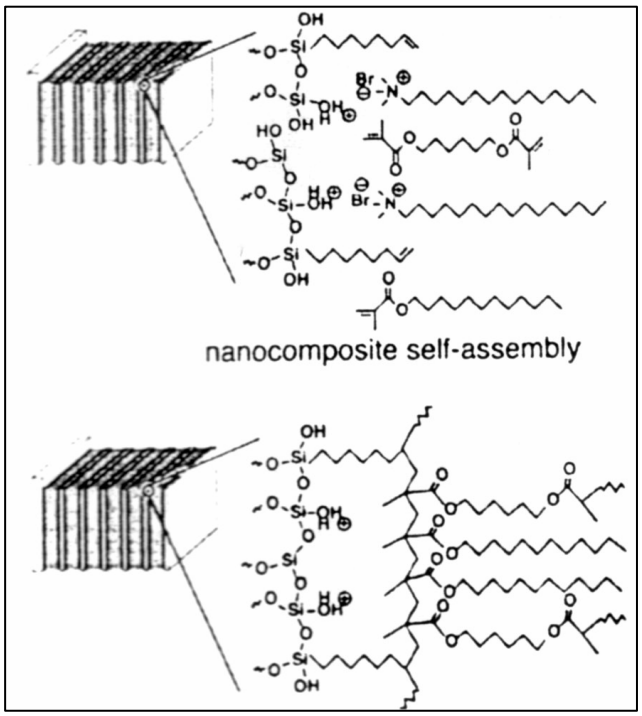

Fig. 1.7: Composition of interconnected layers.[36]

Nanocomposites can be characterized in multiple ways. The easiest and fastest method to analyze the structure is small-angle X-ray scattering (SAXS), whereas Transmission Electron Microscopy (TEM) pictures are certainly more illustrative. The reactivity of the individual components can be explored by routine techniques such as FT-IR and NMR spectroscopy. Thermal analysis (TGA or DSC) provides a means to determine the polymer content and investigate endothermic or exothermic processes occurring either within the silica or the polymer phase.

1.3 *N*-isopropylacrylamide

Hydrogel polymers, in general, have the ability to incorporate a large relative amount of water. Simultaneously, their volume increases, up to 100-fold ("swelling" of the polymer).[37] Changes in the external environment (denoted as "stimuli") can cause the gel to release this water and return to its initial state ("de-swelling"). Some of these polymers have been proved to respond to a variety of stimuli such as pH value, temperature, magnetic fields and electric fields. Therefore, they seem suitable for a wide range of applications, e.g. drug delivery systems, artificial muscles, membrane separations, micro-valves and surfaces in biomaterials.[37]

Thermoresponsive polymer hydrogels exhibit a discontinuous volume phase transition at a critical temperature, the so-called lower critical solution temperature (LCST). Poly(*N*-isopropylacrylamide), poly(NIPAAM), has probably become the best-known of these hydrogels. It shows inverse solubility in aqueous solutions upon heating – it is fairly soluble in water at room temperature but precipitates above the LCST (at 33°C).[38,39] Vice versa, the gel incorporates water and swells below the LCST but de-swells above this temperature. It has been shown that this solubility transition of poly(NIPAAM) occurs by a rearrangement of hydrogen bonds in the polymer-water mixture and by hydrophobic interactions.[40] Generally, a balance of hydrophilic and hydrophobic interactions is crucial for the occurrence of such a transition in hydrogels.[41] The detailed mechanism has not been elucidated yet. The principle of the forces causing the transition in poly(NIPAAM)/H_2O systems, the interaction of hydrophobic and hydrophilic moieties, is shown in Figure 1.8. The first picture (**a**) schematically illustrates the hydrophobic moieties being isolated and stabilized by a surrounding water cage. At the critical temperature, this water cage undergoes a structural change, which causes the system to become unstable. The hydrophobic moieties are attracted to each other and aggregate, which causes the whole structure to contract ("coil-to-globule transition"). It has been shown that also hydrogen bonding is involved, as demonstrated in the lower scheme (**b**).

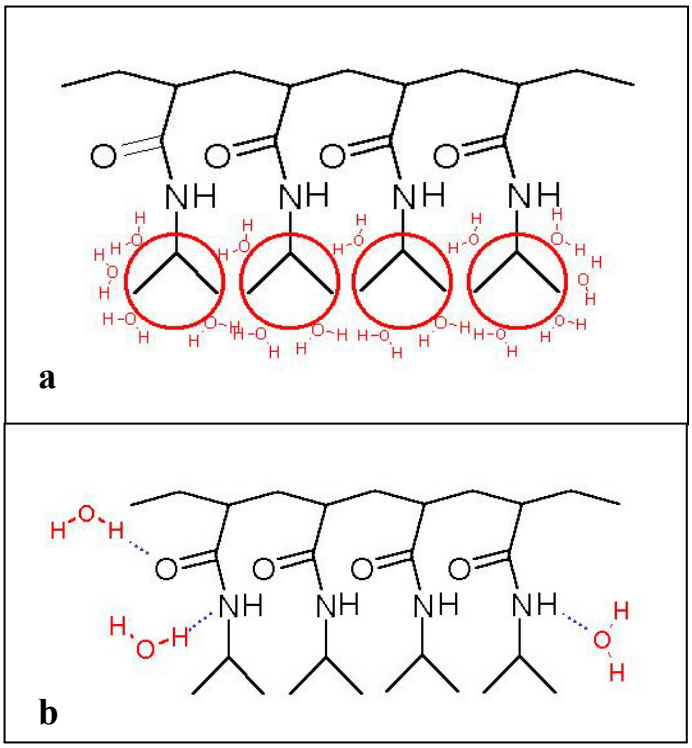

Fig. 1.8: Structure of poly(NIPAAM) and processes involved in thermal transition.

Poly(NIPAAM) gels are synthesized by a variety of techniques, most commonly via free radical polymerization.[38] Bulk gels are obtained by addition of cross-linkers, usually using *N*,*N'*-methylenebisacrylamide (BIS). By reaction of the two double bonds within two different chains (which is likely), those chains become covalently connected. In this way, a 3-D polymer network can be formed. A variety of initiators was used for the polymerization; the most common ones are azobis(isobutyronitrile) (AIBN) and ammoniumperoxodisulfate (APS).

Not only pure poly(NIPAAM) systems, but also co-polymers of NIPAAM with a variation of other organic monomers have been studied intensively to investigate the influence of co-polymerization on the hydrogel properties.[42,43] Especially the co-polymers of NIPAAM and methacrylic acid (or methacrylates) seem very promising, as in some cases, an even higher degree of swelling was observed than for the homopolymers.[44] Additionally, methacrylates show higher reactivity, the co-polymerization therefore is faster and allows more moderate reaction conditions, facilitating the synthesis of the hydrogel. The critical temperature in the resulting hydrogel differs from the NIPAAM homopolymer. Whilst poly(NIPAAM-co-acrylic acid) systems show an elevated LCST, the temperature sensitivity of NIPAAM co-polymers with methacrylic acid also depends on the pH value. At pH 5, co-polymers with a high NIPAAM content were shown to exhibit raised LCST.[44]

It is evident that an increase in the surface-to-volume ratio of a hydrogel enhances the rate of swelling and de-swelling, simply because water has an easier and faster access to the gel. Consequently, studies have shown that the formation of a porous structure effectively boosts especially the de-swelling rate of poly(NIPAAM) gels.[45] Hence, it can be expected that in a nanocomposite, where the interface-to-volume ratio is even higher, also the swelling and de-swelling processes are faster, if water can penetrate the inorganic second phase. It has been recently reported that poly(NIPAAM) can be incorporated into a clay nanocomposite. This was accompanied by a substantial loss in the mesostructural order of the system. Using a coupling agent, however, an unusually large thermal volumetric change of the hydrogel as well as a faster rate of de-swelling was observed.[46] Another study describes the synthesis of poly(NIPAAM)-grafted silica by modification of the silica surface with a coupling agent (e.g. MPS) and then performing a radical polymerization, using AIBN as initiator. Only single polymer chains are grafted onto the silica; in the final system, ca. 100 mg polymer per g silica were obtained.[47]

The incorporation of poly(NIPAAM) or its co-polymers with methacrylates into mesostructured silica, employing evaporation-induced self-assembly, could hence lead to a highly ordered system. Especially lamellar systems appear suitable – the theoretical model of the functionality of such systems is presented in Fig. 1.9. Swelling of the hydrogel results in an increase in thickness of the polymer layer, whereas the thickness of the silica layers remains constant. Upon de-swelling of the hydrogel, the organic layers contract, causing a decrease in thickness, whereas the silica matrix remains unchanged.

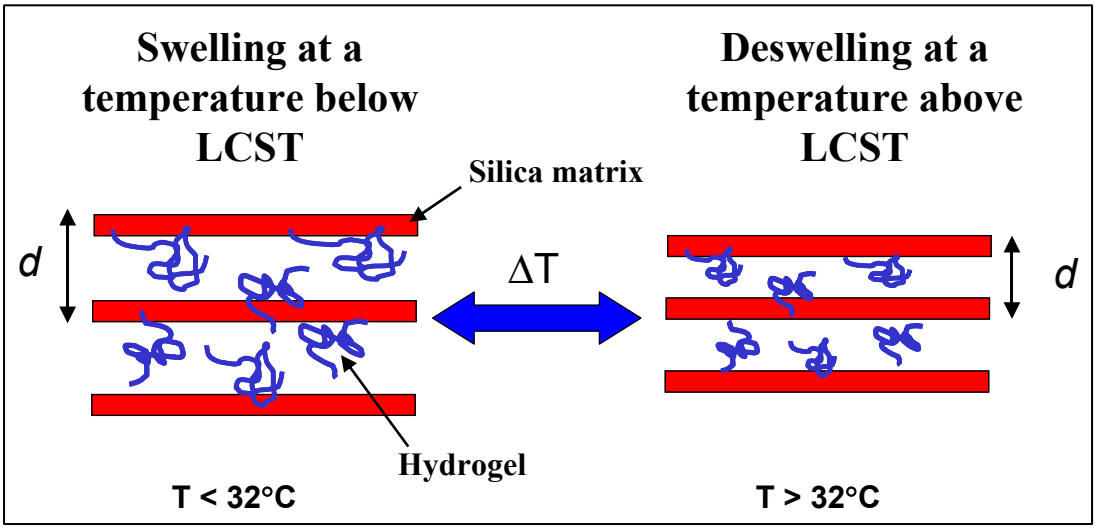

Fig. 1.9: Scheme of the swelling of hydrogels in lamellar nanocomposites.

The advantages of such a system are not only the decreased response time to external stimuli, but also the improvement of the mechanical stability of the polymer through the support of the silica matrix. Furthermore, the preparation process for such nanocomposites is easy and fast. Provided that a rapid and effective polymerization procedure can be found, this would represent an ideal method to obtain functional coatings.

The synthesis of this nanocomposite consisting of silica and a hydrogel seems promising for a variety of applications. Microfluidic systems featuring self-regulated flow control have already been studied for pH-sensitive acrylate-based hydrogels.[48] Being incorporated in a nanocomposite, faster response times of the hydrogel can be expected, and its increased mechanical stability could lead to the development of reliable, resilient micro-valves showing fast response to changes in temperature and pH value or differences in the concentration of specific salts. Sensors could also be created based on these principles.

Since hydrogels can also act as a reservoir for various functional molecules, e.g. in biomedical applications, temperature-dependent controlled release of molecules would constitute one of the most fascinating possible applications.[45] It has already been demonstrated that derivatized poly(NIPAAM) can be used to release insulin responding to the external glucose concentration.[49] Hydrogels embedded in a nanocomposite would show improved stability, and hence could greatly increase the preciseness and the number of potential applications of such systems. As the LCST of poly(NIPAAM) or co-polymers of NIPAAM and acrylates is close to the human body temperature, applications in drug delivery systems seem possible.[44]

2 Conceptual Formulation

Because of their unique properties, nanostructured materials are of high interest. It has been shown that lamellar nanocomposites, consisting of alternating layers of inorganic silica and organic polymers, can be synthesized in a fast and simple way using evaporation-induced self-assembly, a straightforward method to nanostructured thin films. Methacrylates and diacetylenes have been successfully used as precursors.[5] The resulting nanocomposites showed good ordering and enhanced mechanical stability of the polymer.

This work focuses on the synthesis of a similar system. A co-polymer of *N*-isopropylacrylamide (NIPAAM) and dodecyl methacrylate (DM) was intended to be incorporated into a mesostructured silica thin film with lamellar ordering. The co-polymer is a hydrogel exhibiting similar properties as pure poly(NIPAAM) but was used because of the higher reactivity of the methacrylate, which was expected to lead to a faster polymerization. The possibility of the formation of a mesostructure by EISA incorporating these species was to be tested, and consecutively an optimized preparation process to be developed, trying to retain a high ordering of the sample whilst

- achieving a high degree of polymerization of the organic species
- enhancing the condensation of the inorganic network
- establishing a firm connection of the organic layers to the silica
- and, finally, efficiently removing the surfactant but retaining the polymer in the system

Due to the fine distribution of the gel as nanolayers, a fast responsiveness towards changes in the external environment can be expected, and the silica matrix would lead to good mechanical stability of the system. Therefore, samples exhibiting the desired structure and composition after all processing steps, including removal of the structure-directing agent, were to be subject to swelling and de-swelling experiments to explore the functionality of the polymer incorporated in the hydrogel. The response at various temperatures was investigated.

Additionally, several parameters were to be explored to understand the problems involved in the formation of hybrid inorganic/organic nanocomposites and further optimize the sample preparation procedure. These investigations were carried out using a variety of analysis techniques, not only small-angle X-ray scattering (SAXS) but also IR and NMR spectroscopy, thermal analysis techniques (TGA and DSC), transmission electron microscopy (TEM) and ellipsometry.

The work was focused on exploring

- the reactivity and rate of polymerization of the monomers DM and NIPAAM as well as of several coupling agents (which were necessary to create a stable linkage between the layers). Free radical polymerization has been explored extensively for the bulk synthesis of poly(NIPAAM) – but the reaction, if happening at all, might occur very differently in a nanosystem.

- advantages and disadvantages of polymerization by thermal initiation and by photoinitiation

- a gentle but efficient method to remove the surfactant from the system after polymerization, without destroying the structure or eliminating the polymer

- ways to increase the reproducibility of results by improving and standardizing the various preparation steps

- the quantitative amount of polymer incorporated in the sample at different processing steps, and – if possible – the composition of the incorporated polymer

Theoretical models should be applied to selected SAXS patterns to investigate the possibility to calculate and explain the diffractogram of a complex system, and obtain further information about the thickness and variation of the layers within the nanocomposite.

3 Results and Discussion

3.1 Bulk Experiments

The most common initiator for free radical polymerization is AIBN, azobis(isobutyronitrile). This initiator is soluble in acetonitrile or dimethylsulfoxide but not in water or ethanol. The synthesis of bulk poly(NIPAAM) systems is, however, mostly performed in water as solvent, using ammoniumperoxodisulfate (APS) as initiator.[50] APS dissolves in water but not in ethanol, as solubility experiments showed.

Evaporation-Induced Self-Assembly (EISA), on the other hand, relies on a volatile solvent. Also, the A2** sol preparation procedure is optimized for ethanol as solvent. Using a different solvent would lead to changed rates of hydrolysis and condensation. More importantly, it would also greatly influence the solvent evaporation process inducing the self-assembly. This could even result in a different ordering, as the phase diagram of CTAB is different for other solvents, especially if the polarity and proticity differ greatly from EtOH. Therefore, the A2** sol preparation was always performed with ethanol, and also most precursor solutions were assembled only using ethanol as solvents. Interesting results were obtained, though, adding tetrahydrofurane (THF) as solvent to the A2** solution, which resulted in a solvent mixture 1 EtOH : 4 THF, see Chapter 3.2. Other experiments using n-butanol did not give any positive results, probably because its volatility is much lower.

In EtOH or THF, both AIBN and APS could not be used as initiator because of their insufficient solubility. Other initiators which seemed suitable because of their high reactivity and, on the other hand, their high solubility in ethanol were tested. Benzoin dimethylether (BME) is a highly active photoinitiator; its absorption bands are investigated in Chapter 3.7. 1,1'-azobis(1-cyclohexanecarbonitrile) (ACHN) decays rapidly at temperatures above 100°C; it is also soluble in EtOH. The structure of both initiators is shown in Fig. 3.1 **a** and **b**.

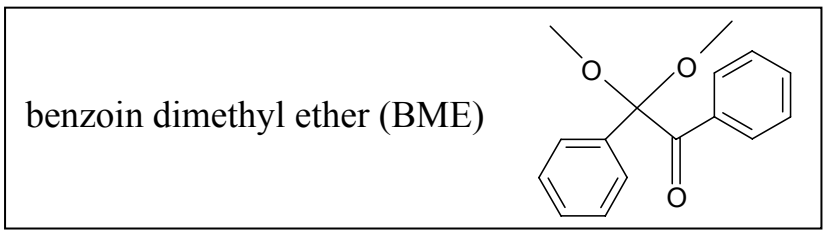

Fig. 3.1 a: Structure of the photoinitiator BME.

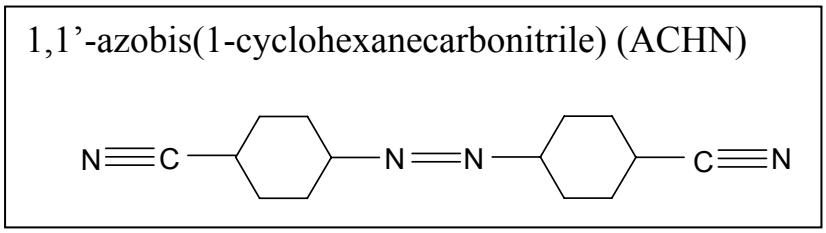

Fig. 3.1 b: Structure of the thermal initiator ACHN.

In order to examine the solubility of other initiators and their influence on the polymerization rate of NIPAAM, DM and 7-OTS, bulk experiments were performed. Only a small amount of solvent (ca. 1 mL) was added to the same amount of monomer as used for standard dip-coating solutions. Various amounts of initiator were added and the vial was sealed with Parafilm to avoid a too high rate of solvent evaporation. For polymerization, the vial was either placed in an oven at elevated temperatures (ca. 80°C) or irradiated with a UV lamp. The viscosity was visually estimated over time, thus getting a very rough measure but a good general idea of the efficiency of various initiators. Table 3.1 shows the observations for the various monomers and initiators.

Monomer	**Solvent, Initiator**	*Polymerization Reaction*	**Color of Polymer**
NIPAAM	EtOH / BME	*apparently **polymerized** after 5 hours / UV irrad.*	slightly yellow
NIPAAM	THF / BME	***fast polymerization**, complete after 4 hours / UV*	slightly yellow
NIPAAM	EtOH / APS	*no experiment possible due to instant **phase separation***	
NIPAAM	EtOH / ACHN	***polymerized** after 6 hours / thermal treatment (120°C)*	nearly colorless
DM	EtOH / BME	*no experiment possible due to **phase separation***	
7-OTS	EtOH / BME	*increased viscosity after 10 hours, but remained colorless and liquid – **no complete polymerization***	
PATMS	EtOH / BME	*very **fast polymerization**, complete within 30 minutes / UV irrad.*	slightly yellow
NIPAAM + 7-OTS	EtOH / BME	***slowly polymerized** within 10 hours / UV irrad.*	slightly yellow

Table 3.1: Polymerization behavior of various bulk systems.

The results clearly show that BME (benzoin dimethylether) and ACHN are suitable for UV resp. thermal initiation. The use of other initiators (APS, AIBN) resulted in instant phase separation; even the addition of further EtOH did not lead to a homogeneous system – these initiators are therefore unsuitable.

The polymerization behavior of DM could not be monitored as the solution became too hydrophobic and the initiators did not dissolve unless a higher amount of solvent was added (preventing the possibility to determine the progress of polymerization by monitoring the viscosity increase). 7-OTS shows a very low reactivity, whereas NIPAAM seems to generally react more rapidly. A mixture of NIPAAM and 7-OTS could also be polymerized within reasonable time. The progress of thermal polymerization was difficult to monitor because of the increased rate of solvent evaporation – however, samples appeared to react in similar rates as upon UV irradiation treatments. Therefore, both photo- and thermally initiated polymerization was employed for structured thin film samples.

3.2 IR Measurements

Infrared (IR) Spectroscopy detects the various kinds of bonds in a sample, giving semi-quantitative information about e.g. the ratio of polymerized double bonds present. Therefore, it is a very useful method to roughly measure the degree of polymerization and polycondensation in the nanocomposite for the organic and the silica species. Also, the ratios of components can be estimated comparing their peaks in IR spectra measured at different stages of the preparation process.

3.2.1 Measurements of Pure Substances

There are a number of components in the system, and some especially complex, high-molecular weight compounds such as the initiator, 7-OTS, NIPAAM or DM that produce many peaks which are hard to separate and identify. Thus, first the pure chemicals were measured in order to obtain reference spectra allowing assignment of the peaks. Nonetheless, it is necessary to concentrate on the main, unambiguous peaks of a substance. Identification of the signals was carried out based on literature tables[51] or electronic assignment tools.[52]

Figure 3.2 shows the IR spectrum of pure cetyltrimethylammonium bromide (CTAB). A small amount of the surfactant (powder) was mixed with KBr in a mortar and then pressed into a pellet.

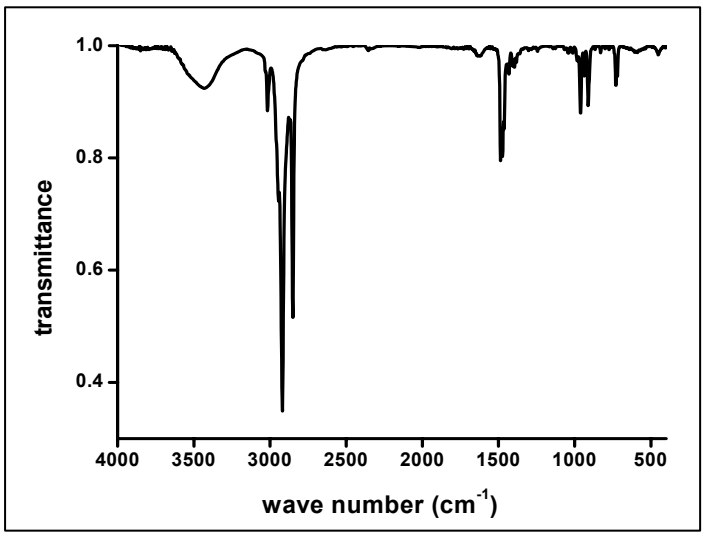

Fig. 3.2: FT-IR Spectrum of pure CTAB.

The stretch vibrations of the $–CH_2–$ groups in the long hydrocarbon chain correspond to two large peaks at 2918 cm^{-1} (asymmetric vibration) and 2850 cm^{-1} (symmetric vibration). The peaks at 1487 and 1473 cm^{-1} are caused by the C–N stretch vibration and $–CH_2–$ scissor

vibration. The peaks below 1000 cm^{-1} are other deformation vibrations or combination vibrations, e.g. the $–(CH_2)_n–$ skeleton vibration at 730 cm^{-1}. The broad signal at ca. 3450 cm^{-1} is the O–H signal, stemming from moisture. As there are no double bonds present, no peaks are visible between 1500 and 2800 cm^{-1}.

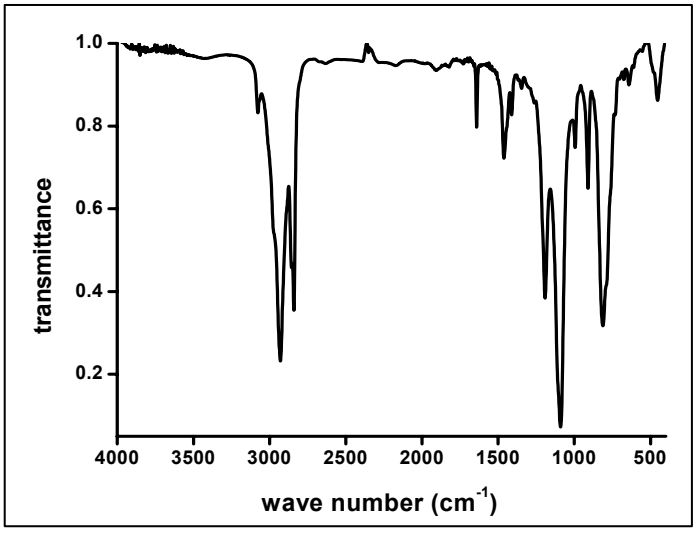

Fig. 3.3: FT-IR Spectrum of pure 7-OTS.

Pure 7-OTS was measured by adding a drop of the liquid to a surplus of potassium bromide powder and homogenizing the wet solid. The substance then was mixed with further KBr and pressed into a pellet. The IR spectrum (Fig. 3.3) shows a small peak for the unsaturated (alkene) C–H stretch vibration at 3077 cm^{-1}, and of course the saturated C–H stretch vibrations at 2929 and 2840 cm^{-1}. The shoulder of the smaller peak (at 2856 cm^{-1}) is caused by C–H stretch vibrations within the $–OCH_3$ groups. The most important signal here is the double bond peak at 1641 cm^{-1} (C=C stretch vibration), whereas the peak at 1463 cm^{-1} is attributable to the $–CH_2–$ deformation vibration. The peaks at 1000-1200 cm^{-1} are caused by the siloxane group, the signal at 1192 cm^{-1} stemming from the C–O stretch vibration, and Si–O–C and Si–C resonances being visible at 1090 cm^{-1}. Out-of-plane deformation vibrations of the vinyl group result in peaks at 994 and 910 cm^{-1}. The large peak at 812 cm^{-1} is attributed to $Si\text{-}CH_2$ rocking vibrations.

For comparison, IR spectra of TEOS are shown in Fig. 3.4; as-received (**a**) and after A2** sol preparation (**b**). The storage conditions of TEOS do not lead to partial hydrolysis, as is visible by the very small –OH signal at approx. 3500 cm^{-1} in **a** (there always was some water in the samples as KBr is highly hygroscopic). Due to the much shorter alkyl chains, the $–CH_2–$ and $–CH_3$ peaks (2977, 2930, 2893 cm^{-1}) are now smaller than the siloxane peaks at 1170, 1109

and 1084 cm^{-1}. In the fingerprint area, there are strong peaks at 966 and 793 cm^{-1}; these signals are attributed to Si–O–Si vibrations in partially condensed silica.

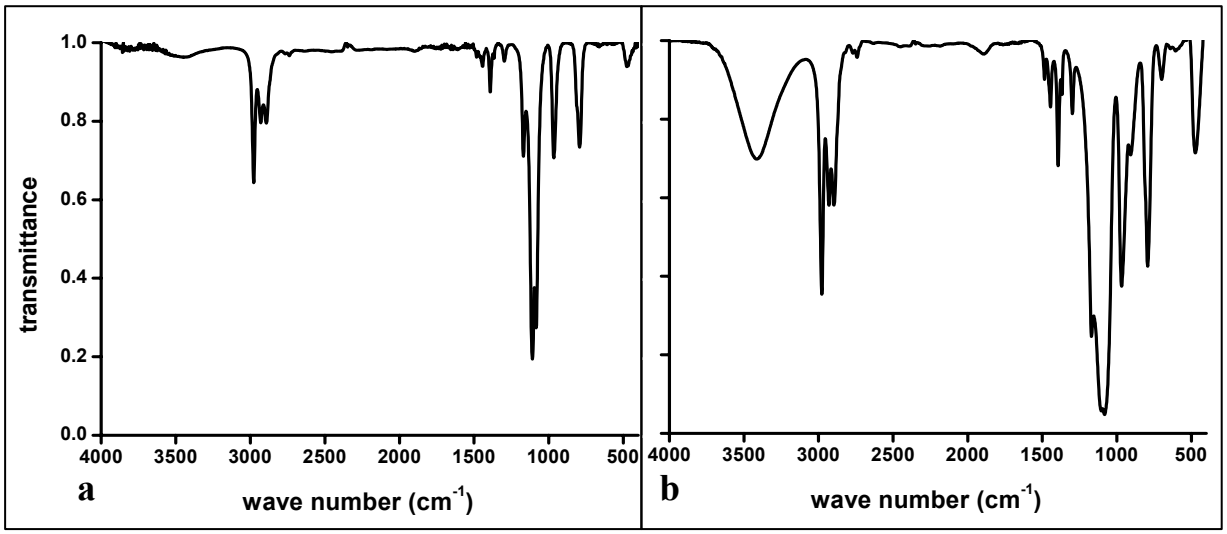

Fig. 3.4: FT-IR Spectra of **a**: Tetraethyl orthosilicate (TEOS), **b**: hydrolyzed TEOS (A2** sol).

During the preparation process of A2** stock solution, TEOS is expected to at least partially hydrolyze, forming ethanol. EtOH is also used as solvent and does not completely evaporate before the measurement; therefore, a large O–H peak (ca. 3400 cm^{-1}) is visible, and the $–CH_2–$ and $–CH_3$ signals around 2950 cm^{-1} increase in intensity (compared to the siloxane/silica peaks). The higher ratio of free alcohol to siloxane also leads to a stronger C–O signal at 1170 cm^{-1}, but as the amount of EtOH evaporated was not measured, also the degree of hydrolysis could not be determined.

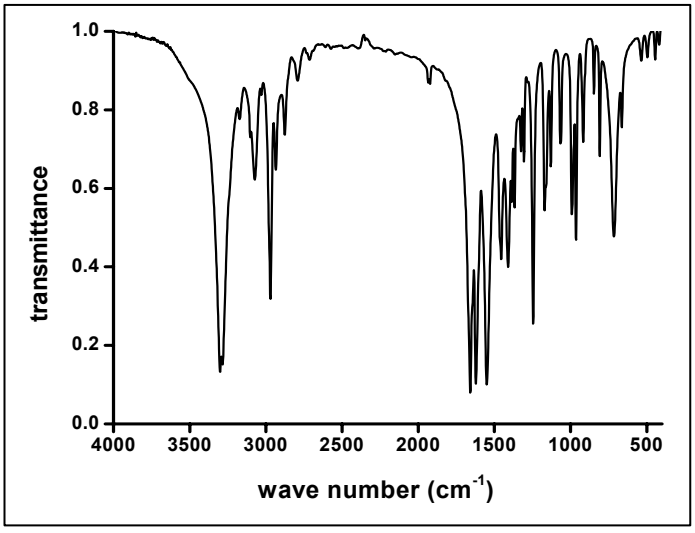

Fig. 3.5: FT-IR Spectrum of NIPAAM.

The spectrum of NIPAAM is illustrated in Fig. 3.5. The measurement was performed using the pure chemical, pressed as usual into a KBr pellet. The number of peaks in the

"fingerprint" area is very high, hence we focus on the most important ones. The doublet peak at 3300 and 3285 cm^{-1} originates from the N–H stretch vibration and is typical for *N*-mono-substituted amides. C–H stretch vibrations are visible at 3073 cm^{-1} (double bond), and at 2970/2935 cm^{-1} (alkyl $–CH_3$ and $–CH_2–$ peaks). The strongest signal is the carbonyl peak at 1658 cm^{-1}; the second amide signal is at 1550 cm^{-1}. In between, there is the C=C stretch vibration peak at 1622 cm^{-1}. The peak at 1455 cm^{-1} is attributed to deformation vibrations of the isopropyl group, where as the C–N stretch vibration causes the peak at 1246 cm^{-1} (amide III peak). C–H deformation vibrations of the amide group result in a signal at 1410 cm^{-1}, whilst the peak at 715 cm^{-1} stems from out-of-plane N–H deformation vibrations.

The photoinitiator BME was measured as well. Fig. 3.6 shows the spectrum obtained from the pure powder, without exposure to UV irradiation.

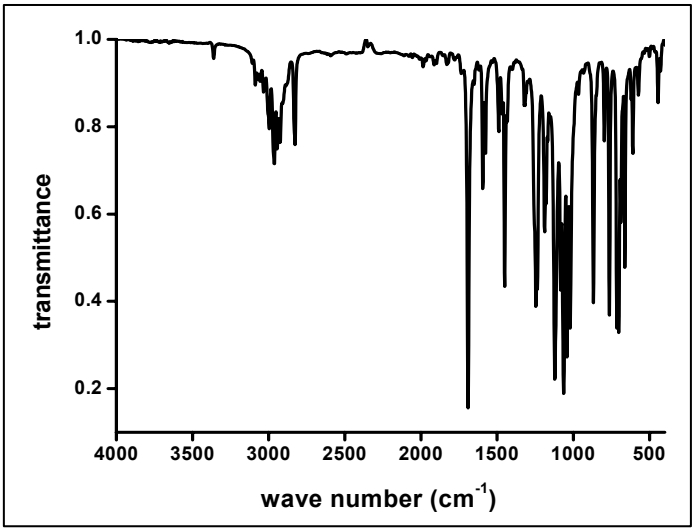

Fig. 3.6: FT-IR Spectrum of the photoinitiator BME.

The multiplet of peaks centered around 2950 cm^{-1} is caused by aromatic C–H deformation vibrations; the alkyl C–H deformation vibration (from the $–OCH_3$ groups) can be seen at ca. 2850 cm^{-1}. The large peak at 1690 cm^{-1} is of course the carbonyl signal. A large number of signals are visible below 1600 cm^{-1}: C=C peaks of the phenyl groups are visible at 1595 and 1577 cm^{-1}, whereas the peak at 1450 cm^{-1} is attributable to $–OCH_3$ deformation vibrations. Most other peaks in the "fingerprint" area are deformation or combination vibrations of the phenyl groups or the ketal fragment (e.g. the conjugated C-O-C-O-C resonance causes four peaks in this area).

3.2.2 Analysis of the Coupling Agent Reactivity

As the double bond signal is a characteristic feature of the 7-OTS FT-IR spectrum, it seems obvious that the degree of polymerization can be monitored by looking at the decrease of this signal. Therefore, systems containing A2** sol and 7-OTS (also containing water and dilute HCl to enhance condensation of the silica network) were investigated with and without initiator after various times of UV irradiation. A precursor solution containing the components was applied to a Petri dish (see *Experimental Section*, Chapter 5) and a film obtained by vertical draining. Samples were either measured as-prepared or after exposure to UV irradiation or heat (by placing the dish into a pre-heated oven). The samples were scratched off the Petri dish with a spatula and then mixed with KBr and homogenized in a mortar. The substance was pressed into a pellet and measured as usual.

Fig. 3.7 shows a sample containing A2** sol and 7-OTS, but no initiator, after drying for 1 hour at ambient conditions (**a**) and after 2 hours of exposure to UV irradiation (**b**).

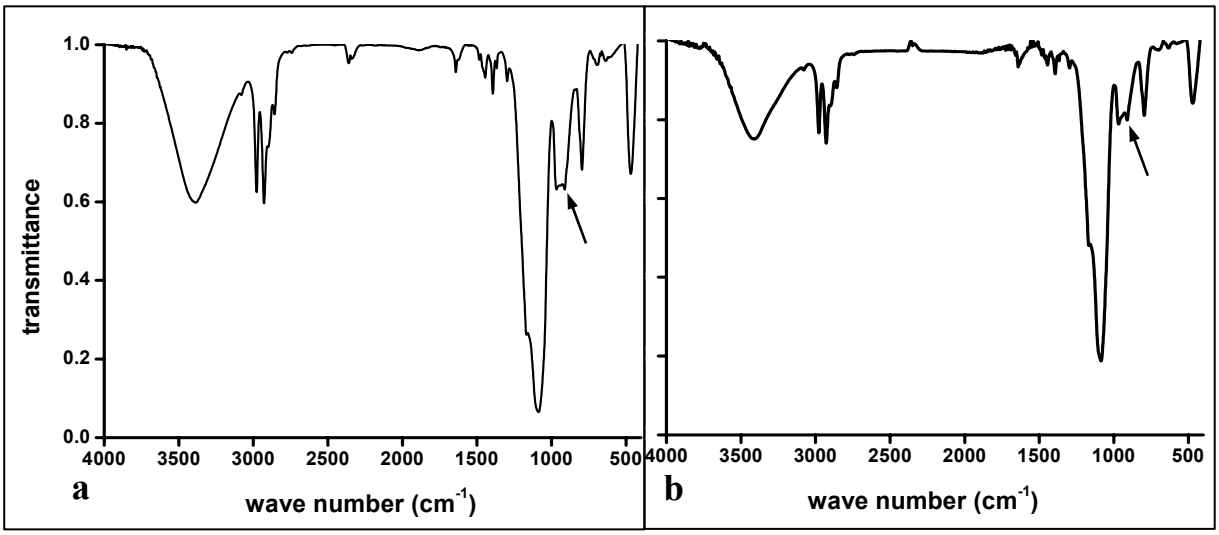

Fig. 3.7: FT-IR Spectra of a 7-OTS/A2** sample **a**: as-prepared, **b**: after 2 h UV irradiation.

In both spectra, the intensity of the Si–O peak at 1085 cm^{-1} is about three times higher than the alkyl C–H peaks around 3000 cm^{-1}, which is consistent with the much higher molar amount of the silica precursor in the system (1 TEOS : 0.16 7-OTS). Hydrolysis of the ethoxysilane and of 7-OTS, however, seems complete, as the broad O–H signal at ca. 3400 cm^{-1} is much larger than the alkyl peaks, which resemble the 7-OTS pattern rather than the TEOS peak shapes. More importantly, the double bond vibration of 7-OTS is still clearly visible at 1641 cm^{-1}, indicating no significant reaction of the monomers. The signals to the right of the peak are all attributable to TEOS/silica resonances, except for a small peak at

910 cm^{-1} which is caused by the *unsaturated* C–H out-of-plane deformation vibration; due to a superposition of other signals it is visible as a small hump at the right side of a doublet (*arrow*). Comparing the spectra before and after UV irradiation, we see that the C=C stretching vibration signal slightly changes its form (it has a broader shoulder in spectrum **b**), but examination of its intensity shows that no reaction has occurred – this is also supported by the steady intensity of the second peak of the unsaturated group at 910 cm^{-1} (compared to other signals caused solely by 7-OTS, such as the alkyl peaks at 3000 cm^{-1}).

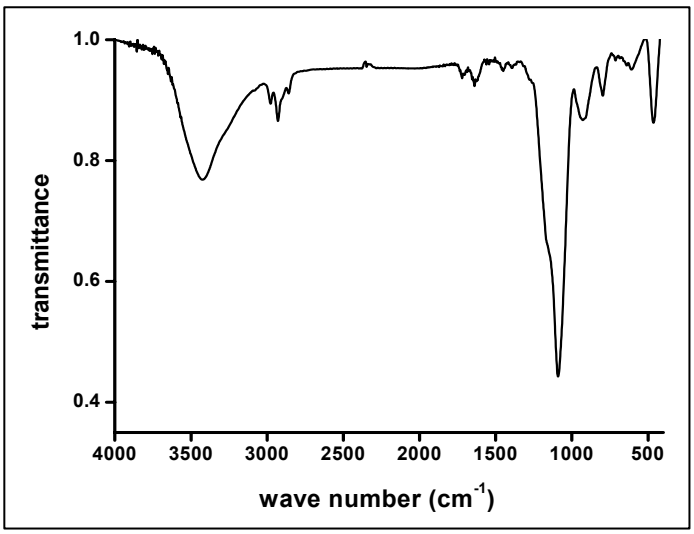

Fig. 3.8: FT-IR Spectrum of 7-OTS/BME after 2 h UV.

A system additionally containing the photoinitiator BME is shown in Fig. 3.8, after 2 hours of UV irradiation. The O–H and Si–O peaks are very strong, indicating a high amount of free silicic acid present in the sample; yet the hydroxy peak could also be caused by a significant amount of solvent (EtOH or H_2O). In comparison with spectra 3.7, now also the carbonyl peak of the initiator is visible; it is very interesting that this signal is slightly shifted (to 1710 cm^{-1}), compared to the pure initiator spectrum (cf. Fig. 3.6); this might be due to solvent interactions. Nonetheless, the intensity ratio of the double bond peak of 7-OTS to the alkyl C–H peaks at 3000 cm^{-1} still has not decreased, thus, it can be inferred that the coupling agent does not substantially react within 2 hours of UV irradiation, even in presence of a photoinitiator.

All samples measured above did not contain any surfactant. Thus, the coupling agent is expected to be randomly distributed within the silica phase. As the amount of 7-OTS is much less than the silica precursor, its double bonds are probably not arranged in proximity to each other as the coupling agent condenses within the SiO_2 matrix, which of course would drastically decrease the polymerization rate. By adding a surfactant (CTAB) to the precursor

solution, an ordered system could be obtained, presumably forcing the hydrophobic alkyl chains of the 7-OTS molecules into organic moieties. In this case, the unsaturated hydrocarbon moieties would sit much closer together – hence, it seems likely that the ordered system has a higher polymerization rate.

Detailed studies were carried out to monitor the decrease of 7-OTS double bond resonance signals over UV irradiation time. The spectra shown in Fig. 3.9 were taken from a system containing A2** stock solution, CTAB as structure-directing agent, 7-OTS and BME. The films were measured after 2 h (**a**), 4 h (**b**), 8 h (**c**) and 24 hours (**d**) exposure to UV irradiation.

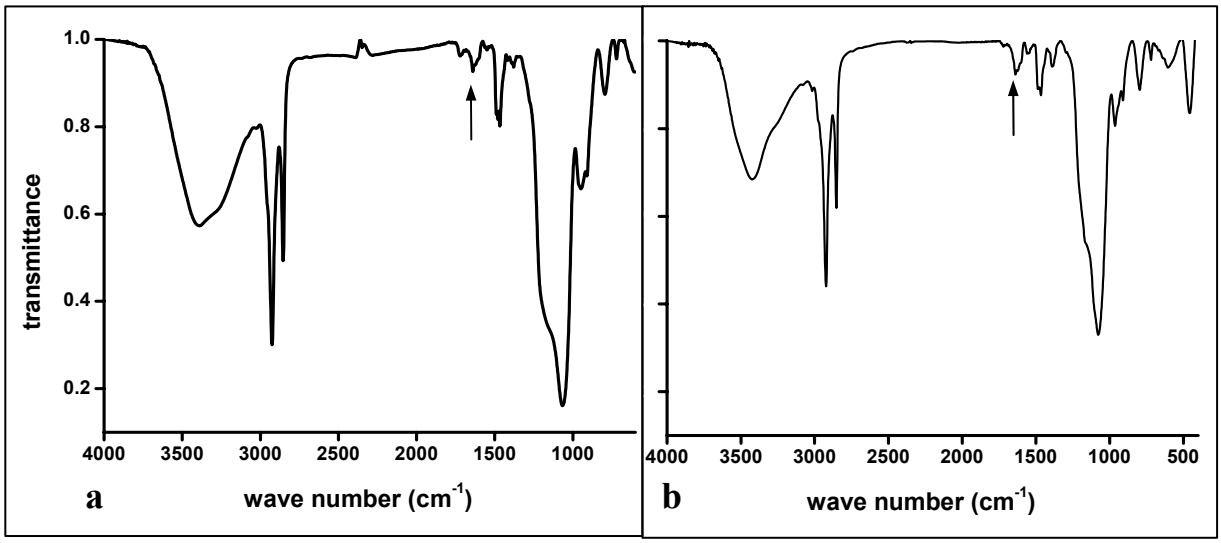

Fig. 3.9: FT-IR Spectra of a system A2**/7-OTS/CTAB/BME. Spectrum **a**: after 2 hours, **b**: after 4 h, **c**: after 8 h, **d**: after 24 h exposure to UV irradiation.

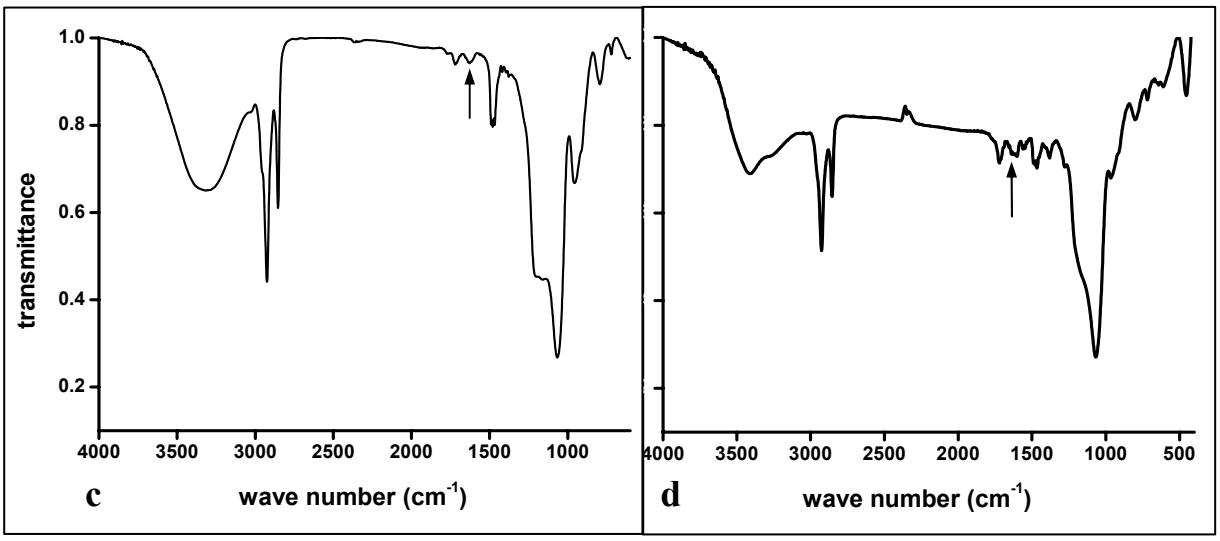

The amount of surfactant used to obtain lamellar ordering was substantially higher than the amount of 7-OTS; therefore, all spectra show pronounced $–CH_2–$ and $–CH_3$ signals around 2950 cm^{-1}. CTAB also causes a multi-jagged peak centered at 1480 cm^{-1} and a signal, fortunately very broad and small, superimposed to the 7-OTS double bond resonance which is observed at 1640 cm^{-1}. Also the second double bond signal is visible at 910 cm^{-1}. The carbonyl group of BME corresponds to the peak at 1715 cm^{-1}. Unfortunately, it was not possible to standardize the transmittance intensity for a sample; therefore, the varying extent of sample dilution with KBr led to a general variation in peak intensity. Hence, the absolute intensities of the double bond peaks cannot be directly compared but have to be related to a constant peak for determining the degree of reaction. It is illustrative to use peaks in close proximity as reference; both the BME carbonyl signal and the CTAB C–N peaks are suitable. After 2 h of UV irradiation, the double bond peak is approximately twice a large as the BME carbonyl, the intensity of the CTAB signal at 1480 cm^{-1} being ca. 2.5 times higher. The ratio of intensities of double bond signal to BME/CTAB peaks is even higher for the sample measured after 4 h irradiation, showing that not much reaction has occurred. Also the unsaturated C–H out-of-plane signal is pronounced in both spectra. After 8 h, however, the double bond peak has decreased dramatically, roughly being as large as the BME carbonyl signal. The intensity of the CTAB peaks is now ca. 6 times higher. There is only a small shoulder left of the second double bond signal. The sample measured after 24 h UV irradiation shows a further reduction in double bond intensity; now the carbonyl is twice a large as the double bond; unfortunately, the quality of this spectrum is not very good. Moreover, superposition of CTAB/BME signals leads to a broad signal around the double bond peak, making it impossible to further quantify the extent of polymerization. We can, however, summarize that 7-OTS exhibits low reactivity and polymerizes slowly. Thermally initiated systems (containing ACHN) produced similar results, showing practically no reaction within 3 h of thermal treatment.

3.2.3 Analysis of the NIPAAM Reactivity

Poly(NIPAAM) provides the functionality of the hydrogel and therefore is an essential component of the system. A high degree of polymerization is one of the main requirements in order to obtain environmentally sensitive nanocomposite films. As the NIPAAM double bond peak is clearly visible, IR analysis constitutes a good means to roughly measure the degree of reaction. Because of the superposition of the 7-OTS double bond signal with the NIPAAM carbonyl, samples containing both components could not be evaluated even semi-quantitatively; therefore, the samples discussed in this chapter were prepared without the coupling agent.

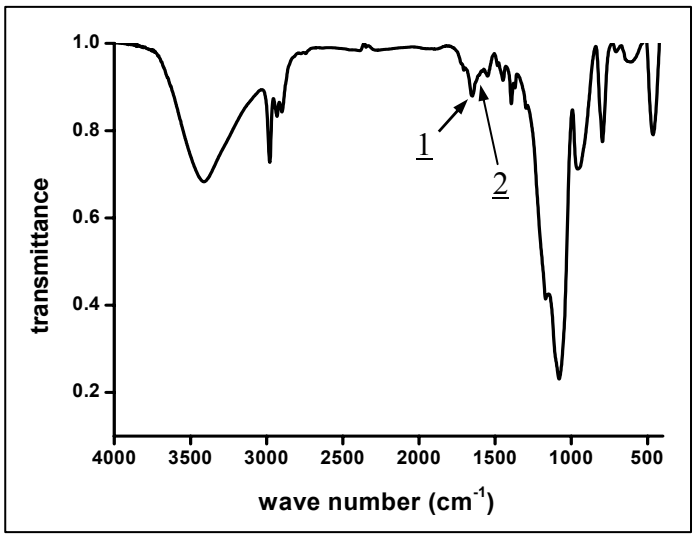

Fig. 3.10: FT-IR Spectrum of NIPAAM/BME after 2h UV.

Fig. 3.10 shows the FT-IR spectrum of a sample containing A2**, NIPAAM and BME after 2 hours of exposure to UV light. The siloxane peaks are very prominent, due to a high silica : NIPAAM ratio. Comparison to the spectrum of pure NIPAAM (Fig. 3.5), however, clearly shows that the monomers have reacted to a large extent. The O–H stretch vibration peak at ca. 3411 cm^{-1} is very large because of contributions from N–H. Furthermore, there are no components in the system with long alkyl chains, therefore the $–CH_2–$ and $–CH_3$ signals are diminished. The unsaturated C–H vibration signal, a prominent feature of the spectrum of pure NIPAAM at 3073 cm^{-1}, has disappeared completely. The actual double bond signal is very close to the carbonyl peak; nonetheless, the decrease in its intensity is unambiguously visible: the as-received chemical shows the C=C stretch vibration at 1622 cm^{-1} in almost the same intensity as the carbonyl (which is at 1658 cm^{-1}), whereas after 2 hours UV irradiation, there is a broader peak centered at the carbonyl position (1), having a shoulder at the double bond site that is only about half the intensity of the peak maximum (2).

Further experiments were carried out to investigate the behavior of NIPAAM upon thermal polymerization (Figure 3.11). Samples containing A2** sol, NIPAAM and the thermal initiator (ACHN) were measured after preliminary drying at room temperature (**a**) and after 3 h at 120°C in an oven (**b**).

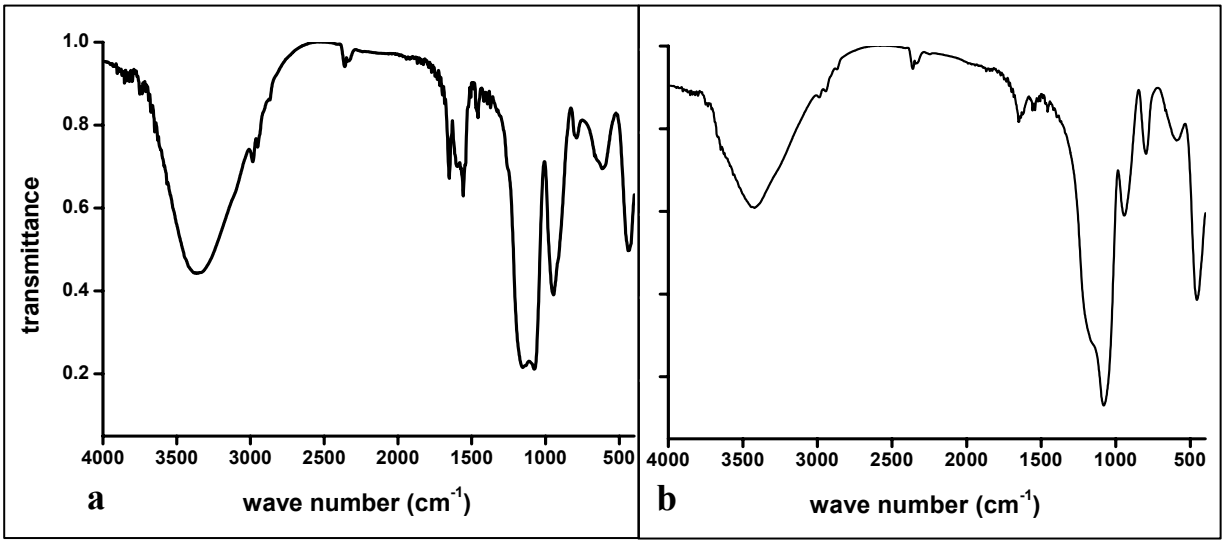

Fig. 3.11: FT-IR Spectra of NIPAAM + ACHN a: as-prepared, b: after 3 h at 120°C.

In both spectra, the O–H/N–H peaks are very large, almost "swallowing" the alkyl C–H peaks. The carbonyl/amide and double bond peaks, however, are pronounced, allowing a detailed evaluation of the spectra. The as-prepared spectrum shows a sharp carbonyl peak at 1657 cm^{-1} and broader double bond and amide peaks at 1618 and 1554 cm^{-1}, respectively. The silica/siloxane peaks are very dominant in both spectra; their intensity even increases during the heat treatment (intensity ratio rising from 3 siloxane : 1 carbonyl to 8 : 1). This strongly suggests that some of the monomer evaporates during thermal treatment, which is probable as NIPAAM has a low boiling point of 90°C (under vacuum). Polymerization and evaporation could be two competitive processes (this is also discussed in Chapters 3.3.1.4, 3.4.1 and 3.5). After thermal treatment, the carbonyl peak is broader but still pronounced, whereas the double bond peak has nearly disappeared, proving a high degree of reaction. Also the amide peak shows significantly lower intensity, which cannot be easily explained but is consistent with results from the UV-polymerized sample (cf. Figure 3.10). Comparing thermal initiation and photoinitiation, it appears that the double bond intensity is higher for the heat treated sample, which would suggest that photoinitiation has a higher efficiency.

3.2.4 Possibilities for the Simulation of FT-IR Spectra of Single Components

In addition to the measurement of prepared samples, a simulation tool was employed and tested in respect to its capabilities.[53] Another goal of these simulations was the facilitation of peak assignments. Due to the theoretical complexity, only the spectra of single components could be calculated. *Telespec*, developed by J. Gasteiger, University of Erlangen/Germany, simulates an FT-IR spectrum emanating from the molecular structure of a compound. From the data input, a three-dimensional structure model is generated and then coded by Radial Distribution Function Coding (RDF). This one-dimensional function is then compared to data stored in an artificial neural network. The program determines a "winning neuron" which acts as a pointer to a spectrum stored in an output block.

The spectra of most components were simulated using *Telespec*. Two calculated spectra are shown as examples in Fig. 3.12: BME (**a**) and 7-OTS (**b**).

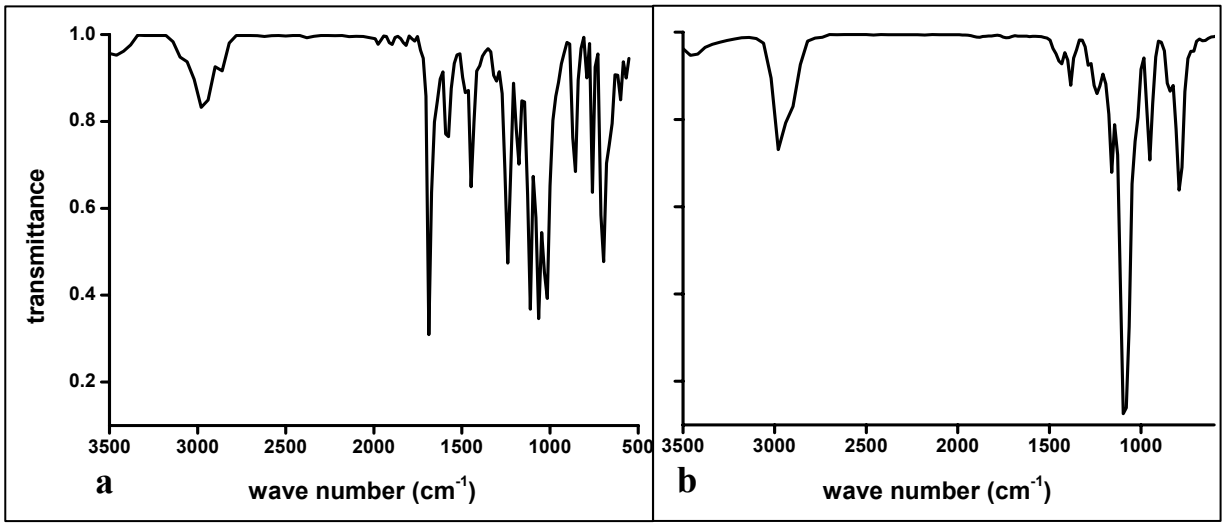

Fig. 3.12: IR spectra obtained from simulation by *Telespec*. **a**: BME spectrum, **b**: 7-OTS spectrum.

Comparison with the measured spectra (Fig. 3.3 and 3.6) shows good agreement. Especially the BME simulation shows all peaks of the measured spectrum, although the resolution is lower. Yet, for general purposes, it can be judged as providing sufficient information in good quality (all peak positions are almost identical as the measured spectrum). The 7-OTS simulation spectrum, however, exhibits one significant blemish: it does not show any double bond peaks. Simulation of trimethoxy(7-octane-1-yl)silane, the saturated 7-OTS equivalent, resulted in precisely the same spectrum. Hence, the spectrum simulation program seems suitable even for complex organic structures but is apparently overtaxed with hybrid inorganic/organic systems such as unsaturated organosilanes.

3.3 NMR Measurements

3.3.1 ^{13}C-NMR Experiments

Due to the large number of organic compounds in the system, solid-state ^{13}C-NMR spectroscopy was a helpful means to explore the reactivity of components (mainly regarding polymerization) or even changes in the concentration of one species compared to another. For peak assignment in the obtained NMR spectra, simple calculation methods (Grant-Paul-Rules) were utilized to be able to theoretically estimate the position of a specific carbon atom of a compound.[54] Also, the spectra of some components were obtained from data bases on the Internet and then compared to measured spectra.[55,56,57] Due to the structural complexity of the surfactant, coupling agent, initiator and the monomers, a detailed interpretation of samples containing the complete system was difficult, especially because of the superposition of peaks. Therefore, many experiments were performed with samples only containing some of the components, risking that their behavior was different than in the standard system. However, this greatly facilitated the identification of peaks and, comparing spectra before and after a certain treatment, allowed the quantification of reactions. It has to be stated, however, that the preparation of samples was difficult, as at least 50-60 mg of substance were necessary for ^{13}C-NMR measurements, but the film on a standard piece of silicon only amounted to ca. 0.5 mg – dip-coating of about 100 standard Si wafers would have been necessary to obtain enough material for one NMR measurement. Therefore, the "Petri dish method" was used, but even the films prepared by this method sometimes yielded less than the actually required amount – however, most of these samples were then measured with an increased number of scans to compensate for the low amount of substance. As practically all samples contained up to 70% silica (SiO_2), which of course does not give any carbon signals unless not fully condensed, the actual amount of the measured species is further decreased, resulting in a sometimes very bad signal-to-noise ratio.

3.3.1.1 Coupling Agent Reactivity

The coupling agent reactivity appears to be a crucial factor for the stability of the films. Upon surfactant removal, lamellar systems without any remaining organic species collapse, resulting in amorphous silica without any structure. Without the coupling agent, it would seem possible that the hydrogel, even if completely polymerized, is washed out of the system

and the film loses its structure. Therefore, a coupling agent appears to be necessary to provide for stability upon washing.

Detailed studies were carried out to explore the double bond reactivity of 7-OTS, trimethoxy(7-octen-1-yl)silane, in systems only containing the coupling agent and not even the surfactant but also in ordered systems, using different initiators and different polymerization techniques. Also, other suitable coupling agents were investigated.

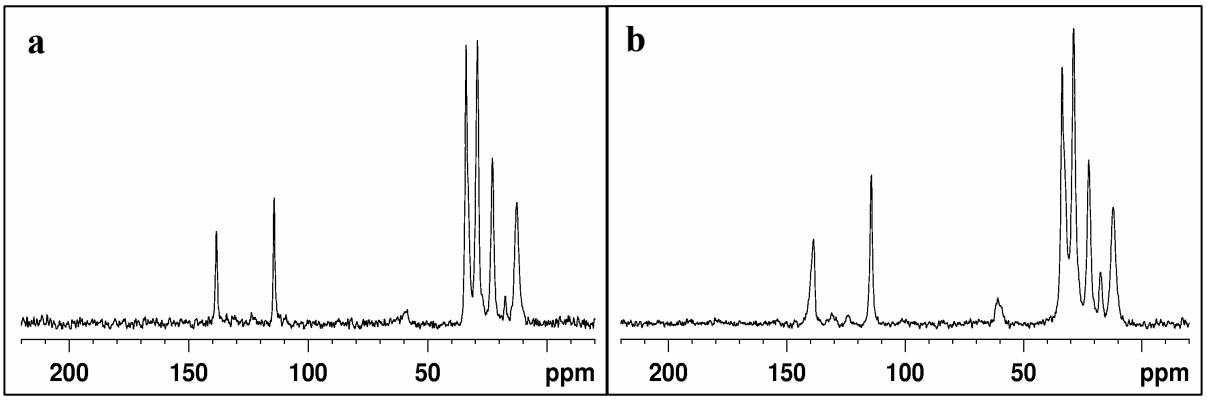

Fig. 3.13: ^{13}C-CP NMR Spectra of an A2**/7-OTS system, **a**: as-prepared, **b**: after 2h UV irradiation.

Figure 3.13 shows the cross-polarization spectra of a sample only containing silica, solvent, water/HCl and 7-OTS, in the as-prepared state (**a**) and after 2 hours of UV irradiation (**b**). The sample was compared to a data base spectrum of 1-octene (obtained from [55]). It has to be mentioned that the amount of substance was very low for these samples, hence the quality of the spectra is not as good as for most other measurements, especially for the as-prepared sample. Nonetheless, we can clearly attribute the peaks at 138.4 ppm and 114.3 ppm to the double bond of 7-OTS. The peaks of the hydrocarbon chain connecting the double bond to the siloxane head group are found at 12.7, 22.9, 29.2 and 33.9 ppm. The spectrum also shows a small peak at 58.5 ppm, which corresponds to ethanol or non-hydrolyzed ethoxy groups of TEOS. These substances also cause a peak at 17.5 ppm, but taking into account the molar ratio of 1 TEOS : 0.16 7-OTS, the intensity of both peaks is low, constituting a qualitative proof that the degree of hydrolysis or even condensation is high even for the as-prepared sample, and that evaporation of ethanol is virtually finished. Non-hydrolyzed 7-OTS features three methoxy groups linked to the Si atom. These groups would theoretically cause a peak at ca. 49.4 ppm; the absence of this peak suggests fast hydrolysis. As cross-polarized spectra are not suitable for quantitative analysis, the peak intensities cannot be directly compared. Also, these spectra are slightly misleading; the slightly higher quantity of sample used for the measurement after UV irradiation resulted in higher peaks, suggesting no reaction. Calculations from spectra measured under direct polarization (not shown because of their

poor quality) however indicate that there is a decrease in double bond intensity (compared to single bond peaks) of about 35%. Still, only a minority of double bonds reacts under these conditions, which is consistent with results obtained from IR measurements (cf. Ch. 3.2.2).

Also, samples containing A2**, 7-OTS plus an initiator (as well as solvent and HCl) were measured. A sample before and after UV irradiation, using the photoinitiator BME, is shown in Fig. 3.14 **a** and **b**. These spectra were measured under direct polarization, obtaining a semi-quantitative spectrum. The quality of the as-prepared sample is very low (the cross-polarized spectrum has much better signal-to-noise ratio), but all expected peaks are clearly visible. We see the double bond peaks at 138.5 and 114.1 ppm, but in between there is a rather broad peak centered around 128.6 ppm which is attributed to the phenyl groups of the initiator. A high amount of initiator was used for this sample (to check for the initiator effect in general); hence, there are significant initiator peaks present. The four peaks caused by the 7-OTS hydrocarbon chain are present as well; their integral ratio is (in order of increasing shift) 1:1:2:2, which is consistent with the theoretical expectation. Even a small peak at 49.4 ppm is visible in this spectrum which probably corresponds to methoxy groups of the initiator but could also be caused by unhydrolyzed methoxy groups of 7-OTS itself.

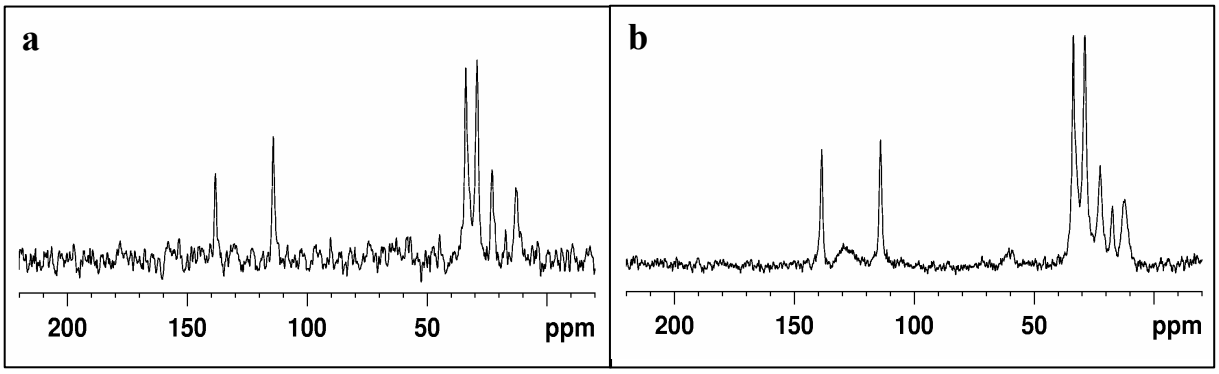

Fig. 3.14: NMR Spectra of A2**/7-OTS/BME, **a**: as-prepared, **b**: after 2 h UV irradiation.

Looking at spectrum **b**, which has much better quality, it is notable that the ethoxy peak at ca. 58.5 ppm is clearly visible; yet it is not nearly as pronounced as the second peak at 17.3 ppm. This suggests the presence of both unhydrolyzed ethoxysilane groups and ethanol, as the $–CH_2–$ groups would differ in their chemical shift corresponding to their different environment, resulting in a broader peak, but the end $–CH_3$ groups basically would differ much less, accumulating to a sharper peak. Yet their intensity is much smaller than the other 7-OTS peaks, signaling a high amount of hydrolysis within the SiO_2 network. Also, there cannot be much EtOH left in the system. Because of a long drying period, it seems obvious that all of the volatile solvent evaporates, but TGA measurements show (see Ch. 3.5.2) that a

significant amount is trapped within the silica network and cannot easily evaporate, especially in non-structured systems. Comparison of the peak integrals proves a decrease in double bond intensity of 40% during polymerization. It seems very interesting that the addition of photoinitiator does not further increase the reactivity of the 7-OTS double bond, however, it must be taken into account that a higher percentage of double bonds reacted even without placing the sample under UV irradiation; comparing the as-prepared sample to the no-initiator equivalent, the mean number of double bond peaks was approximately 10% less. Unfortunately, it is not permissible to directly relate single to double bond peak intensities within one spectrum, so the absolute degree of polymerization for one sample cannot be evaluated.

In order to explore the degree of polymerization upon thermal initiation, samples were prepared using the thermal initiator ACHN instead of BME. Measurements were performed directly after dip-coating and ambient drying as well as after extensive heat treatment (in total, 11 h at 120°C). Fig. 3.15 **a** shows that the thermal initiator only causes a small peak at 130 ppm which is attributed to its nitrile carbon atom. The heat-treated spectrum (**b**) does not show this initiator peak but, like in other polymerized spectra, peaks at 58 ppm and 17.5 ppm indicating the presence of unhydrolyzed TEOS ethoxy groups (as free EtOH is very unlikely to be present after such extensive thermal treatment).

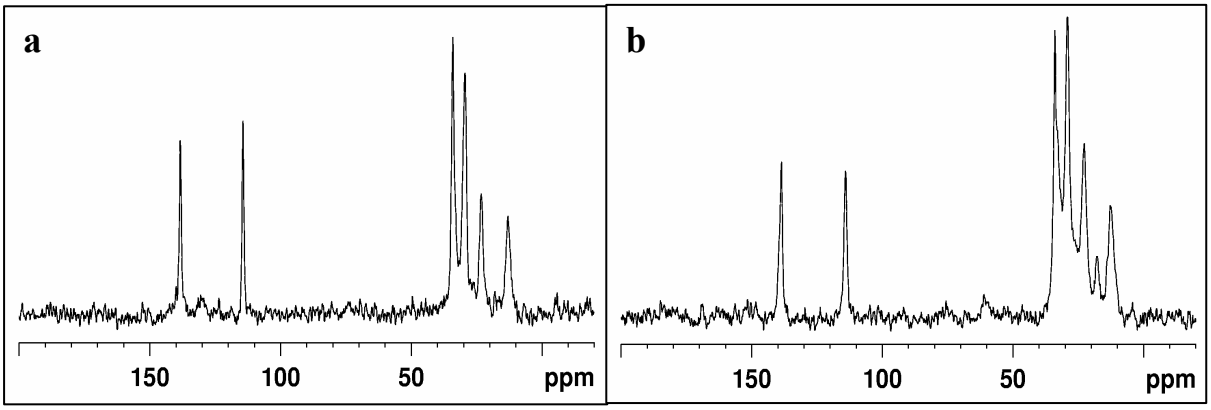

Fig. 3.15: NMR Spectra of a system A2**/7-OTS/ACHN, **a**: as-prepared, **b**: after 11 h at 120°C.

The 7-OTS double bond signals are still present in spectrum **b**. Comparison of the two spectra shows a degree of reaction of ca. 25%. However, the as-prepared spectrum already has a double bond intensity which is significantly lower than in the samples containing no initiator. Hence, assuming no reaction for as-prepared samples not containing any initiator, overall a substantially higher number of 7-OTS double bonds must have reacted within 11 h of thermal treatment.

Polymerizations can generally be impeded by oxygen. O_2 tends to form radicals which act as inhibitors especially for free radical polymerizations. Thus, the presence of air can lead to a lower degree of polymerization. The preparation process for mesostructured films, including solution assembly followed by dip-coating or spin-coating prior to polymerization, does not allow complete handling under N_2 or Ar (unless making major changes to the preparation procedure). However, it was possible to perform thermal polymerization in a special oven flushed with nitrogen. Some samples were polymerized under these conditions to investigate whether an oxygen-free atmosphere leads to a higher degree of polymerization.

Fig. 3.16 **a** shows the direct polarization spectrum of a sample containing the silica precursor, EtOH, 7-OTS and the thermal initiator; sample **b** additionally contained the surfactant, cetyltrimethylammonium bromide (CTAB). In spectrum **a**, the usual 7-OTS peaks are present, but a very interesting fact is the high intensity of the ethoxy peaks at 58.5 and 17.3 ppm. As the presence of EtOH after 3 h at 120°C is not very probable (even if trapped within the SiO_2 matrix), this suggests a low rate of hydrolysis and condensation of TEOS under a dry nitrogen atmosphere. On the other hand, also the rate of polymerization was not much higher than after a standard heat treatment, the integral ratio comparison resulted in a decrease in intensity by 20%, which is even lower than for the sample heat-treated in air. It has to be taken into account that this sample underwent a shorter treatment, but it seems clear that oxygen inhibition does not have a significant effect on the polymerization of 7-OTS.

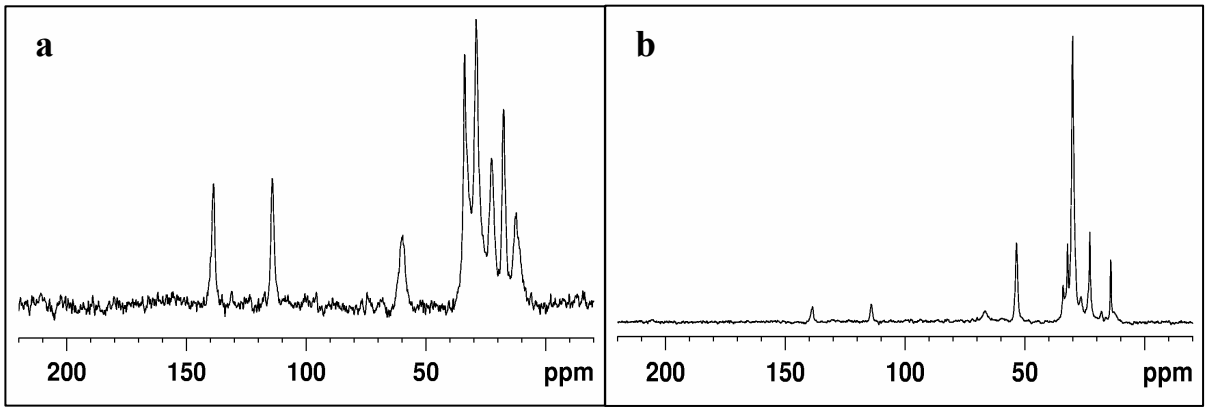

Fig. 3.16: NMR Spectra of a A2**/7-OTS/ACHN system after thermal polymerization under N_2; **b** additionally containing CTAB.

Spectrum 3.16 **b** is dominated by the CTAB signals, as the amount of surfactant used to obtain lamellar ordering was substantially higher than the amount of 7-OTS. A detailed assignment of CTAB peaks is carried out in Section 3.3.1.4. The hydrocarbon signals of

7-OTS are superimposed by the surfactant, but the double bond peaks are clearly visible and a degree of polymerization similar to the non-ordered system was determined.

Overall, the reactivity of 7-OTS proved not to be very high, which is clearly attributable to its structural nature: the double bond is located at the end of a hydrocarbon chain, generally being inactive. A carbonyl or ester group in α-position to the double bond provides the inductive and mesomer effect to significantly activate it, as in the case of acrylates. Hence, a trialkoxysilane featuring an acrylate group at the "end" of its hydrocarbon chain should show much higher reactivity. Fig. 3.17 shows a sample containing 3-(trimethoxysilyl)propyl acrylate (PATMS) instead of 7-OTS. The as-prepared spectrum (**a**) shows the carbonyl peak at 168.2 ppm and the double bond peaks at 129.4 ppm and 130.3 ppm, which is consistent with calculated theoretical peak positions. The propyl group causes peaks at 66.9, 21.6 and 8.4 ppm. The signals at 58.3 ppm and 17.3 ppm are, again, caused by the ethoxy groups of unreacted TEOS; their intensity is higher than in 7-OTS systems. The peak at 195 ppm stems from the carbonyl of unreacted BME, whilst its methoxy groups contribute to the peak at 49.9 ppm; this indicates that the sample has a high initiator content.

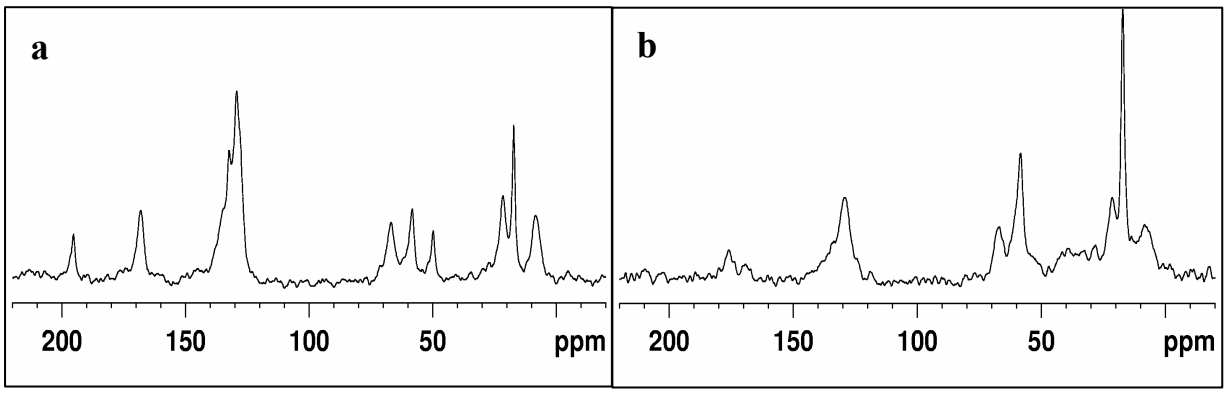

Fig. 3.17: NMR Spectra of TEOS/PATMS systems; **a**: as-prepared, **b**: after 2 h UV irradiation.

There is a clearly visible difference after 2 h UV treatment (spectrum **b**): the double bond peaks have decreased dramatically in intensity, and taking into account that the strong initiator peak is centered around 128.6 ppm, the shape of the peak in **b** (only one not too sharp peak with shoulders compared to two spikes before polymerization) suggests that the initiator is now the main contributor to this signal. Also the carbonyl peak changes upon reaction; it is shifted to 176 ppm. Hence, we now see two smaller signals, the signal at the initial position of course reflecting not reacted molecules. It is easy to calculate the degree of reaction from these two peaks; approximately 62% of PATMS double bonds reacted during the UV treatment, this is a remarkably higher extent of polymerization than any experiment with

7-OTS showed. MPS, 3-(trimethoxysilyl)propyl methacrylate, has a very similar structure (cf. Fig. 1.6); thus, a comparable reactivity can be expected. An interesting phenomenon is the very high intensity of the ethanol/ethoxy peaks (58.5 ppm and 17.3 ppm) after polymerization – they are even larger than the PATMS signals themselves. Thus, there apparently is more ethanol present, or the degree of hydrolysis of TEOS is lower after polymerization. Of course, this is not realistic, but it has to be considered that the as-prepared sample was left to dry for hours or even days (shielded from any irradiation) before the measurement, allowing the steady evaporation of EtOH. As PATMS reacts very fast, probably polymerization takes place before most of the ethanol evaporates or TEOS hydrolyzes. The system would get rigid rapidly and trap the solvent inside the non-structured polymer/silica matrix. On the other hand, organic polymers and oligomers generally are more hydrophobic than monomers. Hydrolyzed TEOS, orthosilicic acid $Si(OH)_4$, is more hydrophilic than tetraethoxysilane itself. Thus, it seems possible that the high hydrophobic organic species distributed in the system also impede hydrolysis of the siloxane.

3.3.1.2 Reactivity of Dodecyl Methacrylate

Ordered, environmentally sensitive films (see Chapter 3.4) were only obtained from solutions not only containing NIPAAM but also dodecyl methacrylate (DM). Because of its activated nature, this monomer is more reactive than the acrylamide; therefore, it can be assumed that it induces NIPAAM to react and form a stable co-polymer with increased molecular weight. NMR experiments were carried out to investigate its reactivity.

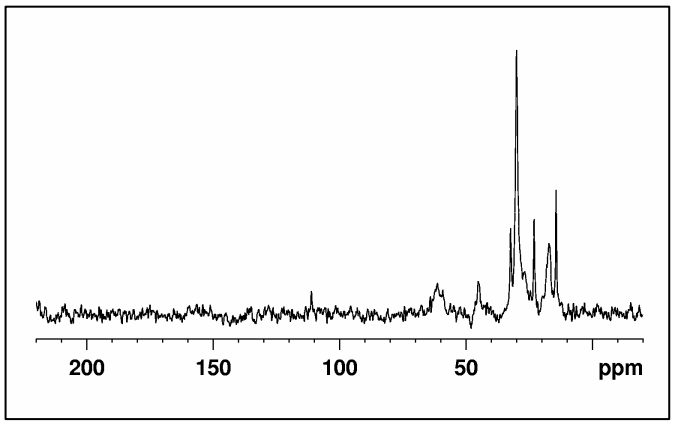

Fig. 3.18: A2**/DM/ACHN system after 3 h at 120°C.

Fig. 3.18 shows a sample only containing the silica network, DM and the thermal initiator to be able to unambiguously identify the DM signals. This sample was treated for 3 h at 120°C under nitrogen (analogously to the 7-OTS experiment) before the measurement. The peaks at

17.0 and ca. 60 ppm again stem from unhydrolyzed TEOS ethoxy groups. DM alkyl signals are found at 14.3, 23.0, 26.5, 29.9 and 32.3 ppm. Double bonds signals are expected at 125 ppm and 137 ppm; their practically complete absence is evidence of the high reactivity of DM. The peak at 45.1 ppm, on the other hand, is caused only by polymerized (or, reacted) DM, corresponding to the quaternary carbon atom next to the carboxyl group. This constitutes further proof of the advanced degree of polymerization of this sample. The carbonyl group of DM usually leads to a signal around 165 ppm; its absence is strange but could be due to hydrogen bond interactions; this is discussed below.

Also, a lamellar ordered system was measured (Fig. 3.19), as-prepared (**a**) and after thermal treatment, again in a N_2 atmosphere (**b**). Below 60 ppm, the surfactant (CTAB) peaks are very dominant, their proximity to DM peaks making an identification impossible. In the as-prepared sample, however, the carbonyl peak of DM is clearly visible at 166.4 ppm and its double bond peaks at 124.8 ppm and 136.7 ppm. The molar ratio of monomer to initiator is substantially higher than in the case of 7-OTS (1 DM : 0.06 initiator), thus, the initiator peaks are not observable in these spectra. The CTAB ammonia group causes a small peak at 64.5 ppm; to its right, there is a spike which is attributed to ethanol being present in the system, as also the second EtOH peak at 18.2 ppm is rather high in intensity. Its slightly higher chemical shift could be the result of interactions with the methacrylate group.

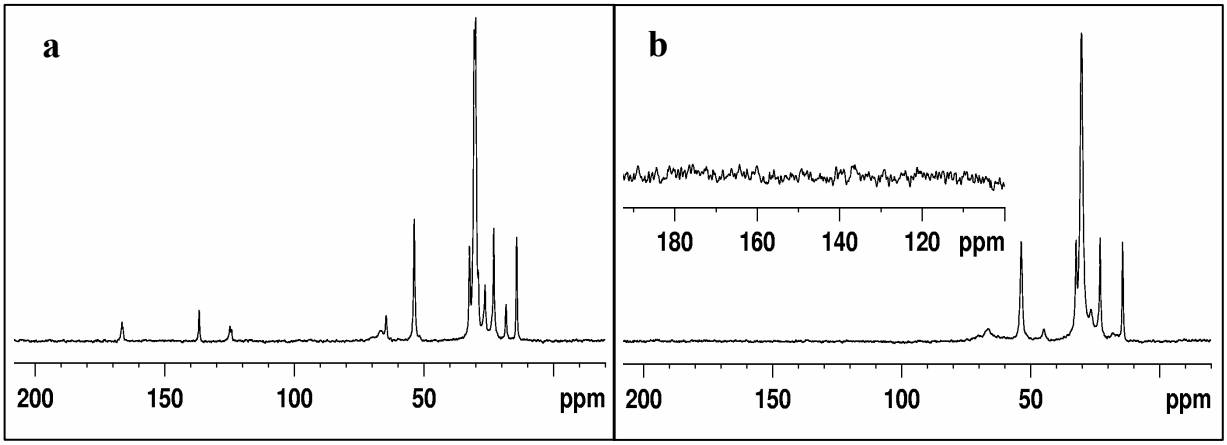

Fig. 3.19: NMR Spectra of a system A2**/DM/CTAB/ACHN, **a**: as-prepared, **b**: after 3 h at 120°C.

After thermal treatment (**b**), the double bonds are completely gone, indicating total reaction of the polymer. Furthermore, the ethanol peaks have disappeared; this seems reasonable as all EtOH is likely to evaporate within 3 hours at 120°C. A very strange phenomenon, however, is the disappearance of the DM carbonyl signal; it cannot be seen even in higher magnification of the spectrum (inset). On the other hand, a new peak at ca. 44 ppm appears which can only

be caused by polymerized DM (as calculations showed[54]). Therefore, poly(methacrylate) must be present in the system – probably after heat treatment, the species are in several possible different chemical environments (as monomer, oligomer, homopolymer, reacted with initiator groups), which leads to a number of small carbonyl peaks which are just invisible because of their low intensity. There could also be hydrogen bond interactions involved, resulting in restricted mobility, which further broadens the carbonyl signal. It is possible, though, that some of the monomer evaporated during thermal treatment; DM is rather volatile, and thus polymerization and evaporation could be two competitive processes. TGA data support this theory of partial evaporation for DM and NIPAAM, see Chapter 3.5.

3.3.1.3 NIPAAM Reactivity

Poly(*N*-isopropylacrylamide) is the functional component in the final system. After the preparation process, it is essential to exhibit a high degree of polymerization; otherwise the remaining monomers are removed upon washing and the final amount of hydrogel in the system is very low. As has been shown in other studies,[37] the swelling and de-swelling processes of the hydrogel however are so pronounced that even a small content can lead to dramatic changes of the whole system.

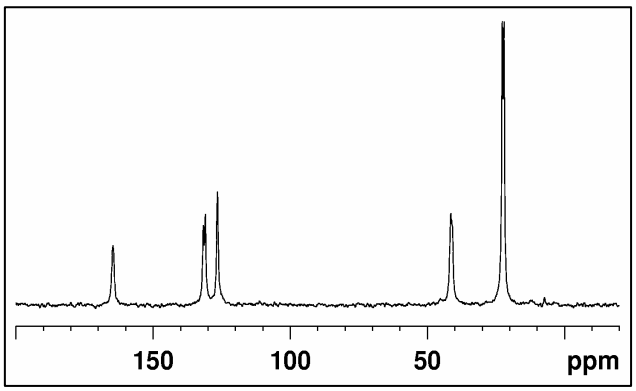

Fig. 3.20: NIPAAM measured in direct polarization.

To facilitate the interpretation of other spectra, pure solid NIPAAM was measured (Fig. 3.20). We clearly see the carbonyl peak at 164.7 ppm and the double bond peaks at 131.4/126.6 ppm. The isopropyl group causes peaks at 41.4 ppm and 22.4 ppm. It is remarkable that even in this spectrum, the carbonyl peak has a low intensity – the integral ratio is approximately 1.00 single bond : 0.64 double bond: 0.32 carbonyl for one atom; thus, this peak can be expected to easily drop below perceptibility in samples only containing a small amount of NIPAAM.

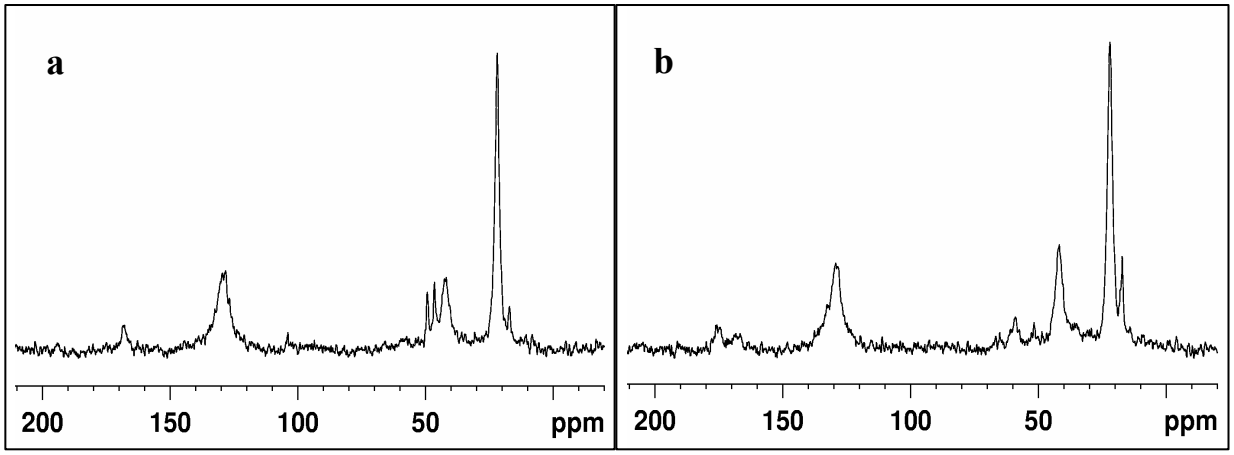

Fig. 3.21: NMR Spectra of the system A2**/NIPAAM/BME, **a**: as-prepared, **b**: after 2 h UV.

The reactivity of NIPAAM upon photoinitiation is displayed in Fig. 3.21. The as-prepared sample (**a**) shows strong initiator peaks at 128.3 ppm and 49.9 ppm as well as small ethoxy/EtOH peaks at 58.5 ppm and 17.3 ppm in addition to the NIPAAM peaks discussed above. There also is a peak at 46.7 ppm which is likely to stem from methanol (formed by hydrolysis of the ketal group of BME) which is trapped within the SiO_2 network. As the molar ratio of reactive species to initiator is slightly lower than in 7-OTS samples and NIPAAM has much less molecular weight, the concentration of initiator is significantly higher, resulting in stronger initiator peaks. Especially the signal centered at 128.3 ppm, which actually results from an accumulation of no less than 12 carbon signals (phenyl groups of BME), is dominant and totally covers the double bonds of NIPAAM. Therefore, it is impossible to compare the double bond peak intensities as in the case of 7-OTS. We can, however, see a shift of the carbonyl peak upon reaction (**b**), as has also been found for PATMS samples. The carbonyl signal of reacted NIPAAM is located at 175.8 ppm; it is easy to see that its intensity is higher than the remaining initial carbonyl peak. Calculations confirm that ca. 58% of NIPAAM reacted within 2 hours of UV irradiation. This is consistent with data acquired from FT-IR measurements, see Chapter 3.2.3.

Thermal initiation experiments were carried out to investigate the influence of different initiation methods on the degree of polymerization. Using the photoinitiator for thermal treatment led to a reaction degree of about 32%. Other samples were prepared using the thermal initiator ACHN (Fig. 3.22). As usual, spectrum **a** is from an as-prepared sample (after drying) whilst **b** was measured after 3 hours at 120°C. The amount of substance obtained from the Petri dish films was low in both cases, leading to a bad quality of the spectra. Also, the initiator content was high, resulting in strong ACHN peaks at ca. 128 ppm (nitrile groups),

71 and 32 ppm (cyclohexyl carbon atoms adjacent to the azo-group). These peaks disappear upon heat treatment, indicating decay of the initiator (its nitrile group, which does not react, remains). The ethoxy peak at 17.3 ppm can still be seen, whilst the second peak at 58.3 ppm is very broad and barely visible. The NIPAAM carbonyl peak has slightly lower intensity, but no clear second peak appears – this could be due to the low spectrum quality, as also the broad peak at 128 ppm is more pointed after thermal treatment, suggesting a decrease in double bond contributions, which would leave a sharper peak due to the higher ACHN contribution. Nevertheless, it is obvious that only a minority of monomers has reacted.

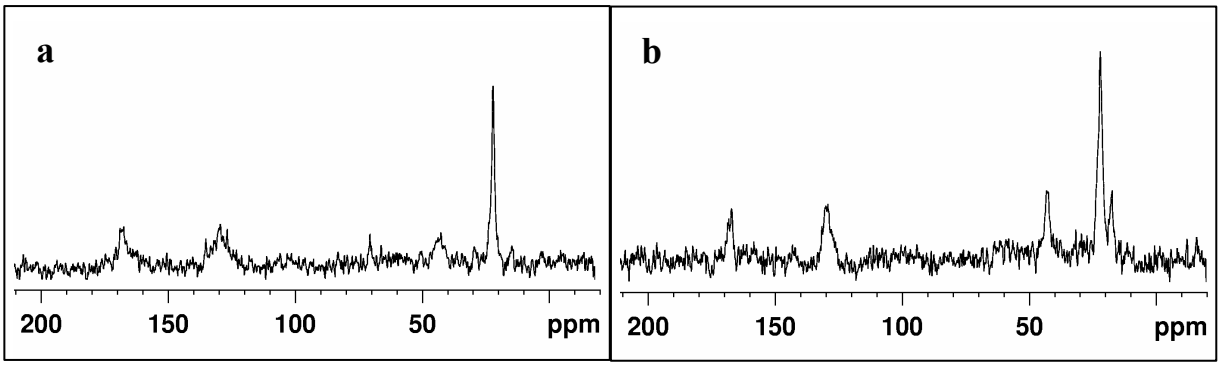

Fig. 3.22: NMR Spectra of A2**/NIPAAM/ACHN, **a**: as-prepared, **b**: thermal treatment.

It can thus be inferred that UV irradiation, using the photoinitiator BME, is by far the more efficient method to obtain a highly polymerized NIPAAM hydrogel. All samples described above were, however, not structured, as they did not contain any structure-directing agent (surfactant). Hence, it can be assumed that the monomers are more or less randomly distributed within the siloxane species and later on the silica matrix. The monomers could even be shielded from each other, which would greatly impede the polymerization. In an ordered system, it seems likely and is desired that most of the monomers migrate into the organic moieties, there being concentrated and separated from the siliceous matrix. Therefore, the ordered system can be expected to exhibit a different and, most probably, higher rate of reaction, but it is imperative to measure an ordered system to probe the polymerization behavior.

3.3.1.4 Investigations of Samples Showing Lamellar Mesostructure

In order to obtain films exhibiting lamellar structure with organic species being incorporated in the hydrophobic moieties, a significant amount of surfactant had to be used, further decreasing the monomer content in the system. Thus, the spectra of these samples are dominated by the surfactant peaks, and magnifications of the spectra had to be used to see the double bond or carbonyl peaks. On the other hand, these signals are not superimposed with surfactant peaks, so calculations could be performed at least for the samples containing only one monomer species (it was focused on NIPAAM). The preparation technique was the same as for the experiments described above, assembling a solution and then employing the "Petri dish method". The films prepared on silicon wafers showed much more homogeneous and less distorted layers than any of the Petri dish films, but because of the relatively high amount of sample required for NMR measurements it was not possible to measure any of these.

A major problem for the evaluation of structured samples was the low polymer content in the system. In many samples, the signals caused by the surfactant are clearly visible, and also the peaks of 7-OTS are present, but NIPAAM or DM signals seem completely absent. Due to a high number of peaks below 35 ppm caused by the hydrocarbon chains of CTAB and 7-OTS, it is nearly impossible to identify any DM or NIPAAM peaks in this region. A clear proof of presence of these species is a peak at ca. 41 ppm. This signal, however, is caused by the NIPAAM isopropyl group but can also stem from polymerized DM. It is thus impossible to tell from this peak whether the organic components are polymerized and whether both NIPAAM and DM or only one of these is incorporated in the system. The double bond signals are superimposed with initiator peaks, as discussed in Chapters 3.3.1.2 and 3.3.1.3. Hence, the carbonyl peak is the only unambiguous signal showing whether DM/NIPAAM is unreacted or polymerized in the system. The signal, therefore, must be visible to be able to determine the degree of polymerization.

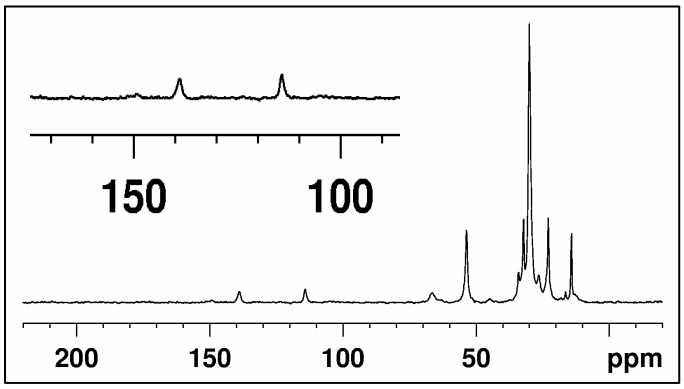

Fig. 3.23: Standard-recipe sample after 3 h at 120°C.

An example of a spectrum featuring an "invisible" carbonyl peak is shown in Fig. 3.23; this sample was obtained using the standard recipe (cf. Chapter 5). The carbonyl/double bond region was magnified (inset). The surfactant is very dominant, its long hydrocarbon chain showing peaks mainly in the region below 35 ppm (at 14.2, 22.9, 26.2 and 32.2 ppm and, most pronounced because of the contribution of 9 carbon atoms, a signal at 30.0 ppm). There are only two other CTAB signals, namely at 53.6 ppm and 66.4 ppm, which both stem from the hydrophilic quaternary ammonium head group. The only other individual sharp peak below 100 ppm is at ca. 17 ppm, most likely being caused by unhydrolyzed TEOS ethoxy groups. Apart from a small peak at 33.7 ppm and a "shoulder" at ca. 12 ppm, the hydrocarbon signals of 7-OTS completely disappear underneath the surfactant peaks. The double bond signals at 138.8 and 114.2 ppm, however, are clearly visible, proving that 7-OTS remains in the system in a significant amount but only polymerizes to a small extent. It is more difficult to detect any NIPAAM or DM in the spectrum. Even the magnification of the region of high chemical shift clearly shows the 7-OTS double bond peaks but no sign of the carbonyl signal that would be caused by both NIPAAM and DM. A splitting of the carbonyl peak into several smaller signals, due to different chemical environments depending on the state of polymerization, could obscure the carbonyl peak; thus, the absence of any peaks in the region around 170 ppm does not necessarily mean that there is no polymer in the system. Actually, there is a clear sign of either NIPAAM or poly(dodecyl methacrylate) in the system, as the spectrum features a hump at ca. 44 ppm which cannot be caused by CTAB or 7-OTS. Also the thermal initiator does not show any signals in this area, and the presence of methanol after thermal treatment is almost impossible. Hence, we can conclude that there must be polymer present in the system, but its amount was too low to produce any detectable carbonyl peaks. Further experiments, employing a higher polymer content and preparing a higher amount of sample, had to be carried out to obtain better spectra and stronger polymer signals.

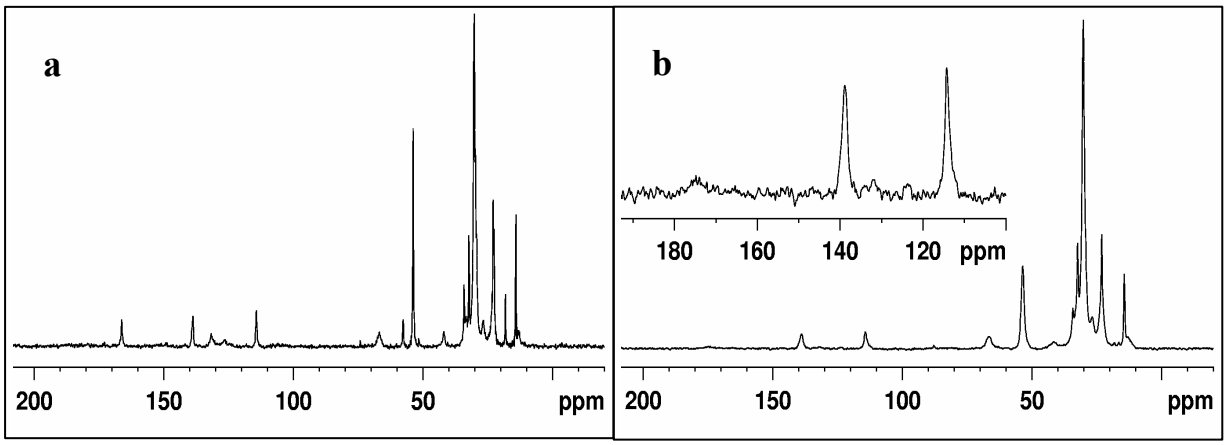

Fig. 3.24: NMR Spectra of a standard system without DM, **a**: as-prepared, **b**: after 3 h at 120°C.

Fig. 3.24 shows the spectra of such a system; the samples were prepared from a standard solution containing no DM to facilitate evaluation. The as-prepared spectrum (**a**) was measured after 2 h of drying in ambient conditions; it shows the carbonyl peak at 166.1 ppm and the NIPAAM double bonds at 126.6 and 131.5 ppm as well as the 7-OTS double bond signals (114.2/138.7 ppm). The CTAB peaks and clearly visible, and also two sharp ethanol signals as in the DM/CTAB system (cf. Fig. 3.19). The NIPAAM isopropyl group appears at 41.9 and 22.5 ppm, and the hydrocarbon chain of 7-OTS at 33.9, 29.3 (shoulder) and 12.8 ppm (the other signal is too close to a CTAB peak). There even is a very small initiator signal at ca. 71 ppm. After heat treatment (**b**), the 7-OTS double bond signals are still visible, whereas the NIPAAM double bond has vanished. The carbonyl peak apparently is gone as well, but higher magnification (inset) shows that only its intensity is decreased and the peak is broader. It has mainly shifted to ca. 174 ppm; comparison of the peak integrals gives a ratio of 80% reacted bonds – the small humps appearing at the double bond positions stem from remaining monomers but also from contributions of the ACHN nitrile signal. Compared to CTAB peaks, all NIPAAM signals decrease in intensity by 55% in average, indicating that more than half of NIPAAM evaporated during thermal treatment – this confirms observations made in IR experiments (Chapter 3.2.3). 7-OTS, on the other hand, does not seem to evaporate at all, which can be explained by fast condensation of its siloxane head group to the silica matrix. The intensity of the 7-OTS double bond remains almost stable, suggesting that only 10-15% of double bonds reacted within 3 hours at 120°C.

A complete system containing both NIPAAM and DM is shown in Fig. 3.25, as-prepared (**a**) and after 3 h thermal treatment (**b**). The insets show magnifications of the regions with higher chemical shifts.

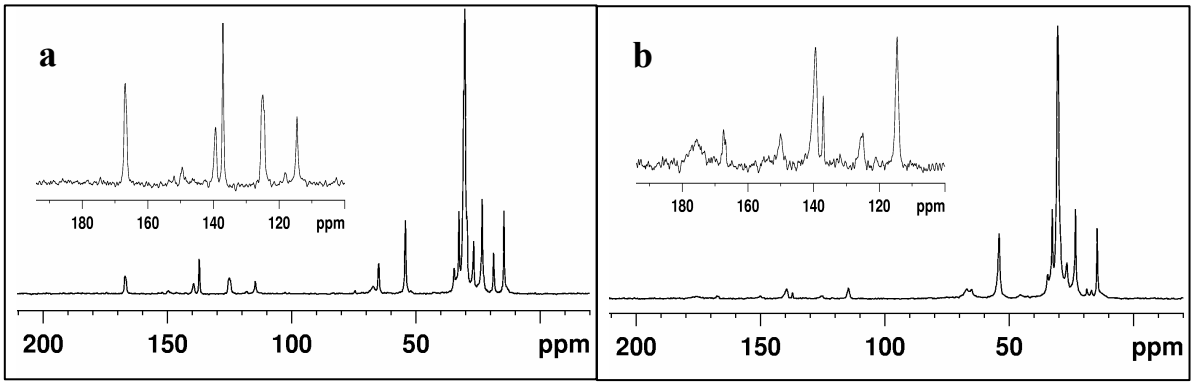

Fig. 3.25: NMR Spectra of a standard system **a**: as-prepared, **b**: same sample after 3 h at 125°C.

There is a large number of pronounced peaks in the as-prepared spectrum; we see a carbonyl peak which stems from both monomers, and the DM double bond at 124.9 and 137.1 ppm. The analogous NIPAAM signals are much smaller (because of a molar ratio of 0.32 DM : 0.14 NIPAAM) and probably are shifted due to interactions with DM; it is not possible to separate them from the DM double bond peaks. The 7-OTS peaks appear at 114.5 and 139.3 ppm. Small ACHN signals are visible at ca. 74 and 118 ppm. For this sample, thermal treatment was carried out using as-prepared sample. After measurement of **a**, the substance was left in the sample holder and directly heated to 125°C, left at this temperature for 3 h and then measured again (**b**). The 7-OTS double bond signals are still visible whilst the DM peaks are substantially decreased, indicating polymerization. Also, a small peak at 45.3 ppm appears, caused by reacted DM. From the shift of the carbonyl peak, it is clear that over 75% of the DM/NIPAAM double bonds have reacted. 7-OTS on the other hand has only reacted to a very small extent. Unfortunately, it is impossible to separate the signals of NIPAAM and DM; thus, we cannot analyze the structure of the polymer and determine whether a random co-polymer or some sort of block co-polymer is formed.

All of these samples were measured before washing, as the washing of films prepared on a Petri dish is problematic because the film thickness is much higher than for standard films obtained when using Si wafers as substrates. Also, these films tend to peel off the dish, making it impossible to perform a washing process analog to the dipping of wafers into solvents. Hence, a thin layer of ethanol and, subsequently, acetone was filled into the Petri dish; then the dish was slightly swayed sideways for 10 s and then the solvent was decanted. This procedure resulted in only incomplete removal of CTAB and monomers. The sample was dried in an oven at 40°C for 20-30 min and then scraped off and measured as usual (Fig. 3.26). This sample contained no DM but twice the standard amount of NIPAAM.

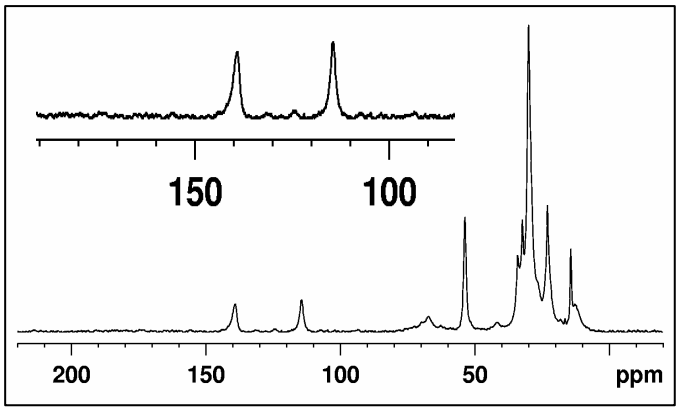

Fig. 3.26: Spectrum of a standard sample after washing.

The spectrum clearly shows that there still is some CTAB in the system. This was expected, as discussed above. The 7-OTS double bond signals are visible, and the magnification also shows that some of the monomer or initiator must have remained in the sample. The NIPAAM isopropyl peak is visible at ca. 41 ppm – it cannot be caused by any other compounds and therefore is evidence for the presence of NIPAAM. Due to the small intensity of the double bond peaks, and the very small carbonyl signal, calculations could not be performed. As we know, however, that for structured samples, most of the remaining NIPAAM is polymerized after a standard heat treatment, this spectrum constitutes an unambiguous proof that poly(NIPAAM) is present in a structured system, even after washing.

3.3.2 ^{29}Si-NMR experiments

The supporting inorganic matrix is formed by SiO_2. As a high stability of the system is desired especially for the washing procedure, a high degree of silica condensation is necessary. The hydrolysis and condensation of the silica species can easily be monitored by ^{29}Si-NMR spectroscopy. TEOS is used as the initial precursor; it is expected to be in a mostly hydrolyzed state after A2** sol preparation (cf. Scheme 1.1). After film formation, it condenses and forms stable Si–O–Si bonds. During the whole process, the silicon atom is connected to 4 oxygen atoms and is therefore called a *quaternary* Si atom (Q). The coupling agent also features a siloxane group, which is expected to hydrolyze as well and then condense to the silica matrix. This Si atom is bonded to the hydrocarbon octyl chain and three oxygen atoms, it is thus labeled a *tertiary* Si atom (T). As these two species have a different chemical environment, they are also subject to different chemical shifts and can therefore easily be separated in ^{29}Si-NMR spectra. Moreover, the group adjacent to the oxygen atoms also influences the peak position; hence even the state of condensation can be determined. The superscript index reflects the number of bridging oxygen atoms surrounding the silicon center.

Fig. 3.27 shows the solid-state ^{29}Si-NMR spectrum of a system containing only A2** and surfactant (and H_2O/HCl). Pure A2** sol was diluted with EtOH as usual before adding the surfactant (the solvent was used to ensure a comparable CTAB concentration in the solution as for standard systems). After adding water and HCl, the solution was cast onto a Petri dish and then exposed to 120°C for 3 h.

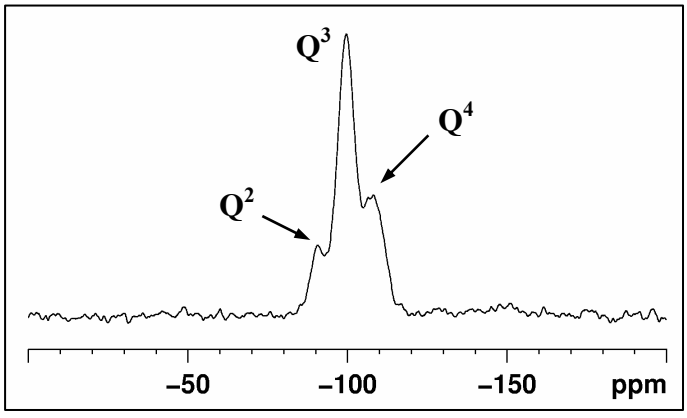

Fig. 3.27: Spectrum of a system A2**/CTAB after 3 h at 120°C.

As the sample contained no coupling agent, there are only quaternary Si signals visible in this spectrum. After heat treatment, there of course cannot be any unhydrolyzed Si–O–R groups left (which would cause peaks between –80 and –90 ppm). Therefore, only Si–O–H and Si–

O–Si groups are present; three distinct peaks can be seen: the signal at –95 ppm is attributed to Q^2 silicon atoms, the largest peak at –100 ppm to Q^3 Si atoms, whereas the third signal at –104 ppm stems from fully condensed Q^4 Si atoms. The signals had to be deconvoluted (assuming Gaussian distribution) to be able to calculate the integral intensity of the actual signals. Assuming only Si–O–Si and Si–O–H groups present (and no Q^0 and Q^1 centers), the number of bridging groups is half of the Q^2 centers, plus ¾ of the Q^3, plus all Q^4 centers. From the intensity ratio of the peaks, a degree of condensation of 79.5% could be calculated, meaning that this percentage of bonds were bridging bonds. As there is no coupling agent in the system, there are of course no visible T-silicon peaks.

The preparation of A2** solution from TEOS, ethanol, water and diluted HCl aims to create a solution of silicic acid or at least partly hydrolyzed TEOS which is stabilized by setting the pH value to the isoelectric point of silica to prevent condensation and gelation. This is of great importance, as only a stable A2** stock solution can lead to reproducible results, and an advanced degree of silica condensation might even impair the self-assembly process. ^{29}Si-NMR allows to monitor the degree of hydrolysis and condensation over time. Fig. 3.28 shows two spectra, measured from pure A2** solutions 3 days (**a**) and 2 months (**b**) after preparation.

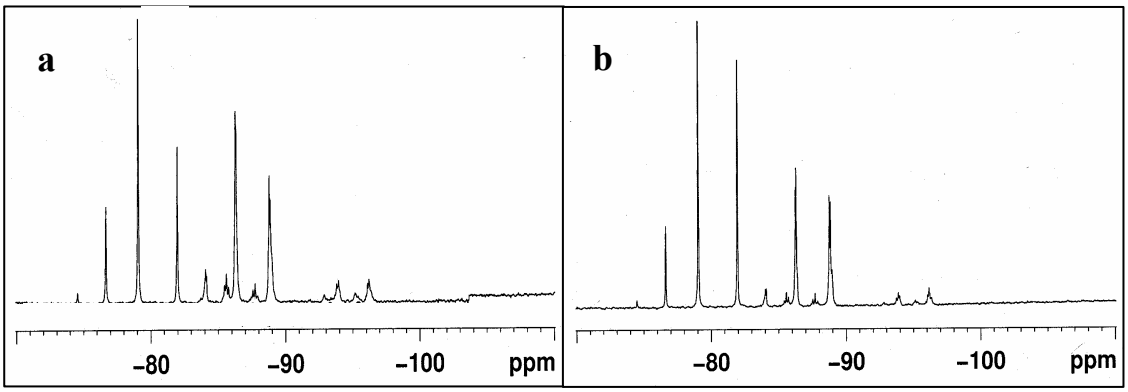

Fig. 3.28: ^{29}Si-NMR Spectra of A2** sols, **a**: 3 days, **b**: 2 months after preparation.

Both spectra were magnified so the individual peaks are visible. A number of Q^0 and Q^1 peaks are visible (the splitting is due to various states of hydrolysis), but the Q^2 peaks are small and there are no higher condensed Si atoms visible. The overall degree of siloxane condensation was calculated to ca. 20%. Hydrolysis, on the other hand, was in a very advanced state (over 85% degree of reaction). Hence, we can infer that the A2** preparation method is very efficient, leading to a highly hydrolyzed sol. Comparison of the two spectra shows no significant changes occurring within two months after preparation – this proves that the pH

value is optimized and the solution remains stable for months (the degree of condensation of spectrum **b** is also not more than ca. 20%).

Polymerization by photoinitiation was followed by ammonia treatment to enhance the condensation of the silica matrix. As mentioned in Chapter 3.4.1, this treatment could not be performed after thermal polymerization without destroying the film structure. Hence, it seems logical to compare the two routes of sample processing to investigate whether the degree of silica condensation after heat treatment is equal to the condensation degree after exposure to ammonia vapor following UV-polymerization.

Two ^{29}Si-NMR spectra obtained from films containing A2**, CTAB and 7-OTS can be seen in Fig. 3.29; one sample was treated in an oven at 120°C for 3 hours (**a**) and the other was irradiated by UV light for 2 h and then exposed to NH_3 vapor for 15 min (**b**).

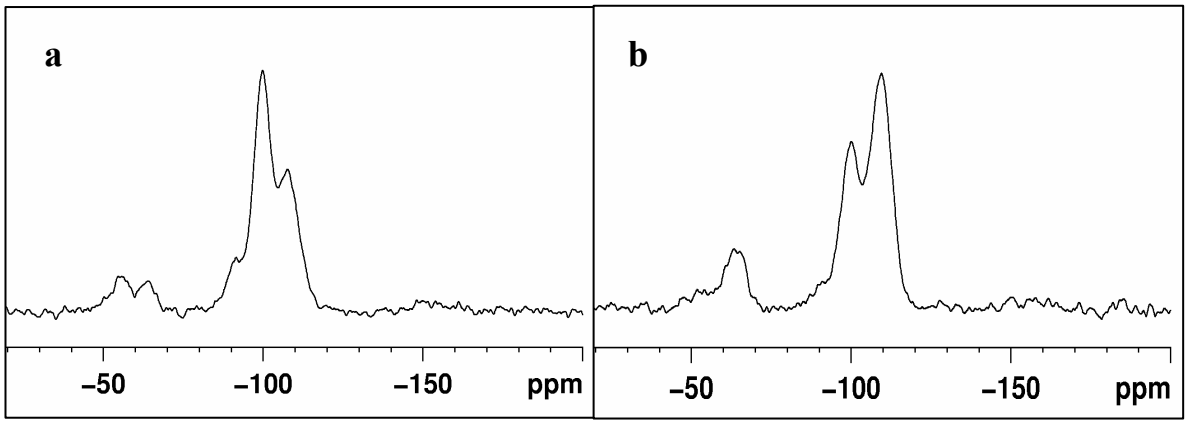

Fig. 3.29: NMR Spectra of samples **a**: after 3 h at 120°C, **b**: after 2 h UV + 15 min NH_3 vapor.

The T-silicon signals appear at –50 to –70 ppm, stemming from 7-OTS. For the heat-treated sample, there are two apparently equal T^3 and T^4 peaks, however the peaks, because of partial superposition, had to be deconvoluted to be able to calculate the degree of condensation. Comparison of the integrals of the two peaks (analogously to sample 3.27) results in a degree of Si–O–Si bonds for 7-OTS of 78.2%. The condensation rate was significantly higher after ammonia treatment, as even the visual comparison with spectrum **b** shows. A value of 90.6% of silica bonds was obtained. After heat treatment, the Q-peaks of TEOS show a slightly higher condensation degree than for the system without 7-OTS (Fig. 3.27), 82.0%, whilst the UV/NH_3 preparation route again leads to a higher degree of condensation of 88.3%. Hence, it can be inferred that the condensation is generally more complete after ammonia treatment, although also heat treatment effectively enhances the silica condensation.

3.3.3 Analysis of Swelling Experiments Using ^{13}C- and ^{1}H-NMR Techniques

Recently, detailed NMR studies were performed with co-polymerized methacrylic acid/NIPAAM bulk gel systems in different states of swelling and deswelling.[58] The transition was detected in ^{13}C- and ^{1}H-NMR spectroscopy. In ^{1}H spectra, measured after immersing the gel in water overnight at various temperatures, a shift to higher field as well as a sudden splitting of one water peak (from DOH) into two peaks was discovered at 34°C, indicating the existence of two species at and above this temperature. The shifting is attributed to less interaction between water and the polymer, leading to a higher shielding of protons. The second water peak above the LCST is believed to be caused by water expelled from the polymer system.

As these results seem very interesting, similar experiments were performed with the nanocomposite hydrogel system to probe for changes in the chemical environment of the H_2O protons (Figure 3.30). Only a poly(NIPAAM) hydrogel nanocomposite was intended to be obtained, therefore, no DM was added to the precursor solution. The sample was prepared in a Petri dish and heat-treated as usual. D_2O was added to a washed sample in the wt/wt ratio of 1:1 and left overnight, at 25°C (**a**) and 40°C (**b**). Then the proton spectra were recorded on a Bruker DRX spectrometer at 399.9 MHz using a 5 mm broadband probe. A sweep width of 50 ppm was used.

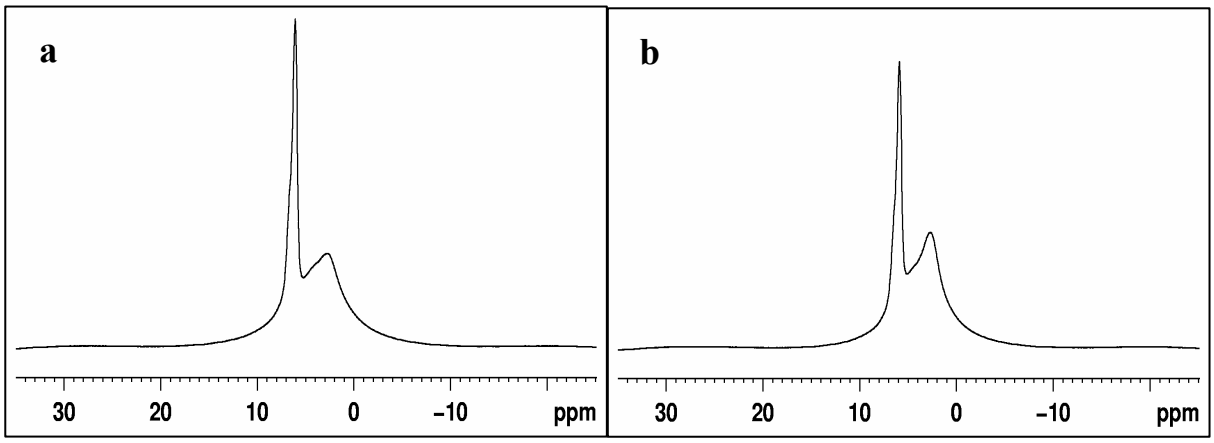

Fig. 3.30: ^{1}H-NMR Spectra of a washed, standard-recipe sample **a**: at 25°C, **b**: at 40°C.

The two images show very similar spectra below and above the LCST; the only difference is the shift of both peaks towards higher field going from 25°C to 40°C by about 0.1-0.2 ppm. This is much less than indicated in the report mentioned above, however, the trend is consistent, but could also simply be caused by the temperature dependence of hydrogen bonding. Yet, the peak exhibits a higher chemical shift compared to the spectra of pure

poly(NIPAAM) spectra. Also, the lower, broader peak at 2.7 ppm is attributed to protons of Si-OH groups which would not be influenced by any polymer phase transition processes.

^{13}C-NMR experiments were performed as well, using the same sample/D_2O mixtures as above (Fig. 3.31 **a** and **b**).

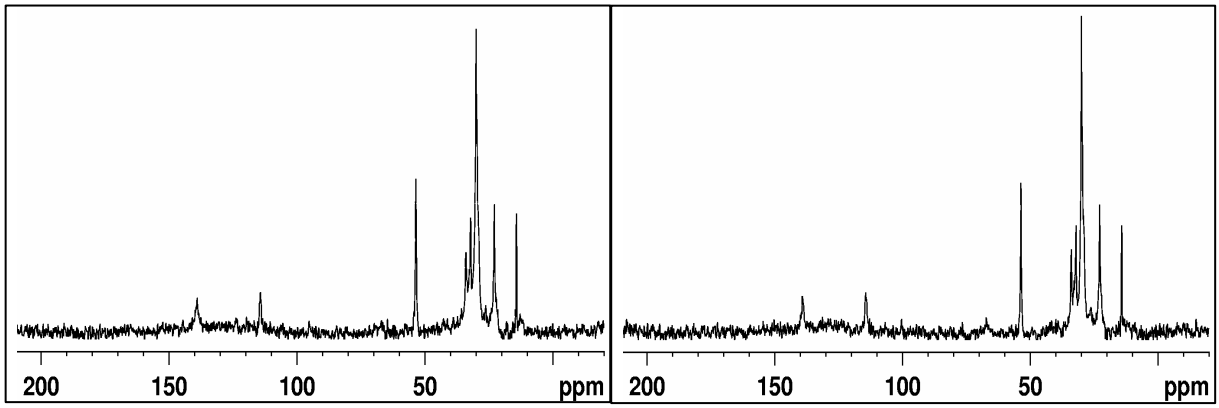

Fig. 3.31: ^{13}C-NMR Spectra of a washed, standard-recipe sample **a**: at 25°C, **b**: at 40°C.

The phase transition should lead to a decreased molecular mobility above the LCST, resulting in the disappearance of the NIPAAM carbonyl peak and a broadening of the isopropyl signals.[59] Looking at the two spectra, however, we see only non-polymer peaks in the water mixture; the quality of the spectra is very low, only showing 7-OTS and CTAB peaks. Even the NIPAAM peak at 41 ppm is hardly visible for the 40°C spectrum and invisible in the 25°C spectrum.

Hence, we can conclude that the amount of poly(NIPAAM) in the sample is too low to be able to observe any phase transition effects of the polymer by ^{13}C- or ^{1}H-NMR spectroscopy. Even the reports mentioned can only show changes when comparing spectra obtained from up to 30,000 accumulations, therefore, it seems obvious that the system investigated in the present work, containing less than 50% polymer, does not allow to watch these processes by NMR experiments. Therefore, analysis techniques much more sensitive to phase transition processes, and swelling in particular, such as DSC and especially SAXS were employed.

3.4 Small-Angle X-ray Diffraction Measurements

As the routine measurement is fast (acquired within 5 minutes) and provides the most essential information about a film sample, such as quality of the structure and mean distance of layers/structure elements, small-angle X-ray scattering (SAXS) was employed as the standard analysis technique for these thin film samples. Also, the desired functionality – swelling or de-swelling of the organic layers – could be monitored best by SAXS. The *d*-spacing corresponds to the mean periodic distance of identical structural elements – in the case of lamellae, this is the distance of one (e.g. inorganic) layer to the next equal (inorganic) one (see Scheme 3.1).

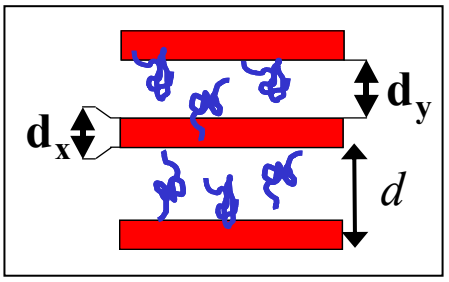

Scheme 3.1.

It can easily be obtained from the measured position of the main reflection (001) using *Bragg's equation with n=1*:

$$d = \frac{\lambda}{2\sin\theta} \qquad (3.1)$$

where 2θ is the scattered angle and λ equals the used X-ray wavelength; in our case: $\lambda = 1.5418$ Å.

The degree of ordering of a sample corresponds to the intensity of a signal, respectively its width. A sharp signal reflects a uniform *d*-spacing, whereas a broad, low (001) reflection is caused by a high variation in *d*-spacing within the sample, stemming from disruptions in the lattice. Also the extension of the lattice plays a role; a low domain size can also cause a broadening of signals. In a lamellar sample, this corresponds to the number of stacked lamellae. TEM pictures (see Chapter 3.9) show that the number of layers within a domain is rather high (over 50 layers); therefore, the domain size can be assumed to be high enough not to cause a broadening of signals.

The routine analyses were performed on a standard X-ray diffractometer in θ-2θ geometry, measuring the sample on the Si wafer in symmetric reflection. Because of an abundance of data, only a selection of the diffractograms can be shown in this chapter. Samples exhibiting high order or good functionality were subject to longer scans, lasting up to 10 hours, in order to get SAXS data of high quality and intensity. Some measurements were carried out on a

Synchrotron Small Angle X-ray Scattering (2D-SAXS) beamline with a 2-D detector at Aragonne National Laboratories, Chicago/U.S.A. For selected highly ordered films, the corresponding SAXS data obtained from the diffractometer were fitted with a suitable theoretical layer model, which produced interesting results (see Chapter 3.4.6). By this method, the thicknesses d_x and d_y (cf. Scheme 3.1) of the two types of layers, as well as their variances, could be calculated.

Summarizing, the following information can be obtained from SAXS analysis in case of the presence of a lamellar structure:

- proof for the formation of a mesostructure
- proof for a lamellar ordering of the mesostructure (from 2D-SAXS)
- the mean distance between the two layers (*d*-spacing)
- changes occurring to the sample structure during the preparation process
- quantitative analysis of the lamellar structure, determining the thickness of the individual layers (applying a theoretical model fit)

SAXS therefore constitutes an excellent means to characterize the mesostructure, and is suitable for qualitative routine scans as well as for detailed quantitative analysis.

3.4.1 Observation of the Sample Preparation Process

The main goal of this work was to synthesize a highly ordered system consisting of condensed silica layers alternating with layers of polymerized organic moieties. As the employed approach was to assemble a homogeneous precursor solution containing all components, the crucial problem was the self-assembly process of the components into organic/inorganic nanophases and especially the maintenance of the high ordering during subsequent polymerization, condensation and washing treatments.

3.4.1.1 Polymerization and Ammonia Treatment

In the as-prepared state, instantly after film formation, the samples generally showed very high ordering, visible in the SAXS plot as sharp signals of high intensity. For most films, not only the (001) reflection, but also second- and even third-order signals were found. The results for similar experiments (using comparable amounts of surfactant, A2**, 7-OTS and monomers) were consistent, also in respect of the positions of the reflections. After polymerization, different results were obtained depending on the initiation method. Thermally treated films showed much lower *d*-spacings than samples exposed to UV irradiation, which is reasonable as significant amounts of solvent remain in the film after dip-coating. Evaporation of this solvent is greatly enhanced by exposure to heat, and also the monomers are rather volatile and partially evaporate (as has been seen discussed in Sections 3.2.3 and 3.3.1). Another factor is the condensation of silica during thermal treatment – hence, both types of layers probably decrease in thickness upon thermal treatment, as confirmed by the detailed SAXS analysis (Chapter 3.4.6). Photoinitiated samples, on the other hand, had to be exposed to ammonia vapor after polymerization to enhance condensation of the silica matrix. This treatment caused a slight decrease in *d*-spacing, which however still was about 1 nm higher than for heat-treated films.

Fig. 3.32 shows the SAXS patterns obtained for as-prepared, polymerized, ammonia-treated (if applicable) and washed films for a thermally polymerized (**a**) and a UV-treated system (**b**). For better visibility of second-order reflections, insets are shown with the intensity being plotted in logarithmic scale.

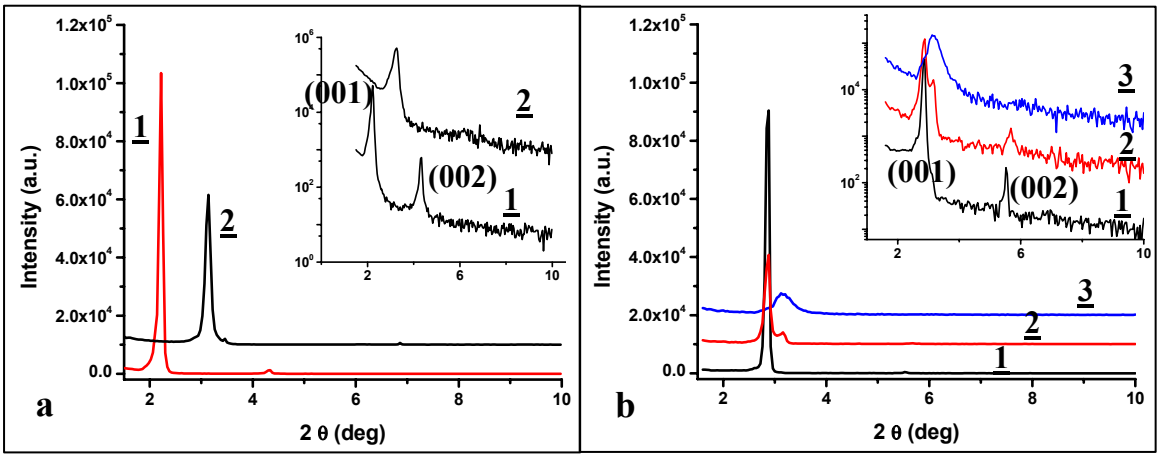

Fig. 3.32: Diffractograms of samples at the subsequent preparation steps of a film, polymerized by **a**: thermal treatment, **b**: UV irradiation; as-prepared (**1**), polymerized (**2**), ammonia-treated (**3**).

Generally, (00*l*) reflections are indicative of a lamellar mesostructure, with the lamellae being parallel to the substrate. For all diffractograms shown in Fig. 3.32, the lamellar ordering is clearly visible by the (001), (002) and, in some patterns, even (003) signals. The shift in the pattern of the heat-treated system is significant, the *d*-spacing decreases from 4.0 to 2.8 nm. The (002) reflection appears very low and broad after heat treatment, which might be the effect of a decrease in ordering of the sample. The UV-irradiated sample showed only a very small shift of the signal and had a very highly ordered structure, but additionally had to be subject to ammonia treatment to induce siloxane condensation – photoinitiated samples not exposed to NH_3 vapor were rinsed off upon washing of the film, or completely lost their structure. On the other hand, extensive ammonia treatment also led to the destruction of the film structure; this is discussed in Chapter 3.4.2. Thermally treated samples, however, already had a high degree of condensation and were not treated with ammonia, as experiments showed that the structure was destroyed upon exposure of these films to NH_3.

3.4.1.2 Washing

The final step in the sample preparation process is washing. This is a crucial operation – on the one hand, most of the surfactant and also unreacted monomers are intended to be removed, but on the other hand of course the structure must be preserved. A general problem was that some films peeled off the substrate as a whole when being rinsed with ethanol or acetone. This problem was diminished by dipping the wafers into the solvent instead of rinsing the wafer. In many cases, though, not the whole film came off but the structure was lost, due to a number of reasons. For a lamellar system, it is obvious that a firm (covalent) connection between the layers must be established up to this point, otherwise the layers would become detached and peel off. Therefore, at least a minimum amount of coupling agent molecules must have reacted, being condensed into the silica matrix but also connected to the polymer. Results obtained by IR and NMR spectroscopy suggest a high condensation rate of the coupling agent (Ch. 3.3.2) but very low reactivity towards polymerization of its double bond (Ch. 3.2.2 and 3.3.1.1). Nonetheless, many samples retained their highly ordered structure upon washing and also upon immersion in water even for days. Thus, it can be assumed that if a connection between the layers is established, only at some sites, the structure remains stable; this appears to be a delicate process, however, as the reproducibility of the SAXS data after washing was limited. This seems reasonable: if not enough sites are connected, or if these connections are badly distributed, the layers would detach and the ordering would be lost.

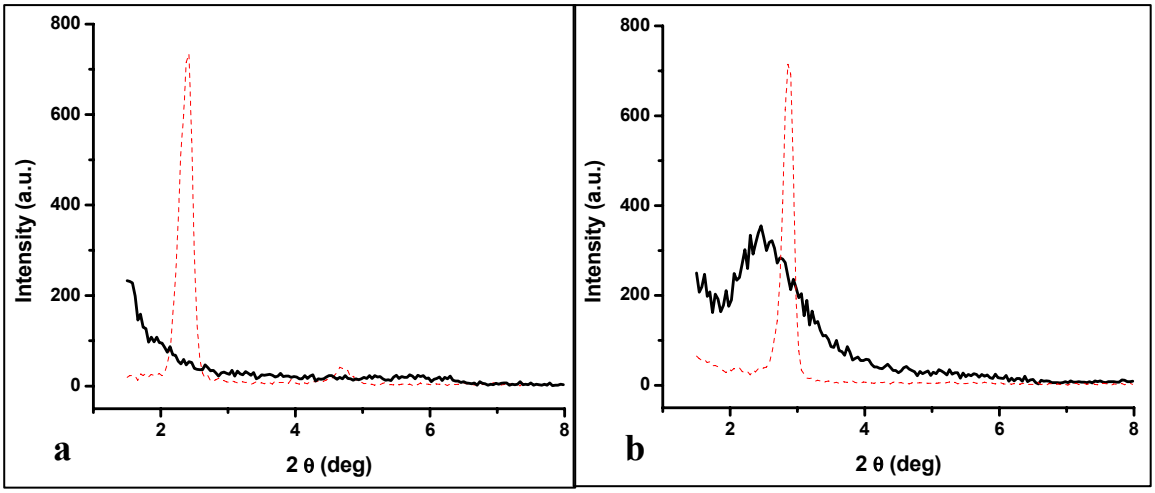

Fig. 3.33: SAXS diffractograms of obtained from thermally polymerized films after washing, **a**: no structure **b**: analogously prepared sample retaining its structure.

Fig. 3.33 shows examples of SAXS patterns obtained after washing. The thin dotted line represents the pattern measured before washing of the sample. In plot **a**, the order is completely lost, with the primary beam reflection leading to higher intensity at low angle of incidence. Pattern **b** shows a broad reflection centered at 3.50 nm. All washed samples showing the layered order with incorporated polymer (*d*-spacing of 2.8 nm and higher) exhibited broad signals with rather low intensity. On the one hand, this is due to the different slit setup that had to be used to diminish the primary beam reflection signal (see Chapter 5.6.1), which led to generally lower intensities of signals but facilitated the detection of reflections with large *d*-spacings. On the other hand, the decrease was much higher than e.g. for polymerized films measured with both slit setups – washing must significantly reduce the ordering of the films. This is easy to explain, to some extent: With the surfactant still present in the system, there is a 'spacer' which keeps the layers in a fixed distance. As this spacer is removed, the structure collapses. In the case of a pure silica/surfactant system, the structure is completely lost and amorphous silica is formed upon removal of the structure-directing agent.[24] With the polymer present in the organic moiety, the layers of course cannot collapse but are kept apart by the polymer. Assuming random distribution of the polymer chains, though, the washed samples would exhibit domains with a variation in thickness of the polymer layer, resulting in a variance in the *d*-spacing, visible as broader signals. One could now think that removing the surfactant would decrease the *d*-spacing, but taking into account that the polymer (being completely dry after thermal polymerization) incorporates some solvent and swells dramatically, higher *d*-spacing is plausible.

Loss of polymer upon washing. There were also other types of SAXS patterns observed measuring washed samples. Some films did not loose their structure completely, but showed one rather pronounced signal at a low *d*-spacing after washing (between 1.40-1.70 nm). As no swelling was observed (see Chapter 3.4.3), it can be deduced that these structures consisted of silica layers kept apart by either remaining surfactant or coupling agent molecules (being condensed to the silica matrix but not polymerized). This is clearly contradicted by a study published earlier by this group.[36] A very similar system was investigated in that work, but only using DM as monomer. The SAXS patterns show rather sharp reflections even after washing at a *d*-spacing as low as 1.46 nm. In the study, the successful incorporation of poly(dodecyl methacrylate) into a lamellar nanostructure is reported even for such a low *d*-spacing; this, however, appears to be a misinterpretation: A stable silica layer must consist of at least two SiO_2 tetrahedrons perpendicular to the interface, equaling a *d*-spacing of 0.6 nm. Therefore, the polymer layer would be less than 0.8 nm thick. Taking into account that the mean C–C bond is 0.15 nm long, the hydrocarbon chain of DM is ca. 1.38 nm long, nearly twice the obtained layer thickness! Even imagining a very tilted hydrocarbon chain, there cannot be much polymer between the layers; it is likely that remaining surfactant or coupling agent prevents the total collapse of the structure and leads to these signals. Thus, such signals obtained from washed samples can clearly be attributed to a system without incorporated polymer. Fig. 3.34 **a** shows an example of such a pattern. The dotted line again represents the diffractogram measured before washing.

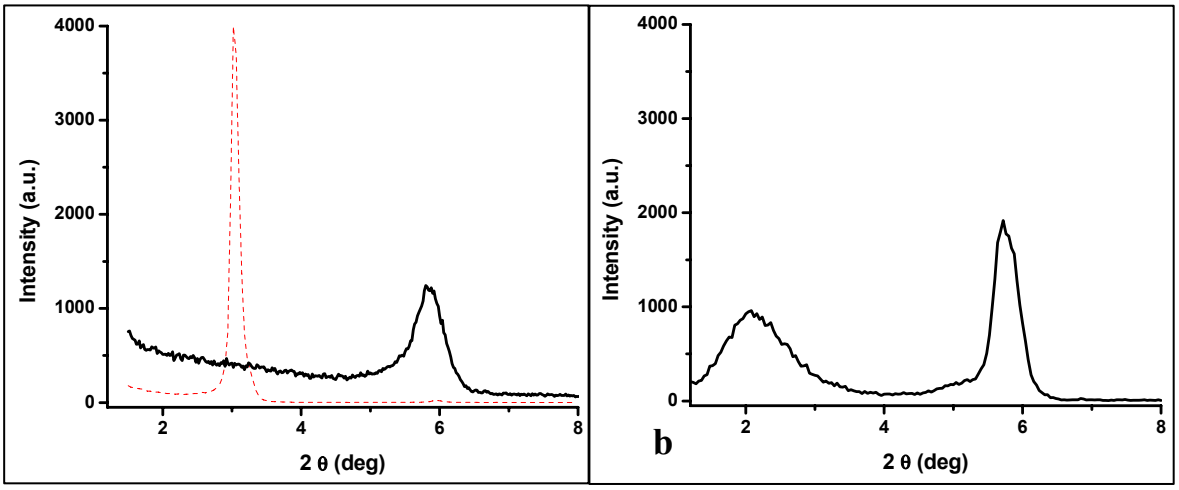

Fig. 3.34: Diffractograms of films after washing, **a**: "no polymer" signal, **b**: both types of signals.

Some SAXS patterns even showed both a broad reflection at a high *d*-spacing (2 θ about 2.1°), indicating a mesostructure with incorporated polymer, and the no-polymer signal discussed above (Fig. 3.34 **b**). It seems that in these samples, the polymer is washed out only

in certain domains (the upper layers?) of the sample, whereas it remains in other sections. This specific sample was prepared using 25% more of the thermal initiator ACHN, and after 3 days of solution aging (discussed in Chapter 3.4.2). The broad signal has a mean *d*-spacing of 4.25 nm, whereas the sharp reflection is at a 2 θ position equivalent to 1.54 nm.

Appearance of CTAB signals. Yet another type of SAXS pattern was observed for washed samples (Fig. 3.35): the diffractograms of some washed wafers featured very sharp reflections appearing at constant positions of 2 θ = 3.49° and 6.93°, equaling *d*-spacing values of 2.50 nm and 1.25 nm (solid line). A reference measurement was carried out to interpret these reflections: a solution of CTAB in ethanol was made and then dip-coating was performed; after drying, exactly these two signals were found (thin dotted line). Therefore, it is inferred that this reflects the structure of crystalline CTAB. One explanation is that, upon washing of a structured film, the surfactant is removed from the layers but becomes concentrated in the washing solution/in the area around the wafer; drying the wafer then causes it to crystallize on the film or wafer surface. As the 'normal' structure signals simultaneously decrease in intensity or even completely disappear, it also seems possible that during the washing process, the surfactant molecules are being concentrated in certain places within a layer and not completely washed out of the film. Then, the solvent evaporates, at a certain point inducing the crystallization of CTAB – smaller structures form, disrupting and destroying the nanocomposite. This would indicate that washing was carried out too swiftly – as longer washing, on the other hand, led to detachment of layers or the whole film. A compromise had to be found, trying to achieve a high extent of surfactant removal whilst preserving the layered structure.

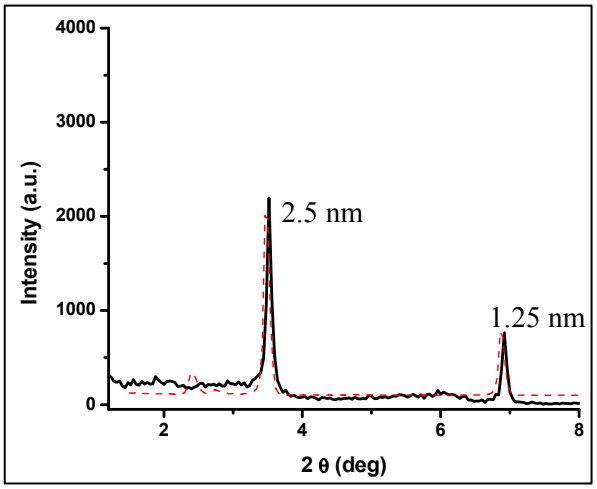

Fig. 3.35: SAXS Pattern of washed film showing "CTAB signals"; thin dotted line: diffractogram of crystalline CTAB.

3.4.1.3 Summary

The incorporation of a significant amount of polymer was desired, leading to a type of diffractogram as shown in Fig. 3.33 **b**. Unfortunately, no optimum precursor solution composition could be developed to achieve 100% reproducibility. Best results were obtained for the standard recipe (as is investigated in Chapter 3.4.2), but even for this composition, some samples lost their structure upon washing. The reason for this could be a too unstable connection between layers, as discussed above. Thus, it was tried to optimize the preparation process to achieve increased reproducibility. Thermally treated samples overall showed to be more stable towards washing. The tendency towards peeling off when being dipped into or rinsed with solvents was much lower for these films. If exposed to heat too shortly after dip-coating, however, the films became cracked, as the solvent remaining from the dip-coating process started to heat up rapidly and vaporize. Improved results were obtained for wafers left at room temperature for 1 hour before thermal treatment. For samples polymerized by exposure to UV irradiation, the subsequent ammonia treatment turned out to be a crucial process – if the exposure time was too short, the film became destroyed upon washing, but too intense treatment also led to a decrease in ordering of the sample. Thus, the presumed advantage of a slightly higher degree of polymerization of 7-OTS and NIPAAM through photoinitiation is compensated by the necessity of a subsequent ammonia treatment which was hard to control and monitor. Upon washing, in all UV-polymerized samples the polymer was at least partially washed out, resulting in a maximum *d*-spacing of 1.98 nm.

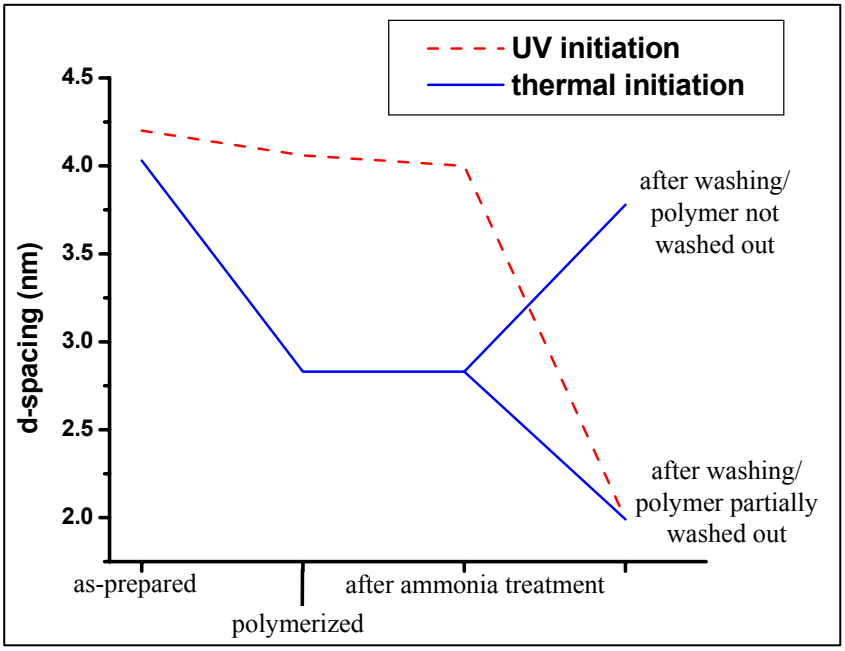

Fig. 3.36: *d*-spacing of samples at various processing steps.

The development of the average *d*-spacing of the wafers over time is illustrated in Fig. 3.36. This diagram summarizes the results discussed above, showing the significant decrease in *d*-spacing upon thermal treatment. The line is split in two after washing, indicating the range of *d*-spacing values obtained for washed samples.

3.4.2 Experiments to Improve the Sample Reproducibility

In order to get more consistent and reproducible results and also to incorporate a higher amount of polymer, the standard recipe was altered in various ways.

3.4.2.1 Optimizing the Composition of the Sample

An important parameter of the system is the nature of the used solvent. Especially the EISA process is greatly influenced by solvent properties (e.g. volatility and polarity). Experiments were performed with other organic solvents than ethanol to probe the influence of solvent parameters. The A2** preparation process was designed and optimized for ethanol as solvent, and was always performed in EtOH. Yet the A2** sol had to be diluted prior to the dip-coating process. In experiments to investigate the influence of other solvents, A2** sol was used unchanged, but then other organic solvents such as tetrahydrofurane (THF) or 1-butanol were added. Their polarity turned out to be relevant; while the addition of THF (which has a polarity and volatility similar to ethanol) led to samples showing good film quality and a well-

defined mesostructure, the more apolar 1-butanol did not produce reasonable results; it is also much less volatile, which could also impair a fast and efficient self-assembly. Fig. 3.37 shows SAXS patterns (in logarithmic scale) of a film prepared with THF as solvent, as-prepared (1), after UV polymerization (2), and after ammonia treatment (3). The results are comparable to samples prepared only with ethanol as solvent; the ordering even being higher (especially after ammonia treatment). Upon washing (4), the pattern shows a rather high reflection, but at very low *d*-spacing, so it seems that no polymer was incorporated into this sample (swelling experiments also were not successful). Other experiments were performed using 1-butanol as solvent (patterns not shown); in these samples the structure was lost after polymerization.

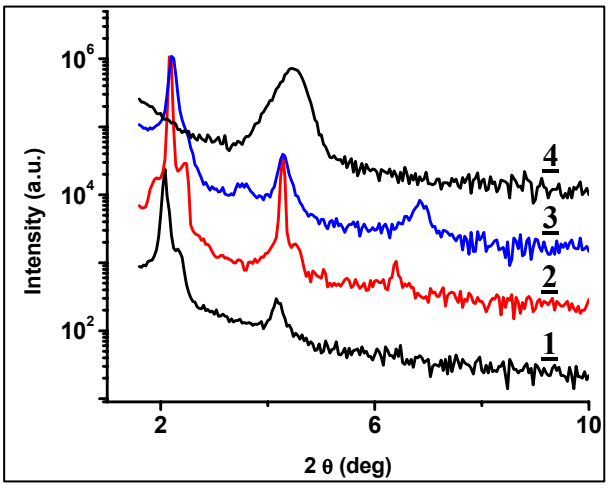

Fig. 3.37: SAXS data of a system with both DM and NIPAAM, using THF as solvent, **1**: as-prepared, **2**: after polymerization, **3**: after ammonia treatment, **4**: after washing.

Increase in Polymer Content. As the hydrogel within the organic layers is the functional component of the system, it seems desirable to produce films with a high polymer content, which would result in thicker organic layers and, therefore, higher *d*-spacing. The incorporation of a larger amount of polymer into the nanocomposite could theoretically be achieved by using higher concentrations of monomer and coupling agent (7-OTS); however, a massive decrease in film quality and also complete de-wetting of the films during dip-coating was observed when using higher concentrations than described in the Experimental Part (Ch. 5.2). None of these samples showed a generally higher *d*-spacing than the standard recipe films.

Investigating Coupling Agents. The detachment of layers, though, is probably the result of an inadequate interconnection. The reason for this could be the too low reactivity of the coupling agent double bond, providing an insufficient number of connection sites, as discussed above.

In fact, an important result of NMR and IR spectroscopy was the low reactivity of the coupling agent 7-OTS, confirming this theory. Other suitable coupling agents such as PATMS and MPS proved to polymerize faster, presumably providing better connection between the nanophases and a more durable connection of the polymer to the silica matrix. SAXS experiments were performed on thin films prepared with PATMS and MPS as coupling agents. In the course of sample preparation, however, problems emerged, possibly just because of the high reactivity of PATMS/MPS. Fig. 3.38 shows SAXS patterns obtained from a UV-polymerized film before (thin dotted plot) and after ammonia treatment (solid line). The precursor solution for this sample was prepared like a standard recipe solution but replacing 7-OTS with 0.42 mL of MPS.

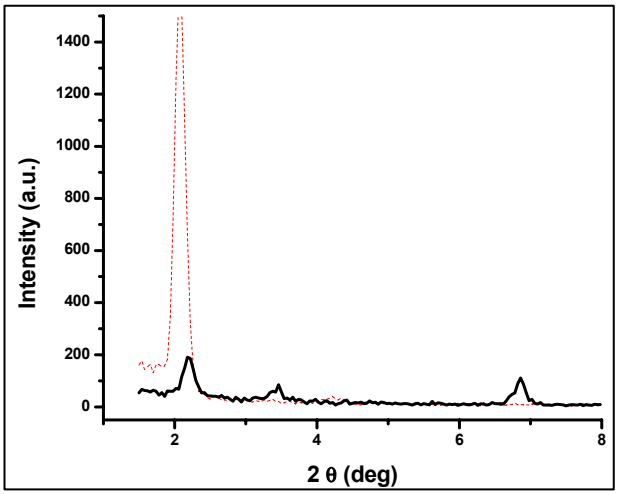

Fig. 3.38: Diffractogram of a sample containing the coupling agent MPS, before (thin line) and after ammonia treatment (thick line).

The SAXS data look 'normal' for the first preparation stages. Yet, after ammonia treatment, the main reflection has decreased dramatically in intensity, and sharp reflections appear at $2\theta = 3.5°$ and $2\theta = 7.0°$. They are at the same positions and have the same appearance as the 'CTAB signals' as described for washed samples in Chapter 3.4.1. So, their existence must be caused by the same process – the crystallization of CTAB, substantially disrupting the lamellar mesostructure. These signals always appeared after ammonia treatment for samples containing PATMS and MPS, but only after too harsh ammonia treatment for samples containing 7-OTS. Hence, PATMS and MPS are unsuitable as coupling agents for the system in question. Probably, their high reactivity causes them to polymerize very fast, providing a too rigid link between the layers. When NH_3 treatment is performed, the silica layer condenses and contracts, but the organic layer is inflexible, resulting in an increase in mechanical stress. At a certain point, the polymer cannot sustain this stress, and the whole layered structure becomes disrupted. The surfactant then re-arranges and crystallizes. Another

possible explanation is that PATMS and MPS already form oligomers before dip-coating, which would aggravate the self-assembly, leading to an unstable system.

Many approaches to synthesize NIPAAM hydrogels employ cross-linkers to obtain connectivity between polymer chains.[50] In our system, this is not absolutely necessary for stability as every polymer chain is linked to the silica matrix via the coupling agent. The use of a cross-linker, on the other hand, seems suitable to further improve the stability of the polymer itself. Two cross-linking agents were tested, *N*,*N'*-methylenebisacrylamide (BIS) and 1,6-hexanediol dimethacrylate (HDM), corresponding to the acrylamide and methacrylate monomers. Both BIS and HDM (used in various, yet very low concentrations) did not lead to improved results, to the contrary – the ordering of films containing significant amounts of cross-linker was relatively low even after polymerization, and the structure was completely lost upon washing. Samples containing very small amounts of BIS showed comparable results as standard-recipe films, but it is questionable whether the cross-linker exerts any influence. We can thus infer that the cross-linkers do not significantly improve the interconnectivity of polymer chains, which is comprehensible, as the calculations performed above (Chapter 3.4.1) indicated that the chain length of a DM molecule is over 1.40 nm– thus even a layer which is 3-4 nm in thickness can only consist of a few polymer chains. The environmental condition in one of these organic nanophases is therefore very different to a bulk system, so it is no surprise that a cross-linker which requires some steric freedom does not provide the desired interconnection.

Fig. 3.39 shows a sample containing 0.075 mL cross-linker (HDM) after UV polymerization (1) and after washing (2). The structure is totally destroyed upon washing.

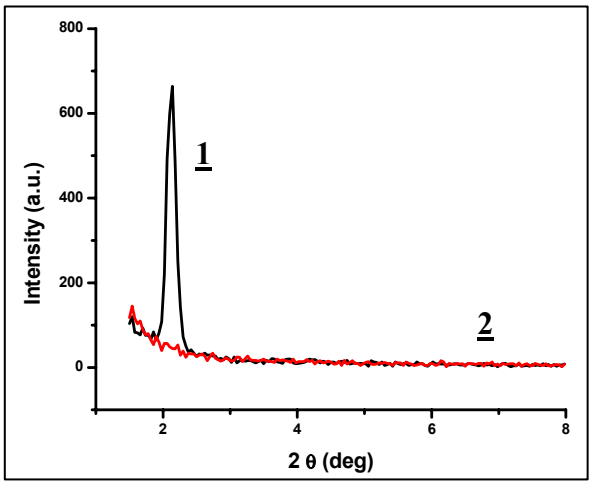

Fig. 3.39: Diffractogram of a sample with the cross-linker HDM.

3.4.2.2 Optimizing the Preparation Process

For greatly improved reproducibility, it turned out to be essential to filter the solution prior to dip-coating. This drastically reduced the tendency of films to de-wet from the surface or peel off upon washing. It has not been analyzed which species is removed by this procedure; it seems possible that oligomers are formed by reactive species in the precursor solution, either organic monomers or condensed siloxane species. In the case of organic substances, these oligomers are more hydrophobic than the monomers, which would be an explanation of a higher inclination towards de-wetting of the films. The oligomers, being adsorbed in the pores of the filter, are absent in the freshly filtered solution; upon instant dip-coating, this leads to improved film quality, substantially reducing the tendency towards de-wetting. Oligomers, however, would then also gradually be formed in the filtrate, again causing a decrease in film quality. Thus, aging experiments were performed, and surprising results were obtained: overall, aging of the solutions after filtration generally tended to improve the film quality and the order of the mesostructure. This, however, was only the case for a limited time; aging for more than two weeks seemed to give less satisfying results. Yet, this strongly suggests that oligomers or condensed siliceous species are not the main factor for the low quality of films prepared before filtration. It seems more plausible that initially there is a lot of dust and dirt (stemming from chemical impurities) in the precursor solution, which possibly aggravates the structure formation upon dip-coating (as large dust particles would disrupt the surfactant mesostructure). Once these impurities are removed, the films show a generally higher quality.

The phenomenon of aging could also not be completely explained. As stated above, aging for several hours up to a few days after filtration slightly increased and certainly not decreased the quality and ordering of prepared films. It is, however, very difficult to determine the real cause for the improved stability and ordering of a film which was prepared after aging the solution, as other factors, e.g. a different temperature during the dip-coating process or a slightly higher degree of polymerization of the coupling agent due to a slightly longer thermal treatment, might have played a role as well. Analogously prepared samples sometimes gave different results, independent of aging or not. Yet, the general results seem to suggest a small positive effect if solutions were aged for about 5-15 days.

The SAXS patterns of two films prepared after 1 day of aging (1) and after 14 days of aging (2) are presented in Fig. 3.40. The films were both measured after heat treatment. Due to the generally only medium reproducibility after washing, it seems less informative to compare SAXS data measured after washing. Comparing the two diffractograms, it seems that there is less polymer incorporated in the sample prepared after 2 weeks aging. The ordering, on the other hand, seems slightly higher than for the film prepared after only 1 day of aging.

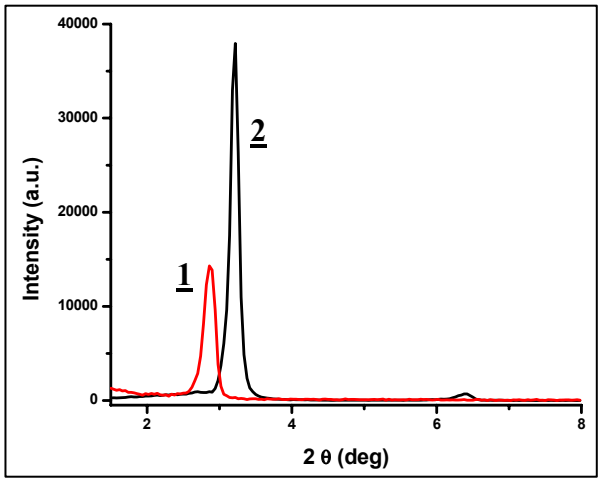

Fig. 3.40: SAXS patterns of films after heat treatment, after aging for **1**: 1 day, **2**: 14 days.

3.4.3 Swelling Experiments

Samples with a significant amount of incorporated polymer, visible as a rather broad signal at a *d*-spacing of over 2.8 nm in the SAXS pattern after washing, were subject to swelling experiments. Bulk poly(NIPAAM) hydrogels exhibit swelling when exposed to water at temperatures below the LCST of about 32°C; this process however takes up to 80 hours for nonporous gels.[50,60] As the hydrogel in the system discussed here is a co-polymer of DM and NIPAAM, the LCST is not precisely known and may even vary, depending on the methacrylate content of the polymer. In order to ensure that the environment was well below the actual critical temperature, the standard swelling procedure was carried out at 5°C. This temperature also was unproblematic to maintain, as the samples were simply placed into a refrigerator. To accelerate the process of water incorporation, the wafers were put in a Petri dish filled with de-ionized water pre-cooled to 5°C. De-swelling experiments were also carried out by immersion of the wafers in water. The reason for this is obvious: as the de-swelling had to be carried out above the LCST, at elevated temperatures, de-swelling of

the sample could have occurred simply because of water evaporation. This was most efficiently avoided by putting the films in water. The standard temperature used was 50°C. Other experiments were carried out at room temperature or at 30°C/40°C to investigate the swelling behavior of the system at temperatures closer to the LCST.

3.4.3.1 Experiments at 5°C/50°C

Significant and consistent swelling and de-swelling were observed only with samples prepared by thermal polymerization. The SAXS patterns in Fig. 3.41 were measured from a standard-recipe film polymerized by thermal treatment and then washed. This film was subject to several cycles of swelling and de-swelling.

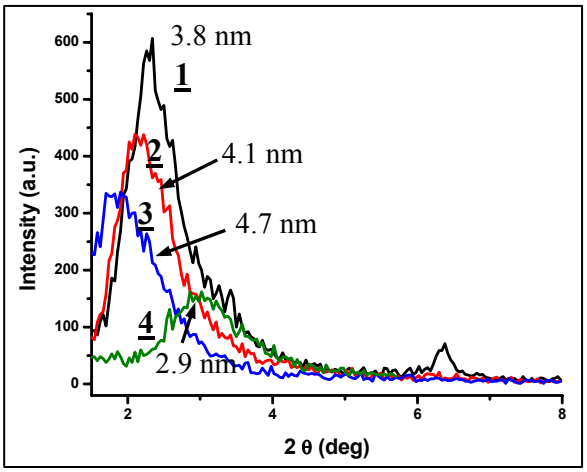

Fig. 3.41: SAXS plots of the 1st swelling cycle of a thermally polymerized film.
1: after washing; **2**: after 36h in 5°C water; **3**: after 4h in 50°C water; **4**: after 6h in 50°C water

The SAXS profiles of the film after washing and for the first cycle of swelling and de-swelling are presented, showing that the first cycle required rather long times of exposure to cold respectively warm water: after washing (1, *d*-spacing of ca. 3.8 nm), the film was left in water at 5°C for 36 hours before observing significant swelling in the obtained pattern, to ca. 4.1 nm (2). Next, the sample was immersed in water at 50°C, but after 4 hours, the signal was at an even higher *d*-spacing of 4.7 nm (3). Further 2 hours of exposure to warm water, though, produced a SAXS pattern showing substantial de-swelling to 2.9 nm (4). There seems to be a trend towards decreasing intensity, which is, however, only coincidental and was not found for other samples. This proves that in principle, the swelling and de-swelling response of the nanocomposite is similar to bulk poly(NIPAAM) hydrogels, and is significant, but for the first cycle of exposure, the response time is relatively high.

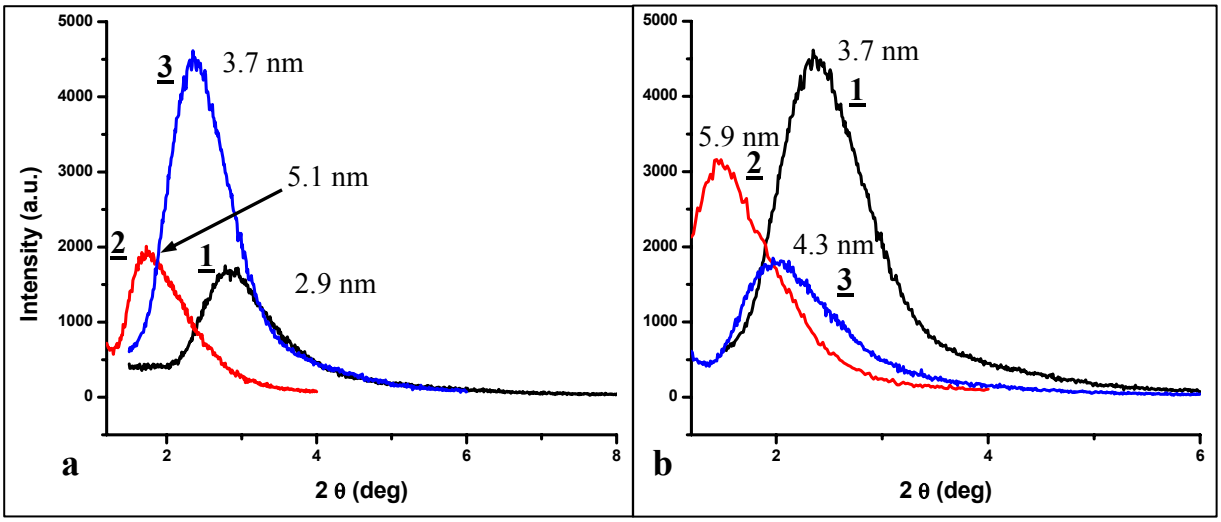

Fig. 3.42: SAXS patterns of the **a**: second, **b**: third swelling cycle of a standard-recipe film; **1**: initial state, **2**: after immersion in 5°C water, **3**: after immersion in 50°C water.

Further swelling cycles by exposure to water at 5°C and 50°C are illustrated in Fig. 3.42. In **a**, the second cycle is shown (using the same sample as measured for Fig. 3.41). A longer scan after the first cycle was performed in order to get better and more precise data (1). After only 12 hours in cold water, the reflection had shifted from 2.9 nm to 5.1 nm (2), suggesting a dramatically increased rate of response. Immersion in warm water was carried out for 5 hours, leading to diffractogram (3) at an equivalent to $d = 3.7$ nm. Further exposure to warm water would probably have resulted in a shift to even lower *d*-spacing; however, a next cycle was started by placing the sample in cold water again (Fig. 3.42 **b** 2; 1 is the same as **a** 3 for better illustration of the swelling process). The sample swelled from 3.7 to 5.9 nm. This signal is situated at such a low angle of incidence (corresponding to its high *d*-spacing value) that its left shoulder could not be measured as it disappeared behind the very strong reflection of the primary beam; this problem is extensively discussed below. Immersion in water at 50°C for 6 hours caused de-swelling to 4.3 nm (pattern 3). These results clearly show that the swelling rate increases from cycle to cycle, whereas the rate of de-swelling remains practically constant. An explanation for this phenomenon is that water might be 'stored' in the silica layers upon release from the hydrogel, thus facilitating and accelerating the swelling process in the next cycle. De-swelling would take much more time, as water has to be released from the whole system although the silica matrix is (allegedly) saturated with water. The swelling, however, is completely reversible, and the preservation of the shape of the signal proves that only the *d*-spacing changes but the lamellar structure of the sample remains stable.

Development of d-spacing over multiple cycles. Several more cycles were performed with this sample, and the trends discussed above proved to persist. Other influences were observed as well: when leaving a sample under ambient conditions overnight or over a weekend, the film started to swell (if in the de-swollen state), which had to be compensated by allowing for longer de-swelling time in warm water. In general, it turned out to be difficult to reach a specific degree of swelling (a specific *d*-spacing), due to the effects stated above. The signal of structures with a too high *d*-spacing disappeared under the primary beam reflection signal; their actual *d*-spacing could only be estimated. Fig. 3.43 illustrates the change in *d*-spacing over several cycles of swelling and de-swelling.

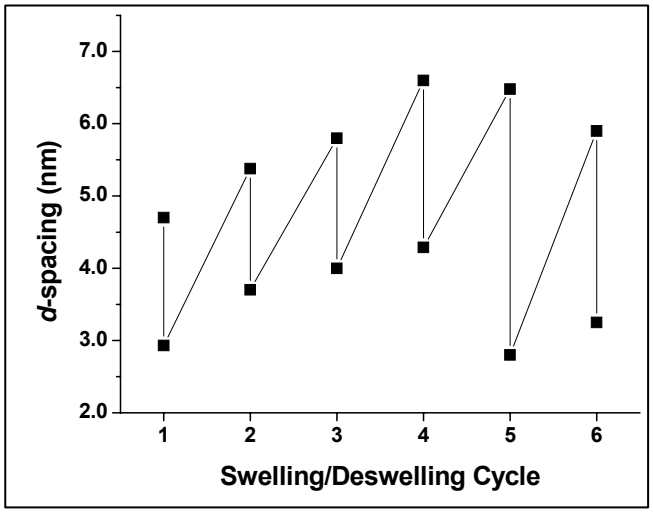

Fig. 3.43: *d*-spacing of a sample over swelling cycles.

Over the first four cycles, the phenomenon of increasing speed of swelling but steady rate of de-swelling is manifested in generally increasing values of *d*-spacing (as the exposure times were more or less kept constant, see above). For the fifth cycle, however, the time allowed for swelling was cut substantially (from 4 hours to 1 hour) but then the sample was immersed in water at 50°C for a slightly longer time (7 hours). The sample de-swelled drastically from 6.48 nm to 2.80 nm. The sixth cycle, however, was performed by immersion in water at room temperature (25°C) instead of cold water for swelling, whilst de-swelling was achieved as usual.

3.4.3.2 Experiments at Room Temperature

As swelling at room temperature seemed to happen even faster than in cold water, detailed studies were carried out to investigate the rate of swelling under these conditions. Using the same sample as above, the film was immersed in 25°C water for 10 minutes, then measured, again immersed in water for 10 minutes and measured and so forth. The resulting patterns are displayed in Fig. 3.44.

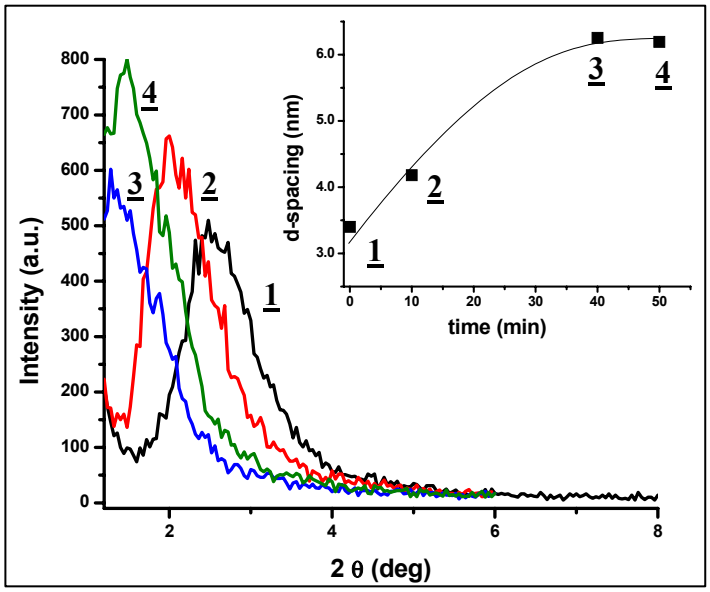

Fig. 3.44: Swelling performed by immersion in 25°C water, starting from the de-swollen state (6 h in 50°C water).

The initial pattern (1) was measured after de-swelling the sample in 50°C water for 6 hours; the *d*-spacing is 3.5 nm. After 10 minutes (2), a significant shift to 4.3 nm is observed. The diffractograms taken after 20 and 30 minutes (not shown) exhibit no substantial changes in *d*-spacing, but after 40 minutes, a strong increase to 6.5 nm is visible (3). The sample seems to remain at this state, as after 50 minutes, no further swelling is observed but even a slight decrease to 6.2 nm (4). On the other hand, the sample had to be removed from the sample holder for immersion in water; therefore, it is possible that a different spot was measured, being in a different state of swelling or even containing a different amount of the hydrogel, therefore exhibiting a slightly different *d*-spacing. The observed trend, as shown in the inset in Fig. 3.44, is clear and significant, constituting unambiguous evidence for a fast response of samples after a few cycles. Also, these experiments prove that the LCST of the co-polymer incorporated in the nanostructure must be above 25°C, as substantial swelling was observed.

As mentioned above, samples left at ambient conditions overnight showed a change when measured again. Also, the last experiment proved a very fast swelling when immersed in water at room temperature. Therefore, it seemed interesting to also explore the swelling behavior of a sample when being left in air at room temperature. During the experiments, humidity amounted to ca. 40%. The sample was first de-swollen as usual at 50°C for 4 hours. After measuring the SAXS pattern, the sample was repeatedly taken out of the sample compartment of the XRD device, left outside for 10 minutes and then measured again. Fig. 3.45 shows the obtained results.

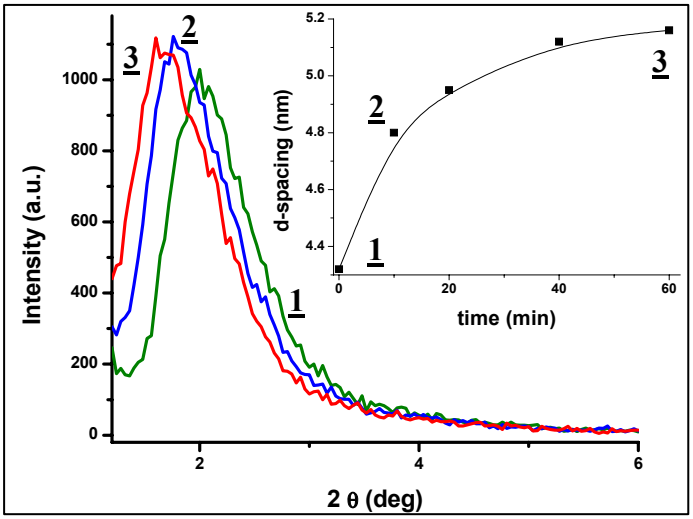

Fig. 3.45: Swelling Experiments performed in dry conditions at 25°C.

The patterns exhibit a steady increase in *d*-spacing, from initially 4.3 nm (1) over 4.8 nm after 10 minutes (2) to 5.1 nm after 60 minutes (3). Measurements carried out in between are not shown due to the closeness of signals. The *d*-spacing value over time is plotted in the inset of Fig. 3.45 to illustrate the swelling properties under these conditions. The swelling is fastest immediately at the beginning of exposure, then slowing down in a manner similar to a saturation effect.

3.4.3.3 Experiments to Narrow the Range of the LCST

The LCST of the co-polymer incorporated in the nanocomposite could not be precisely determined. The experiments described above show that the critical temperature must be above 25°C and below 50°C. This is a broad range; thus, experiments were performed to further narrow this range. The sample, after de-swelling at 50°C as usual, was measured and then placed in water at 30°C for 2 hours. After a SAXS scan, 2 more hours of exposure followed. The data are shown in Fig. 3.46 **a**; they were taken from a thermally polymerized,

washed sample after several cycles of swelling and de-swelling. This sample contained a very small amount of cross-linker (2.7 mg, equaling 1.4%wt of NIPAAM). The *d*-spacing, initially amounting to 4.04 nm (1), steadily increased to 4.85 nm after 2 h (2) and 5.86 nm after 4 h (3). This clearly shows that the LCST must be situated above 30°C. On the other hand, experiments were also carried out at 40°C, again immersing the wafer in water at this temperature (Fig. 3.46 **b**). Within 2 hours, the *d*-spacing decreased from 5.15 nm (1) to 3.34 nm (2), providing clear evidence that the LCST is below 40°C. Because of the rapid swelling even in air below the LCST, as was shown above, and also due to problems with providing a stable environment at a precise temperature close to the LCST, it was not possible to perform experiments to further restrict the possible range of the critical temperature.

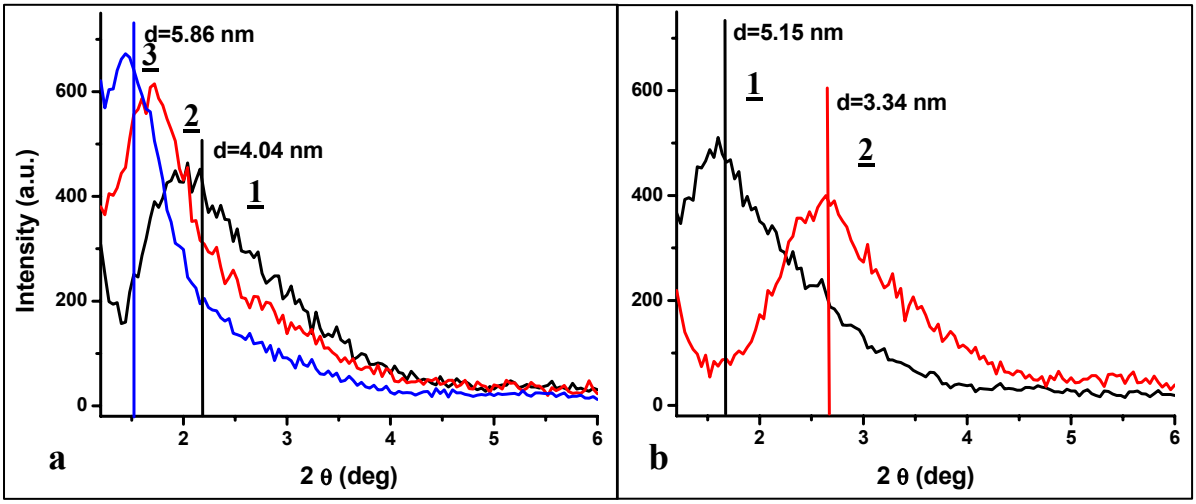

Fig. 3.46: Swelling Experiments performed in water at **a**: 30°C, **b**: 40°C.

3.4.3.4 Responsiveness of Films Prepared without NIPAAM

In order to prove the influence of NIPAAM on the functionality of the films, it was also necessary to probe the swelling behavior of samples prepared without poly(NIPAAM). Poly(dodecyl methacrylate) can also act as a hydrogel but does respond to changes in the external pH value rather than temperature. Fig. 3.47 shows the results of swelling experiments performed with a thermally polymerized film not containing any NIPAAM. After washing, the film shows a *d*-spacing of 3.11 nm (1). After 4 hours in water at room temperature, the reflection has shifted to 3.36 nm (2). Then the sample was immersed in water at 50°C and left for 4 hours, causing de-swelling to 3.10 nm (3).

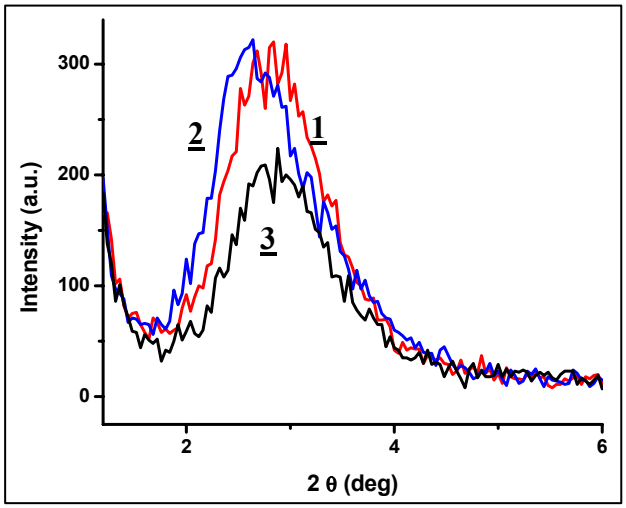

Fig. 3.47: Swelling Experiments with a no-NIPAAM film.

This system seems to be switchable as well, it is however clearly visible that only small changes occur upon swelling and de-swelling. Longer exposures to water were carried out for this sample as well without achieving a higher degree of swelling. The poly(dodecyl methacrylate) layers probably swell significantly upon washing, later only showing minor swelling and de-swelling upon variation of the temperature. These results prove that the use of NIPAAM is necessary to obtain a substantially thermo-responsive system.

3.4.3.5 Problems Found for the Analysis of Swelling Experiments

In several experiments discussed above, it has been found that samples showing a very high *d*-spacing could not be characterized by SAXS on a standard XRD device because of a strong primary beam reflection. It has been shown that the rate of swelling increased for each cycle; therefore, the time allowed for the swelling process had to be cut for each cycle in order to be able to characterize the sample. For a sample not showing any reflection within the normal 2θ range, one could think that the structure was lost, however the signal 'reappeared' upon de-swelling, confirming the theory that the structure still existed and just was superimposed by the much larger primary beam reflection – one of these samples is shown in Fig. 3.48 **a**. The patterns were measured using a standard recipe sample polymerized by heat treatment, after washing and several cycles of swelling and de-swelling. After one de-swelling process, the signal was situated at 4.2 nm (1). The wafer was then exposed to water at 5°C for only 4 hours before measuring plot (2). Although a higher intensity at low angles (2 θ > 2°) suggests the presence of a structure signal in addition to the primary beam reflection, no clear maximum is visible. Due to the steep incline, the measurement could not be extended beyond

this point (too high intensity). Next, the sample was de-swelled at 50°C for 1 hour before pattern (3) was taken. The initial signal has reappeared at slightly lower intensity but at nearly the same position.

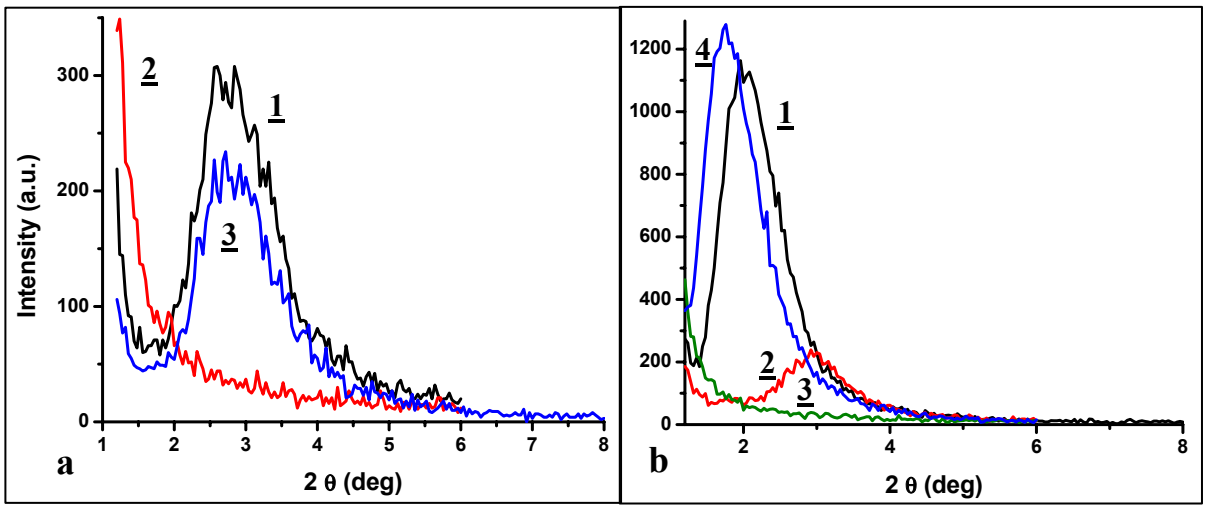

Fig. 3.48: Problems found for the analysis of swelling experiments.
a: primary beam reflection, **b**: loss in intensity upon de-swelling.

Another difficulty appeared after a few cycles of swelling and de-swelling: the intensity of reflections at high *d*-spacing values always was higher than the intensity of low *d*-spacing signals. At some point, the signals of de-swollen samples completely disappeared. Such a case is shown in Fig. 3.48 **b**. Initially (1), the sample showed very high ordering, corresponding to a strong reflection at 4.31 nm. After 4 hours in water at 50°C, the sample had de-swollen to 2.99 nm, but also the intensity of the signal had decreased to only one fifth (2). Two more hours of de-swelling treatment produced pattern (3), where no signal at all is visible (apart from the primary beam reflection). The sample was then placed in cold water (5°C) for only 30 minutes and again analyzed, resulting in plot (4). The initial reflection has reappeared, even at a slightly higher intensity and a *d*-spacing of 5.02 nm. The sample had been subject to several cycles before this experiment; therefore the very high rate of swelling is (to some extent) comprehensible. The drastic decrease in intensity upon de-swelling, though, can only be explained by decreasing contrast between the polymer and silica layers within the sample. In general, the scattering intensity I (2 θ) of a mesostructure composed of two phases 1 and 2, can directly be related to the average electron densities δ_1 and δ_2 of the two phases: $I(2\theta) \propto (\delta_1 - \delta_2)^2$. Therefore, assuming a change in the average electron density of the polymer layer upon variation of the water content, the measurable XRD intensity of the lamellar mesostructure could eventually drop to an undetectable limit because of a too similar

electron density of the two phases at some stage of swelling or de-swelling. From the experiment, it is clear that the structure is present at all times.

3.4.4 Alternative Preparation Methods

All samples discussed above had been prepared by dip-coating. Furthermore, alternative preparation methods were tested as well, employing casting of films as well as spin-coating techniques.

3.4.4.1 Spin-Coating

Spin-coating usually results in a more homogeneous film thickness and film distribution on the substrate. Especially in our case, this could be expected to lead to greatly improved reproducibility. Experiments were carried out using square-cut wafers; the pre-treatment was performed as usual. Spin-coating was performed at 1000 and 2000 rpm. Then the samples were thermally polymerized. The SAXS patterns of samples after polymerization are presented in Fig. 3.49 **a**. For comparison, the diffractogram of a dip-coating film (1) is shown as well as the plot corresponding to films prepared by spin-coating at 1000 rpm (2) and 2000 rpm (3). The dip-coated film, surprisingly, shows by far higher intensity, which could be caused by a higher film thickness, whereas the spin-coating samples have slightly higher *d*-spacing (3.2 nm and 3.0 nm). The intensity of the second-order reflection, on the other hand, is higher for the spin-coated samples. The results suggest that spin-coating at lower rotation speed leads to higher ordering. “CTAB reflections” are visible as well; they appear to be especially pronounced for the sample prepared at 1000 rpm but are still much smaller than the signal due to the nanocomposite lamellar structure.

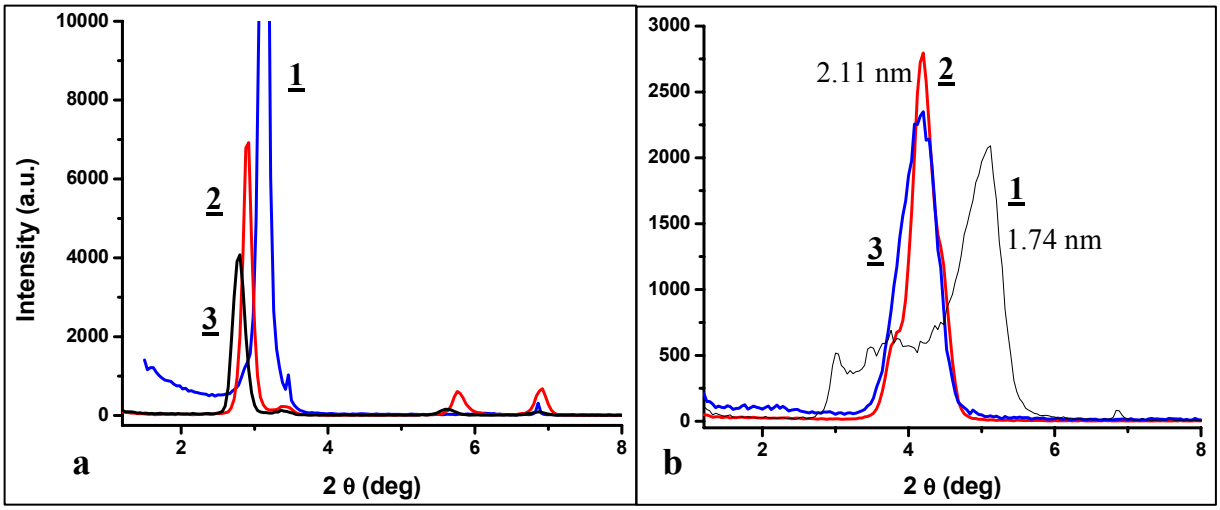

Fig. 3.49: SAXS patterns of spin-coated films, **a**: after thermal treatment, **b**: swelling experiments.

The SAXS pattern after washing is shown in 3.49 **b** (1); this sample was prepared at 2000 rpm. There is a high, rather sharp reflection (similar to the diffractograms for dip-coated washed samples presented in Chapter 3.4.1), and smaller, broader signals at lower 2θ values. The main signal corresponds to a *d*-spacing of 1.74 nm. As discussed in Chapter 3.4.1, a simple calculation shows that there can not be much polymer incorporated in the system. Nevertheless, swelling experiments were performed. After one week in water at 5°C, there is only one sharp signal left, at a position of $d = 2.11$ nm (2). Then, the sample was immersed in water at 50°C for 7 hours before measuring pattern (3) showing a *d*-spacing of 2.14 nm. These results clearly prove that no hydrogel is present in the system; the sample only undergoes a slight increase in *d*-spacing as some water is incorporated into the silica layers, but of course this process is not reversed at elevated temperatures. These results were very consistent for all spin-coated samples; it can hence be inferred that spin-coating is not suitable for the preparation of lamellar films with incorporated hydrogels. It seems possible that the spinning process causes the polymer to be centrifuged towards the edge of the wafer, thus not leading to a stable linkage between the layers and, consequently, to the complete removal of polymer upon washing.

3.4.4.2 Casting of Films

For the application of functional nanocomposite films onto larger and eventually also non-plane substrates, or for micro-molding, it is obvious that a dip-coating process would be very difficult to control. Thus, simple casting of films seems much more suitable for large-scale application. Apart from Petri dish experiments necessary to prepare samples for NMR, TGA and IR measurements (see below), films were also cast on silicon wafers to explore the influence of the different preparation technique on the film quality and functionality. The main difference to the Petri dish films was that the samples cast on Si wafers were applied with a syringe and left to evaporate in a horizontal position, whereas the Petri dish was always arranged vertically before the sample was left to dry. Precursor solutions were prepared as usual, but then applied to the pre-treated silicon wafers in quantities of only ca. 20 µL. The samples were left at ambient conditions for 1 hour and then thermally polymerized. Because of the higher thickness of the samples, the optical appearance at all stages of processing was not the typical interference pattern of thin films but a matte, gray color. Looking at the SAXS data of a sample (Fig. 3.50 **a**, intensity in logarithmic scale), as-prepared (1) and after heat treatment (2), we see high ordering also after polymerization, and a decrease in *d*-spacing from 3.87 nm to 3.12 nm. The pattern of a polymerized dip-coated sample (3) is shown for comparison. The cast sample has higher *d*-spacing but less ordering. The third signal visible in (2) and (3) stems from crystalline CTAB. The highly ordered lamellar structured of cast samples is also proved by TEM measurements (cf. Chapter 3.9) and 2-D SAXS experiments (Ch. 3.4.5).

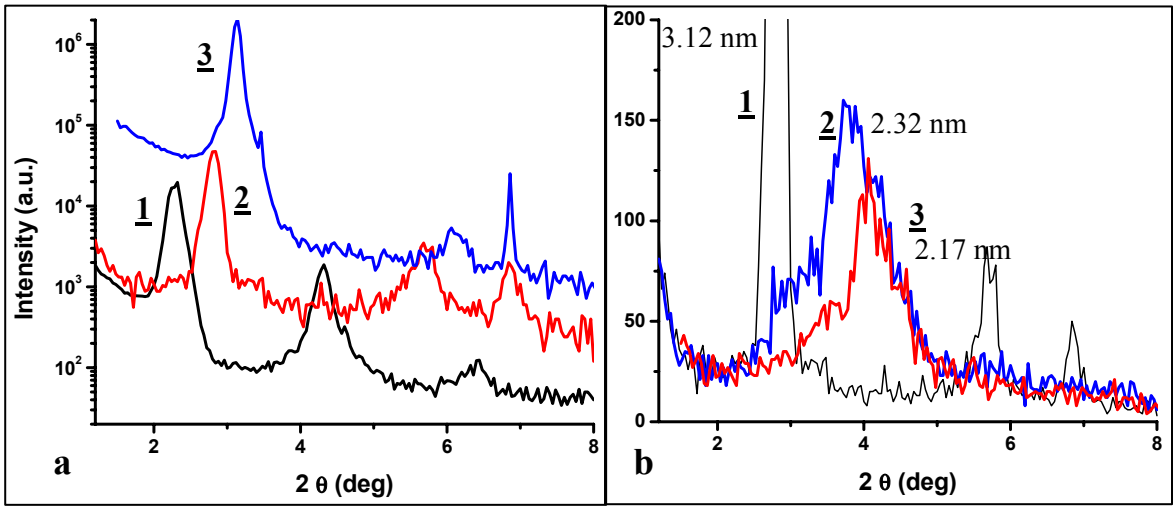

Fig. 3.50: Patterns of cast films, **a**: as-prepared and after polymerization, **b**: swelling experiments.

Swelling experiments were performed with cast films as well. Fig. 3.50 **b** shows the pattern of a film after washing (1), at $d = 3.12$ nm. This sample was immersed in cold water (5°C) for 15 hours and then measured again (2). There is no swelling visible, but even a small shift towards lower *d*-spacing (2.32 nm). Next, de-swelling was performed (3) at 50°C for 4 hours, and now a slight shift towards smaller *d*-spacing is observed (to $d = 2.17$ nm). Subsequent immersion in cold water for 7 hours led to an interesting phenomenon: the signal is split in two, one signal remaining at the 'de-swollen' position whereas the other appears at 2.31 nm.

This clearly shows that the high thickness of cast films leads to inhomogeneous accessibility of the hydrogel layers to water. It can diffuse to the layers close to the film surface, resulting in swelling, but the deeper layers are shielded and therefore do not swell. As the casting technique leads to very inhomogeneous films, it was not possible to determine the film thickness by ellipsometry, but certainly cast films are much thicker than dip-coated samples, probably several µm compared to a few hundred nm. Hence, it is comprehensible that dip-coated films would show much faster and more uniform swelling than cast samples. It is unclear, though, why we see two rather sharp signals instead of one broad distribution in *d*-spacing which would represent a gradual decrease in accessibility of water to the layers. The SAXS results were consistent for all cast samples, which comes unexpected, as the casting process constitutes a much less controllable technique compared to dip-coating or spin-coating. The structure of the samples, however, always exhibited low ordering. On the other hand, the application process is of course much less complicated than for dip-coating or spin-coating (although the possibility of controlling the film thickness is practically not existent). The prospect of a very simple application technique suitable also for larger and non-even substrates probably outweighs the disadvantage of slower and less uniform response of the resulting nanocomposite film.

3.4.4.3 'Petri Dish' Method

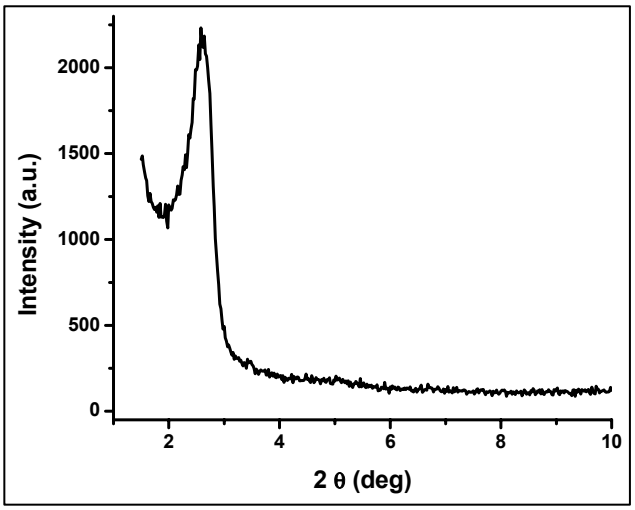

Fig. 3.51: Powder SAXS pattern of a 'Petri dish' Sample.

In order to obtain sufficient amounts of sample for NMR and IR analyses, the 'Petri dish method' had to be used, applying some solution into a Petri dish which then was dried by vertical draining. Yet, it needs to be shown that this method leads to structured films, as the film thickness and hence the evaporation process is different to standard Si wafer substrates. Therefore, a standard film was prepared by the 'Petri dish method', but due to the experimental setup it was not possible to measure the film being on the Petri dish. The substance (measured after heat treatment) had to be scratched off the dish and measured as a powder sample. A small amount of silica gel was applied to a SAXS sample holder and then some of the powder pressed onto the gel. Next, the sample was measured as usual. The pattern (Fig. 3.51) shows a rather sharp reflection at 3.40 nm. Its intensity is hardly comparable to thin film samples, but this is not surprising as the SAXS setup was intended and optimized for measurement in symmetric reflection mode and not for powder samples. Thus, for the purpose of NMR, TGA and IR measurements, it is satisfying to know that lamellar structure is present, and also that the *d*-spacing value is comparable to thin film samples.

3.4.5 2-Dimensional Small-Angle X-ray Scattering

The measurement of films in symmetric reflection can theoretically lead to the same pattern for a lamellar and a 2-D hexagonal structure, if the structure elements are oriented parallel to the substrate surface. If only the (00*n*) reflections are visible in these SAXS patterns, it is not possible to unambiguously identify the structure as lamellar or hexagonal. Therefore, 2-dimensional small-angle X-ray scattering (2-D SAXS) was employed to clarify the structural character of the samples. The experiments were carried out on a 2D-SAXS device at the University of New Mexico, Albuquerque, as well as on a Synchrotron 2D-SAXS at Aragonne National Laboratories, beamline 1 BM C, using a wavelength of 1.27 Å. The samples were measured under He to minimize scattering by air. The scattering patterns were recorded using a CCD camera.

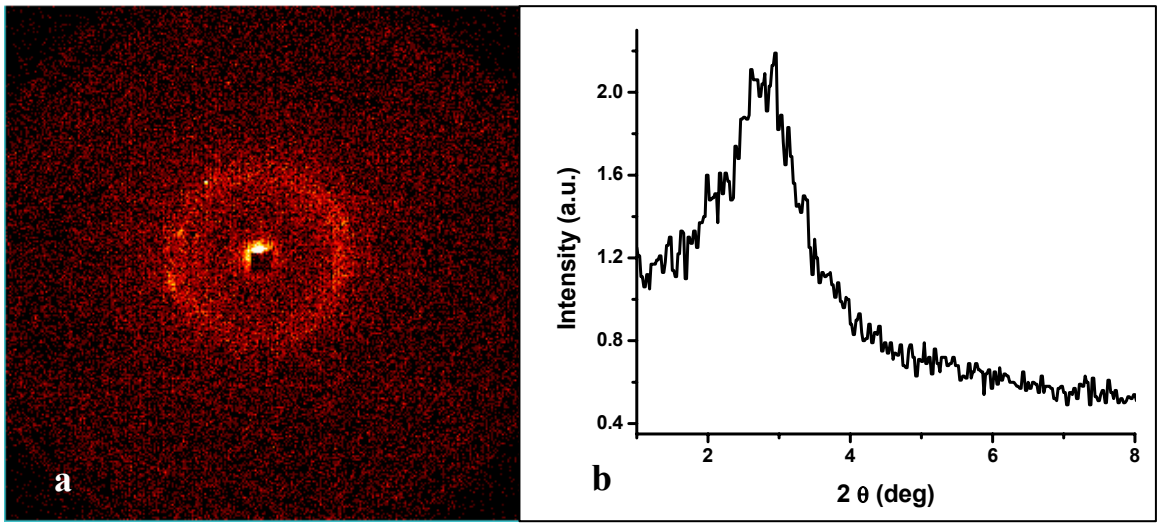

Fig. 3.52: Powder SAXS of a standard sample after washing, **a**: 2-D pattern, **b**: linear plot.

Fig. 3.52 shows the pattern of a dip-coated sample containing the standard components after polymerization, before washing. It was measured on the standard 2D-SAXS device at the University of New Mexico. The sample was scratched off a wafer and measured as powder, therefore showing less ordering than film samples. The 2-D scattering pattern is displayed in **a**, whereas the corresponding linear plot (calculated from the 2-D picture) is shown in **b**. In the 2-D picture, the bright spot at the center is the (partially shielded) primary beam, whereas the (001) reflection is now visible as a ring around the primary beam – this is due to the powder measurement, as now the lamellae are arranged randomly, causing reflection of the beam in all directions. The ring is clearly visible, being evidence for the good ordering of the sample. A hexagonal structure would lead to a rather pronounced (011) signal – its absence shows that the structure possesses lamellar and not hexagonal ordering.

Further 2-D SAXS experiments were performed at the beamline in Argonne, now measuring film samples, as shown in Fig. 3.53 **a** . The (001) reflection is now visible as a bright spot, proving high ordering of the sample. Again, the absence of any (011) signal (there would be two bright spots visible to both sides of the (001) reflection) clearly proves that the structure is not hexagonal. Fig. 3.53 **b** shows a 3-D plot of the pattern; the intensity of the reflections corresponds to the vertical height of the signals.

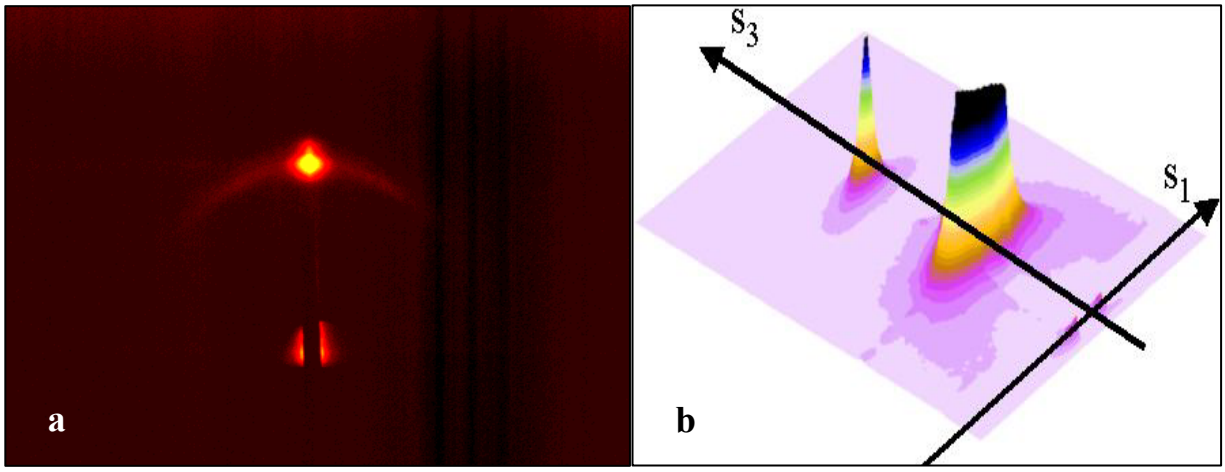

Fig. 3.53: SAXS of a standard film after washing, **a**: 2-D pattern, **b**: 3-D plot of the signal intensity.

3.4.6 Calculations

The only quantitative information obtained from all patterns shown above is the position of the reflections, corresponding to the *d*-spacing of the structure. In the case of lamellar ordering, the *d*-spacing equals the cumulated thickness of an organic and one neighboring inorganic layer (denoted "*d*" in Scheme 3.1). It was not possible to determine the thickness of only one of those layers. There are, however, elaborate theoretical models for the calculation of diffractograms of oriented two-phase lamellar systems.[61] There are two methods that seem appropriate to describe the synthesized systems, the 'staple model' and the 'lattice model'; of course several simplifications and assumptions need to be stipulated, e.g. a perfectly parallel orientation of the layers to the film surface. Both approaches are characterized by a limited number of physically meaningful parameters describing a lamellar system. In these models it is assumed that the stack height is sufficiently large to be neglected, that it is approximated to be infinite. This assumption is supported by the TEM results (see Chapter 3.9).

Staple Model. This model emanates from the assumption that the thickness of each layer is independent of the thickness of the previous one. The only parameters are the mean thickness $\bar{d}_j$ of each of the two types of layers (cf. Scheme 3.1), and their variance σ_j. The postulation for the intensity (in dependence of the length **s** of the scattering vector) is:

$$I_1(s) = \frac{1}{2\pi^2 s^2} \cdot \mathrm{Re}\left[\frac{(1-H_1)\cdot(1-H_2)}{(1-H_1H_2)}\right] \tag{3.2}$$

with $$H_j = \exp\left(2\pi i \bar{d}_j s - 2\pi^2 \sigma_j^2 s^2\right) \tag{3.3}$$

and $$s = \frac{2\cdot\sin\theta}{\lambda} \quad \text{(in our case: } \lambda = 1.5418 \text{ Å)}. \tag{3.4}$$

Lattice Model. In this model, only the thickness of one of the layers is a fitting parameter, $\bar{d}_1$ (and σ_1), and of course it again cannot be determined which type of layer corresponds to $\bar{d}_1$. The other parameters are the distance *L* of the centers of two equal layers (equivalent to the *d*-spacing) and its variance σ_L. The model says,

$$I_1(s) = \frac{1}{2\pi^2 s^2} \cdot \left\{1 - \mathrm{Re}\, H_1(s) + 4\cdot\left[\mathrm{Im}\, H_1(s/2)\right]^2 \cdot \mathrm{Re}\left[\frac{H_L(s)}{1-H_L(s)}\right]\right\} \tag{3.5}$$

with (3.3), (3.4) and $H_L = \exp\left(2\pi i \bar{L} s - 2\pi^2 \sigma_L^2 s^2\right)$. (3.6)

The models were applied in the following way: first, a diffractogram obtained from a long scan (for high signal-to-noise ratio) was chosen, and then tried to be fitted by a calculated pattern of either the layer model or the lattice model, electronically optimizing the parameters.

The results are surprising: very good fits were achieved, which comes unexpected, as the structure was assumed to be disrupted (due to e.g. the exothermic polymerization reaction, and the assumed inhomogeneous polymer distribution), strongly differing from the ideal layer system stipulated in the theoretical models. The SAXS patterns could even be evaluated at all states of processing. Fig. 3.54 **a** shows the SAXS patterns of a standard sample as-prepared (1) and after heat treatment (2), dotted curves, as well as their theoretical approximations

(using the staple model), visible as thin lines (in logarithmic scale). The calculated parameters are stated in **b**.

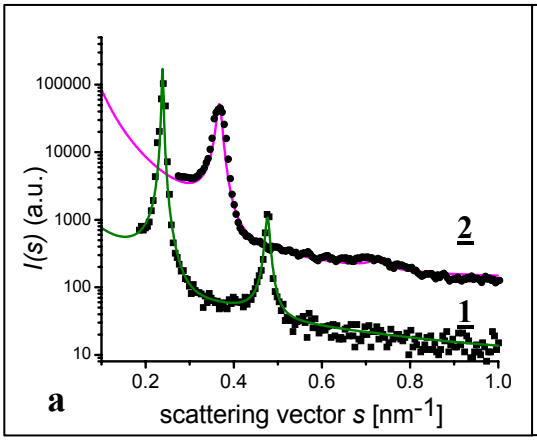

Pattern	Param.	(nm)	
as-prep	$\overline{d}_1$	1.25	± 0.5
	$\overline{d}_2$	2.94	± 0.4
polymerized	$\overline{d}_1$	0.70	± 0.3
	$\overline{d}_2$	2.00	± 0.5

b

Fig. 3.54: Theoretical fits for SAXS patterns of as-prepared (**1**) and polymerized (**2**) samples.

Based on the results of TGA measurements (cf. Chapter 3.5), which show a very high amount (over 50%wt.) of organic species present, the parameter $\overline{d}_1$ is related to the mean thickness of the inorganic silica layers, whereas $\overline{d}_2$ corresponds to the thickness of the organic layers. Upon thermal treatment, we see a decrease in thickness of both the organic and inorganic layers, which is attributed to shrinkage of the siliceous phase (by siloxane condensation and solvent evaporation) and of the organic moiety (mostly contraction by polymerization, but also partial evaporation of monomers).

Fig. 3.55 **a** shows the diffractogram of a washed sample in a de-swollen state (1) fitted with a curve calculated using the layer model (thin line), and the data for a sample in the swollen state (2), after 6 hours in 5°C water, and its approximation. Apart from the primary beam reflection, which of course cannot be expected in theory, as it is not attributable to the sample structure, the fit shows almost perfect approximation over the whole range of measured scattering angles. The measurement was, unfortunately, not extended up to higher angles; hence we cannot tell whether calculated second-order signals are also reflected in the measured patterns. The calculated parameters (3.55 **b**) seem reasonable and possible.

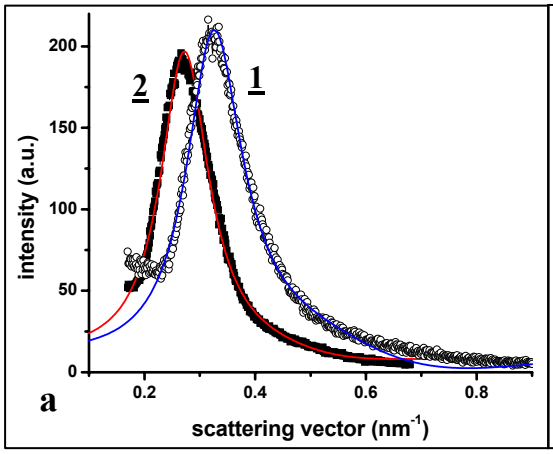

Pattern	Param.	(nm)	
de-swollen	$\overline{d}_1$	1.3	± 0.3
sample (**1**)	$\overline{d}_2$	1.6	± 0.8
swollen	$\overline{d}_1$	1.4	± 0.3
sample (**2**)	$\overline{d}_2$	3.7	± 0.9

b

Fig. 3.55: Theoretical fits for diffractograms of samples subject to swelling experiments.

Comparing the obtained parameters for both patterns, we clearly see that one type of layer has nearly remained constant in thickness, whereas the second type increased from 1.6 nm to 3.7 nm. This strongly suggests that the first type is equivalent to the silica matrix, which of course is expected to hardly swell or de-swell, and the second type corresponds to the hydrogel. Therefore, the calculated results clearly support and confirm the theory of a highly ordered lamellar system, consisting of alternating layers of silica and polymer.

3.5 TGA Measurements

Thermo-gravimetric analysis (TGA) is performed by heating a sample at a constant rate whilst precisely measuring its weight. A decrease in weight is observed upon evaporation (of solvent or monomers) or thermal decomposition, especially of organic substances. The temperature of such a transition can be used to identify the reactive species, whilst the amount of weight loss tells its content in the sample.

Silica, in its fully condensed state, is thermally stable up to high temperatures (over 1500°C). Hence, TGA appears to be an ideal method to determine the polymer content of samples at all stages of processing. The minimum amount of material necessary for a measurement was about 10 mg; thus, the samples were prepared mainly by the 'Petri dish method' for preliminary experiments to investigate the decomposition behavior of components. Some measurements were performed with samples prepared on a Si wafer, employing a special preparation method (see Ch. 5.6.6). All experiments were carried out in an argon atmosphere, unless stated otherwise.

3.5.1 Thermal Analysis of Pure Components

The thermal decomposition behavior, especially of compounds with high molecular weight, such as co-polymers, is very complex. Therefore, first the pure chemicals and samples only containing a small number of components were measured.

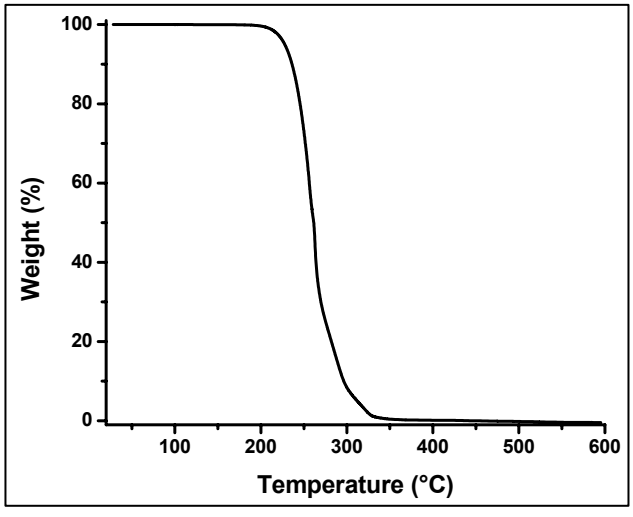

Fig. 3.56: TGA plot of pure CTAB.

Figure 3.56 shows the TGA plot of pure cetyltrimethylammonium bromide (CTAB), the relative weight over temperature. A very sharp step is visible, resembling the thermal decomposition of the surfactant. The process begins at 210°C and ends at ca. 325°C, with only 2% of initial weight left. We can thus infer that CTAB decomposes rapidly at comparably low temperatures.

The thermogram of only the inorganic species is presented in Fig. 3.57. Pure A2** solution (water and dilute HCl were added to achieve a comparable rate of condensation as in standard-recipe samples) was applied to a Petri dish and then left to dry at ambient conditions (leading to partial evaporation of EtOH and water). After 12 hours, the film was scratched off the dish and measured. The plot shows a steady decrease in weight up to ca. 125°C; this is clearly attributable to solvent residues because of insufficient drying of the sample; the weight loss amounts to 10%. Only a minor decrease in weight is observed at higher temperatures, this is due to gradual condensation of the silica matrix and inherent ethanol formation and evaporation. The additional weight loss caused by these processes, however, is small; the further decrease is only 6% of the initial sample weight up to 600°C.

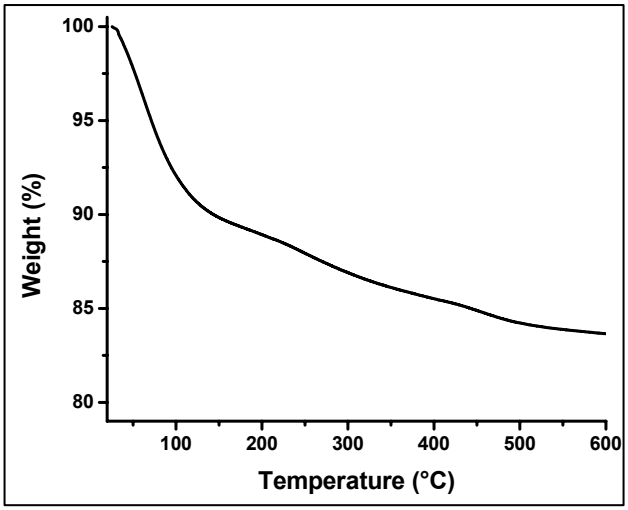

Fig. 3.57: TGA graph of condensed A2**.

The evaporation of organic monomers, especially NIPAAM, constituted one of the problems identified for the polymerization process. To further elucidate this phenomenon, TGA analysis of pure NIPAAM (as-received) was performed. Fig. 3.58 **a** presents a plot of the weight loss over temperature. Two very pronounced steps are visible. The dramatic loss (about 85%) below 200°C is of course due to evaporation of the monomer; however, approx. 12% of sample is left and remains stable up to 360°C - this is attributed to polymerized NIPAAM. This seems surprising, as the sample did not contain ACHN or BME – obviously,

thermal treatment effectively induces NIPAAM polymerization even without the use of any initiator. The material decomposes at 360-410°C. **b** shows the derivative weight over temperature, featuring strong signals at points of maximum weight loss rate. The monomer evaporation corresponds to the signal at 170°C, whereas the smaller signal centered at 398°C stems from polymer decomposition.

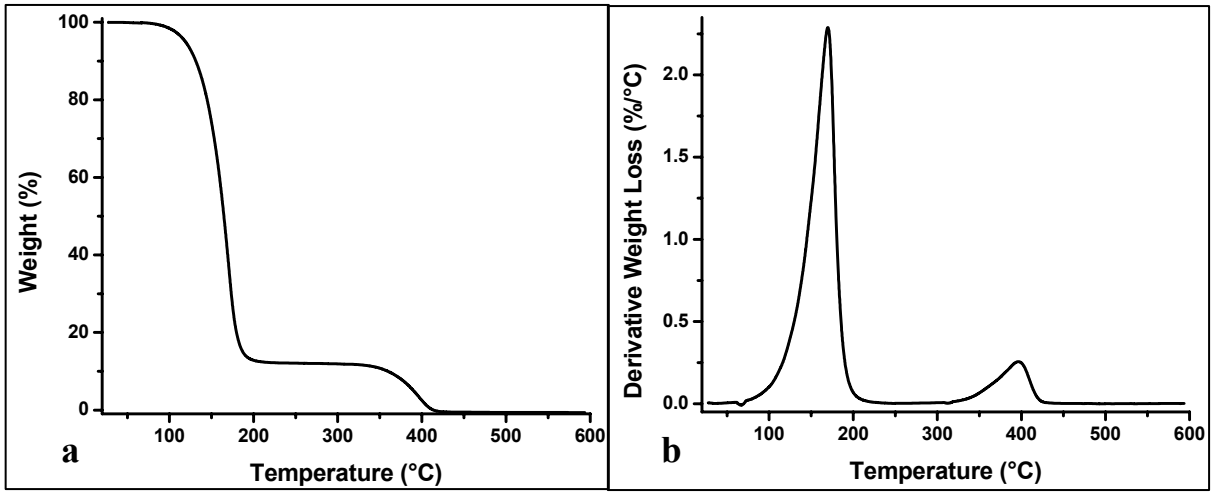

Fig. 3.58: TGA plots of pure NIPAAM, **a**: weight loss over temperature, **b**: derivative.

Similar experiments were carried out with DM and 7-OTS; these TGA plots only show the total evaporation of monomers at low temperatures and no polymer degradation.

The thermal decomposition behavior of bulk co-polymers of NIPAAM and methacrylic acid has already been studied.[62] Comparing co-polymers with increasing NIPAAM content, a general decline in decomposition temperature is found. Also, a second decomposition step is found for systems with a high content in poly(methacrylic acid). Because of the structural similarity of DM to methacrylic acid, an analog thermal behavior can be expected.

It was difficult to explore the thermo-gravimetric behavior of the pure polymer as present in the nanocomposite films, as a substantial amount of surfactant had to be used to obtain the ordered nanocomposite, which decreased the polymer content. Therefore, also non-structured systems were measured to facilitate the assignment of decomposition processes to single components.

3.5.2 Decomposition Behavior of Non-Structured Systems

As the dried silica precursor solution does not undergo a massive weight loss upon heating, it seems promising to study systems containing the inorganic components and solvents but only one of the monomers – thus, a simple thermogram is obtained which allows unambiguous identification of the signals.

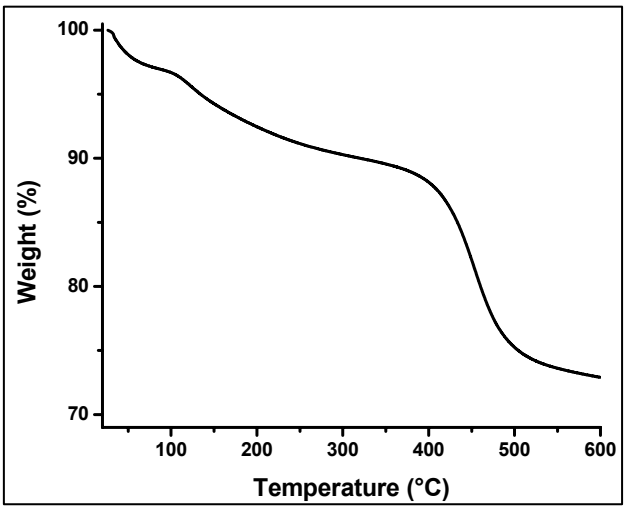

Fig. 3.59: TGA trace of a 7-OTS/silica system.

7-OTS was added to A2** stock solution and pre-hydrolyzed (by addition of water and HCl). The solution was applied onto a Petri dish and measured after drying at room temperature (Fig. 3.59). As the coupling agent is now linked to the silica matrix, the substance cannot evaporate. Its degradation (of course only the organic groups decompose) is visible as a significant step at 450°C – this seems very high, and it is possible that the 7-OTS monomers (in the absence of any structure-directing agent) are distributed within the silica matrix and are thus shielded, enhancing the thermostability of the organic moieties.

The decomposition properties of a silica/DM system were investigated analogously (Fig. 3.60 **a** and **b**). The sample was dried at 80°C for 1 hour before the measurement. Four maxima are found in the derivative plot. The signal at 130°C is caused by evaporating monomers; as the sample was not subject to a thorough heat treatment, it is surprising that only 7.2% of the sample evaporated at this point (compared to a total amount of at least 30% DM in the sample). This is clear evidence for the high reactivity of DM. The main decomposition was found at 248°C and 465°C and is attributed to poly(dodecyl methacrylate). In the literature, the decomposition of poly(methacrylic acid) is reported to occur in two steps, at 240°C and 473°C.[63,64] This is in very good conformity to the results

obtained in this experiment. The smaller signal found at 358°C is probably caused by the decomposition of the long alkyl chain of DM.

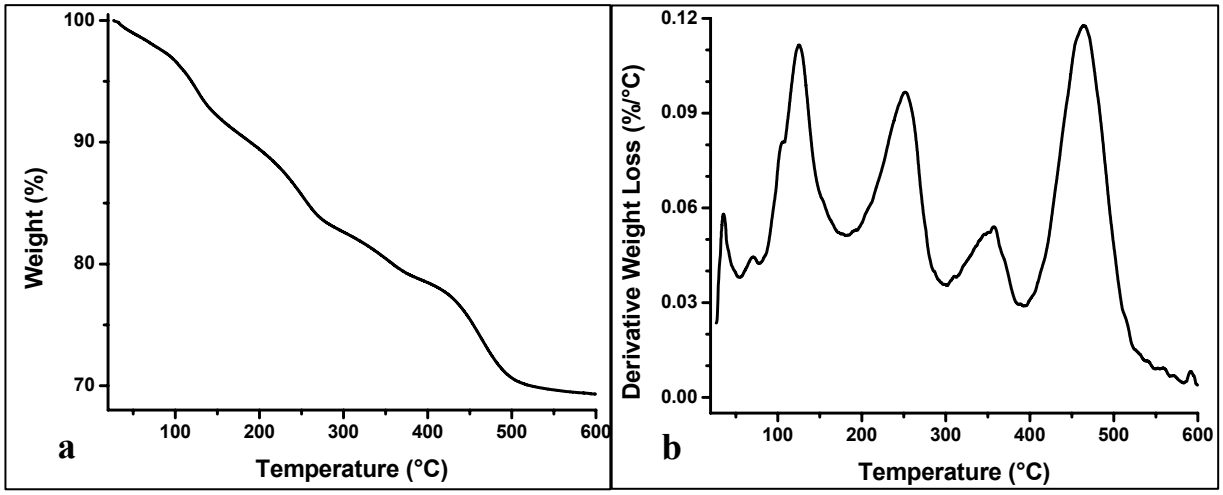

Fig. 3.60: TGA traces of a dodecyl methacrylate/A2** system.

3.5.3 Decomposition Behavior of Structured Films

In non-structured films, the polymer is expected to be homogeneously distributed within the silica matrix. In contrast to this, samples prepared with the surfactant are expected to contain the polymer arranged in nanolayers, being separated from the silica phase and therefore easily accessible (especially as the surfactant burns out at low temperature). Therefore, it seems reasonable to assume that the decomposition of the polymer happens at lower temperatures than in non-structured films.

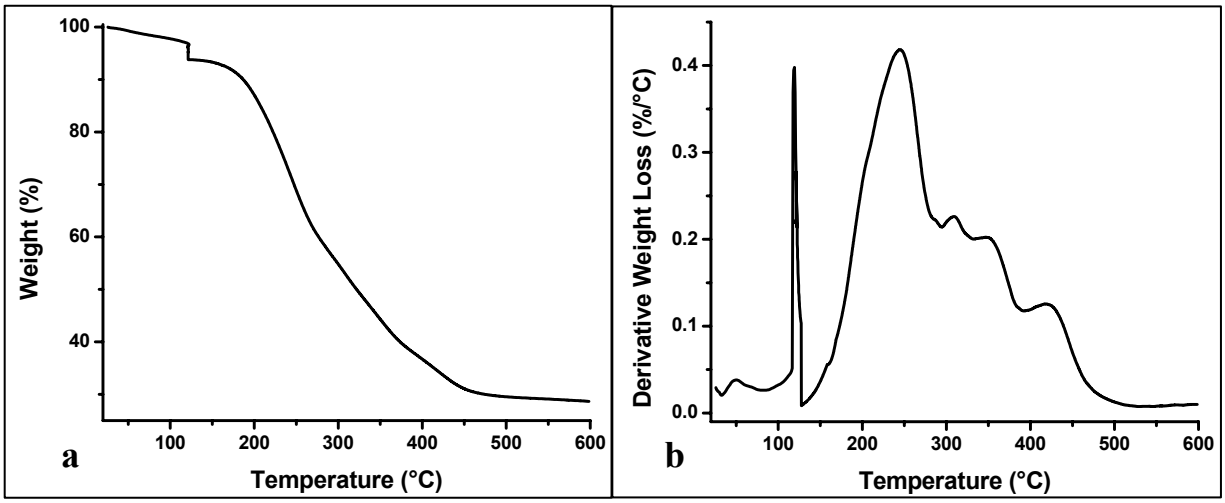

Fig. 3.61: TGA traces of a CTAB/DM/silica system, **a**: weight loss over temperature, **b**: derivative.

Fig. 3.61 shows the TGA plot obtained from a structured sample containing CTAB, DM and A2** solution. In contrast to the sample shown in Fig. 3.60, this sample was only dried at room temperature before the measurement but then held at 120°C for 3 hours (to simulate polymerization) before heating up further. Therefore, a vertical step is visible in the thermogram, and the signal at 120°C is very pronounced in the derivative. The weight loss at this point amounts to 6%. A strong decrease in weight, by 36%, occurs at 244°C, resembling mainly the decomposition of CTAB. The total amount of surfactant in the system, however, was calculated to ca. 30 wt.%, thus, a partial decomposition process of poly(dodecyl methacrylate) must also contribute to this signal. Further signals are visible at 310°C and 355°C; these are likely to be caused by the dodecyl groups (cf. the discussion of Fig. 3.60). The last decomposition step of the polymer occurs at 424°C (decline by 8%) – this constitutes a significant shift compared to 465°C for the non-structured sample. This can be interpreted as a clear sign that the polymer is in a different chemical environment, and cannot be situated within the silica matrix but must be situated in a separate 'organic' layer.

The TGA pattern of a system additionally containing NIPAAM is plotted in Fig. 3.62. It is interesting to see that the total weight decrease up to 600°C is practically equal to the sample discussed above, indicating the same amount of polymer present – whereas the added NIPAAM should of course lead to a higher polymer content. As both samples were measured as-prepared, though, it is easily possible that this sample contained less solvent, producing less weight loss in the TGA plot and thus indicating a lower polymer content than actually present in the film. Also, the amount of NIPAAM added is comparatively low. The derivative (**b**) shows a maximum at 225°C and a shoulder at the CTAB degradation point at 244°C. Further signals are visible at 295°C, 335°C and 410°C. In the literature, the degradation steps are reported to be at 234°C, 377°C and 410°C for NIPAAM/methacrylic acid co-polymers containing 30% (mol) NIPAAM.[62] Especially for the highest signal, the obtained results are in good accordance with the literature results, which confirm the observed trend of a shift towards lower temperature. Pure poly(NIPAAM), on the other hand, decomposes at ca. 400°C, hence superposition of two separate poly(dodecyl methacrylate) and poly(NIPAAM) signals could also cause the weight loss maximum to lie between the decomposition temperatures of the two pure polymers. Therefore, it cannot be unambiguously verified whether a *block*-co-polymer or a genuine randomly distributed co-polymer is formed within the organic layers of the nanocomposite.

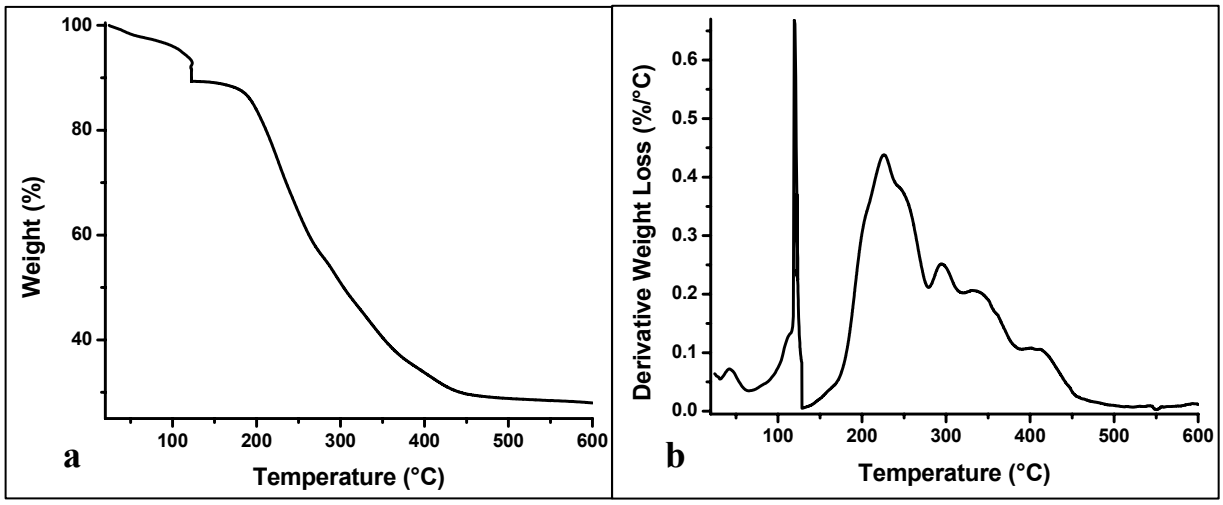

Fig. 3.62: TGA plot of a standard film without 7-OTS, **a**: weight loss over temperature, **b**: deriv.

The standard system, including the coupling agent, was also thermo-gravimetrically analyzed in the as-prepared state, see Figure 3.63. The derivative plot (**b**) is very similar to the system without 7-OTS discussed above, the only difference being a higher decrease around 295°C and a slightly shifted, more pronounced signal at 418°C. In the original plot (**a**), we see a slightly higher residual weight at 600°C, which is reasonable because of the presence of additional silica stemming from the coupling agent – in total, the silica content amounts to 29% of the sample. The first visible degradation step can clearly be attributed to CTAB; also the decrease by 28% is consistent with the calculated theoretical surfactant content of 26 ± 2%. (The degradation of CTAB seems to occur at slightly lower temperatures as in the 'bulk system', analogously to the polymer – this has also been confirmed by measurements of a pure silica/CTAB system.) Therefore, the polymer present in the system (including the octyl chain of 7-OTS) is proved to amount to at least 35% (theoretical value: 38%).

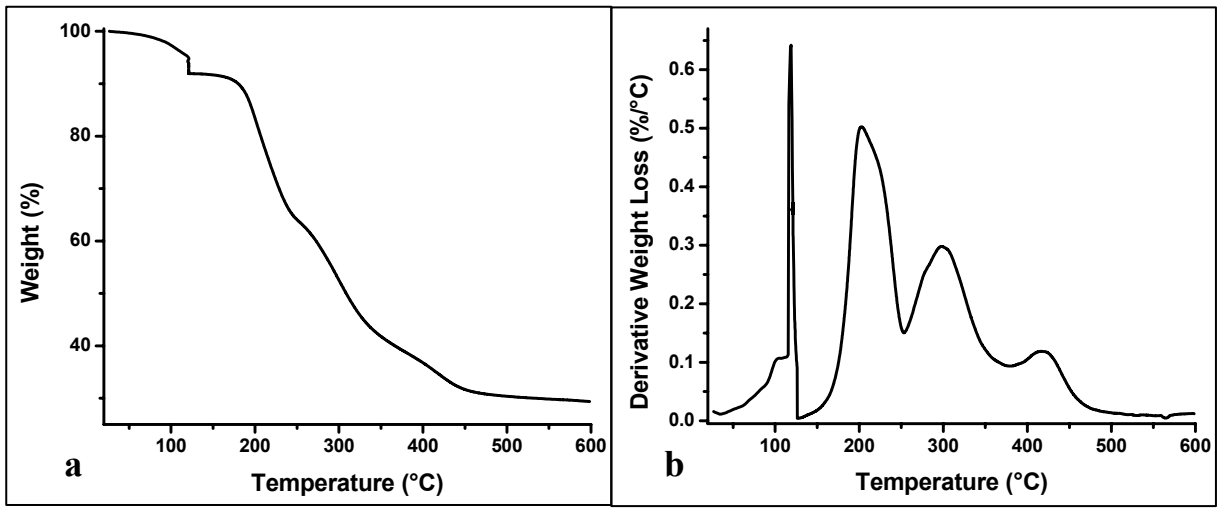

Fig. 3.63: TGA traces of a standard recipe system, **a**: weight loss over temperature, **b**: derivative.

3.5.4 Analysis of Washed Samples

In other sections of this work (cf. Chapters 3.3, 3.4) it is discussed that especially the washing process after polymerization is a crucial step for the preparation of polymer nanocomposite films. Therefore, one of the most important factors for obtaining a functional nanocomposite is the actual amount of polymer remaining in the system after washing. Because of the substantially higher film thickness, however, the washing treatment for 'Petri dish' samples had to be carried out in a different manner as for films on silicon wafers. This could also lead to a different amount of polymer incorporated in the final system. To ascertain the authenticity of results, films were prepared on Si wafers by dip-coating, similar to samples produced for SAXS experiments, but in a special way to obtain enough material for reliable TGA measurements (see Chapter 5.6.6). Subsequent thermal treatment and washing was performed analogously as for the SAXS samples.

The TGA trace of a standard recipe film prepared according to this method is presented in Figure 3.64. The film was dried at 80°C for 1 hour after washing to remove the solvents. For comparison, it was measured under O_2 (1) and under argon (2).

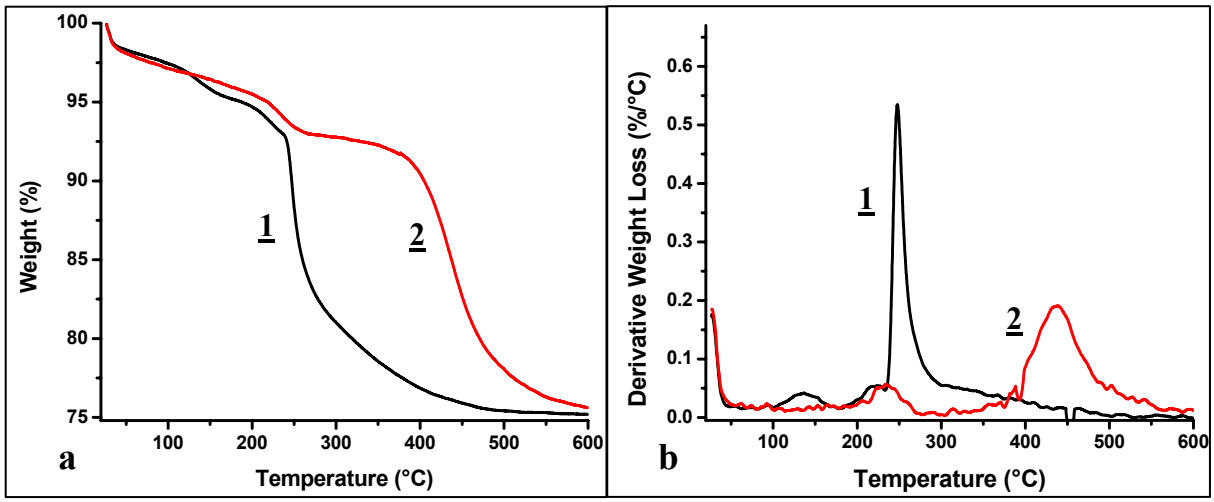

Fig. 3.64: TGA traces of a washed thin film, measured in O_2 (**1**) and Ar (**2**), **a**: weight loss over temperature, **b**: derivative.

After washing, all of the surfactant should of course be removed, but it cannot be a priori excluded that some CTAB remains in the system. In Chapter 3.5.3 (sample 3.63), it has been shown that CTAB, being in the nanocomposite, decomposes below 260°C. As the sample was thermally treated at 120°C for 3 hours, it can be assumed that the weight loss due to further silica condensation is practically equal to zero. Therefore, all decrease occurring above 260°C is attributable to polymer present in the system. This amounts to 17% polymer for the sample

measured in Ar, and ca. 19% polymer for the O_2 sample (the decomposition behavior of CTAB in oxygen, however, was not explored, thus a more precise number could not be calculated). On the other hand, the first decomposition step of poly(dodecyl methacrylate) in the nanocomposite occurs below 260°C – hence, the actual amount of polymer in the system must be higher. The DM/A2** system (Ch. 3.5.2) exhibited a weight loss of at least 5% in the first decomposition step, and of 13% in the subsequent steps at higher temperatures (in other words, 29% weight loss of pure poly(DM) in the first decomposition step), whereas poly(NIPAAM) and condensed 7-OTS practically do not decompose below 350°C. As the exact composition of the organic layers is not known, the total amount of polymer can only be roughly estimated: initially, the DM : 7-OTS : NIPAAM weight ratio is 1.00 : 0.47 : 0.23. The evaporation rate of NIPAAM monomers certainly is higher than of DM monomers (which was found to be relatively low); thus, the ratio of DM must be equal or higher in the washed system than initially. The siloxane group of 7-OTS hydrolyzes, creating volatile alcohols (which evaporate during heat treatment) and stable silica – only the hydrocarbon octyl chain decomposes, which changes the weight ratio to 1.00 DM : 0.23 7-OTS octyl chain : 0.23 NIPAAM, equaling a DM content of 68% in the polymer. Assuming that the ratio of weight loss for the multiple decomposition steps of poly(DM) remains stable even if a co-polymer is formed, the total amount of polymer is calculated to 22%. This shows that indeed practically no CTAB remains within the thin films after washing.

3.6 DSC Measurements

Differential scanning calorimetry (DSC) is used to measure the heat flowing to or from a sample whilst heating up or cooling down. This is useful to be able to detect exothermic or endothermic processes within the sample and determine their extent and the temperature at which they occur. DSC measurements are often performed on polymers, especially to determine the glass transition temperature.

For a complex system, as the hybrid nanocomposite discussed in this work, DSC can be useful to explore thermal transition processes of components; however, this only works if the investigated process gives a pronounced signal and the amount of the corresponding species within the sample is high enough. The poly(NIPAAM) hydrophilic/hydrophobic phase transition is an endothermic process which only gives a small – but distinctive – signal at the lower critical solution temperature (LCST). The measurements discussed in this chapter were aimed to detect a signal of the poly(NIPAAM) phase transition – on the one hand, to prove the occurrence of a hydrogel phase transition in the lamellar nanocomposite, and, on the other hand, to determine the temperature of the LCST. It was not intended to quantitatively investigate the heat flow of the hydrogel transition, as the instrument's precision was too low to obtain reliable data.

The DSC device used for the measurements was mainly intended for the analysis of metals, metal oxides and glasses at high temperatures; therefore, it did not include a cooling device to regulate and maintain temperatures below ambient conditions. The critical temperature (LCST) of poly(NIPAAM), however, is situated at ca. 32°C, which is too close to room temperature to be able to start a reliable measurement without prior cooling, as the device needs some time for stabilization before useful data are obtained. Therefore, it was inevitable to cool the sample compartment before the experiment was started. The only available cooling device was a can for liquid nitrogen (see *Experimental Section*, Chapter 5.6.7, for the detailed proceeding). It must be stated, though, that the measurement conditions were far from ideal and the system was rather unstable even during the measurements up to a temperature of 40°C. The output data were plotted in normalized units (W/g) to be able to compare the traces of various samples. The curves are shown in 'Exo Down' mode, meaning that the heat flow to the sample is measured – in other words, endothermic processes produce a positive signal and exothermic processes a negative signal.

3.6.1 Measurements of Bulk Polymers

Preliminary tests with bulk polymers showing well-defined polymer phase transitions were performed on the device to test its ability to detect such processes and to investigate the precision of the instrument.

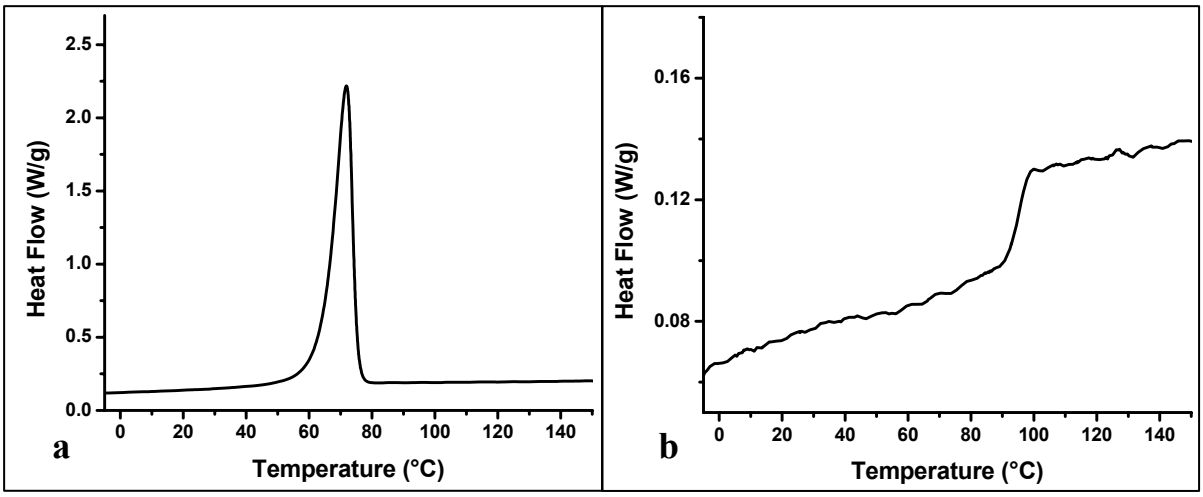

Fig. 3.65: DSC traces of **a**: poly(ethylene oxide), **b**: polystyrene.

The DSC curve of pure poly(ethylene oxide), PEO, is shown in Fig. 3.65 **a**. The polymer granulate (ca. 9 mg) was filled into a sample pan and measured using a heating rate of 5°C/min. PEO exhibits a melting point of ca. 65°C.[65] The obtained signal is rather broad, owing to the high heating rate, but has a very high intensity. The steep increase starts at 63.5°C, indicating sufficient precision of the measurement. The thermogram of polystyrene, a polymer undergoing a glass transition process at about 100°C,[66] is illustrated in 3.65 **b**. A step is clearly visible starting at 95°C, indicating an endothermic process. The intensity of the glass transition, however, is far less than found for the melting of PEO.

A PEO-polystyrene *block*-co-polymer was measured as well, again heating at a rate of 5°C/min. The plots (Fig. 3.66) illustrate one of the major problems for obtaining reliable, precise information from DSC. In the first run (**a**), two signals are visible (centered at 0°C and 22°C) which are not caused by the polymer. The first signal looks as if caused by water, but the absence of a signal at its boiling point (100°C) rules out that possibility. The system apparently did not stabilize up to about 30°C, producing signals just caused by the unstable thermal conditions. The right-hand trace (**b**) was measured from the same substance in the same sample pan, simply repeating the experiment without even opening the sample compartment. These results are accurate, only showing the true melting point of the co-polymer at 29.7°C.

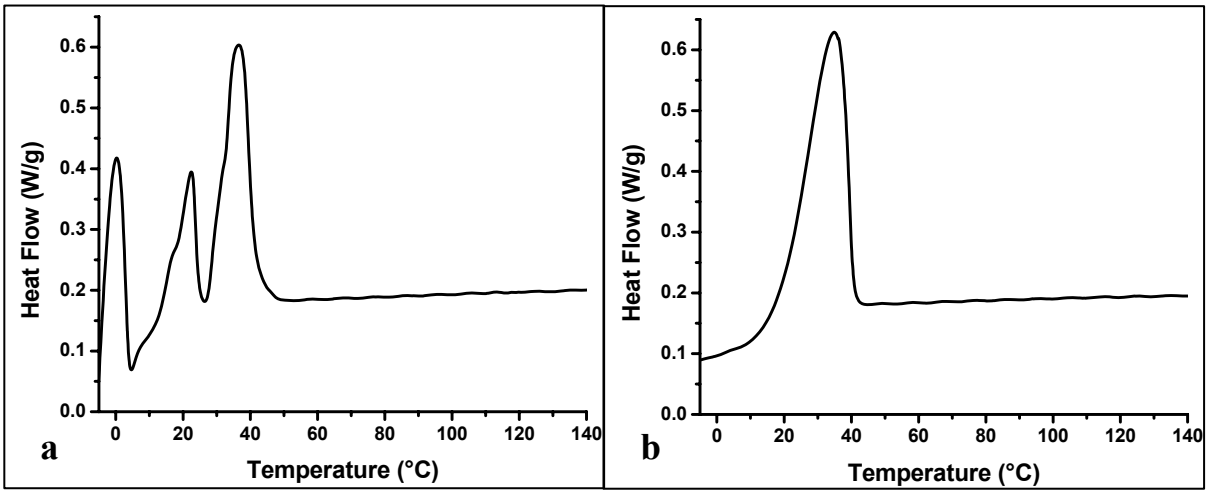

Fig. 3.66: DSC curves of a PEO/PS block co-polymer. **a**: 1st run of measurement, **b**: 2nd run.

In order to examine a DSC plot obtained from a bulk poly(NIPAAM) system, solution-polymerized NIPAAM (see Chapter 3.1 for preparation details) was ground in a mortar and then mixed with water (approx. 1:1 wt/wt). Ca. 15 g of the wet solid were measured in an Al sample pan, heating by 5°C/min (Fig. 3.67).

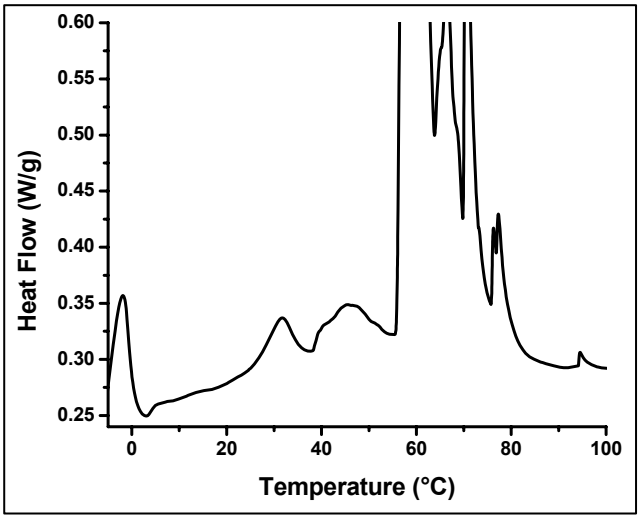

Fig. 3.67: Thermogram of bulk poly(NIPAAM).

The trace (magnification) shows one signal at -1.99°C which is caused by melting water. At this point, the temperature of the sample could easily be slightly warmer than in the sample compartment, as the Al pan is heated through its socket on the bottom of the chamber. The poly(NIPAAM) transition corresponds to the signal at 31.5°C which is rather small (ca. 0.05 W/g). At 45.2°C there is another signal which might be caused by solvent evaporation, as the bulk polymer – though hard and rigid – was not completely free of the solvent (THF was used for this sample) before adding water.

3.6.2 Measurements of Nanocomposite Systems

It has been shown in the literature that the LCST of pure PNIPAAM is shifted to higher temperatures for co-polymers with methacrylic acids.[62] Also, the specific enthalpy involved in the transition process decreases as NIPAAM is 'diluted' in the co-polymer. The standard co-polymer incorporated in the nanocomposite films, synthesized from the monomers in a molar ratio of ca. 30% NIPAAM / 70% DM, is reported to exhibit a very broad signal barely higher than the baseline, even in a bulk system.[62] Thus, it can be expected that the transition is hardly visible when measuring the hybrid nanocomposite system, as the polymer is practically diluted to 50% by the inorganic silica matrix.

A standard recipe sample was prepared in a Petri dish and then thermally polymerized and washed. Afterwards, the sample was scraped off the dish and mixed with de-ionized water (1:1 wt/wt) in a mortar. The substance was filled into an aluminum pan and measured at a heating rate of 5°C/min (Fig. 3.68). After the first measurement (**a**) the Al pan was carefully opened and some more water added. The pan was re-closed using another Al lid and then a second measurement was started (**b**), this time heating at only 1°C/min.

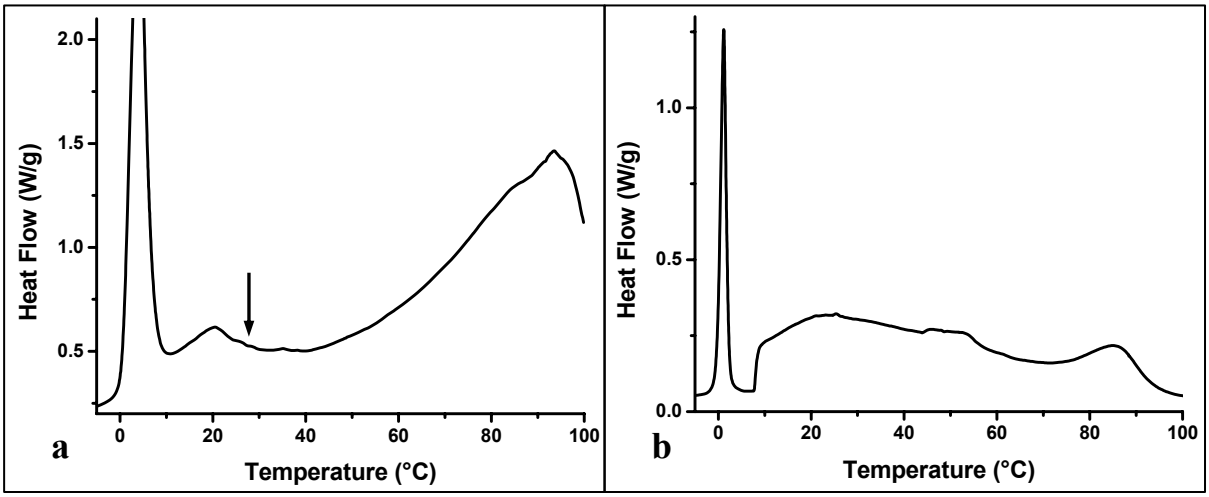

Fig. 3.68: DSC traces of a washed standard-recipe sample, **a**: 1st run of measurement, **b**: 2nd run.

The first run gives a very large water signal at ca. 5°C, followed by another signal at 20°C, but within the expected range of the critical temperature, only a very small hump is visible at ca. 28°C (arrow) – probably this measurement is influenced by a large amount of solvent (ethanol) incorporated in the sample which is released continuously. As the aluminum pan was non-hermetically sealed, it can be expected that the solvent has completely evaporated from the sample, not affecting further measurements. In the second run, there is a much sharper water signal which is followed by a strange sharp step at 10°C. A maximum appears

at 25.4°C which could correspond to the NIPAAM phase transition, but on the other hand it seems unrealistic that the heat flow then drops steadily going up to 100°C.

A thermogram obtained from a nanocomposite not containing any NIPAAM gave very similar results. The two traces are compared in Fig. 3.69, the thin dotted line representing the NIPAAM system already shown in Fig. 3.68 **b**. It is very interesting that both traces feature a steep incline at 8-10°C. The no-NIPAAM sample reaches a maximum heat flow at 13°C, followed by a minimum at ca. 40°C – hence, there is no signal at about 35°C comparable to the other sample. The signal at 76°C (probably stemming from remaining solvent) seems to be shifted to 85°C for the system containing NIPAAM.

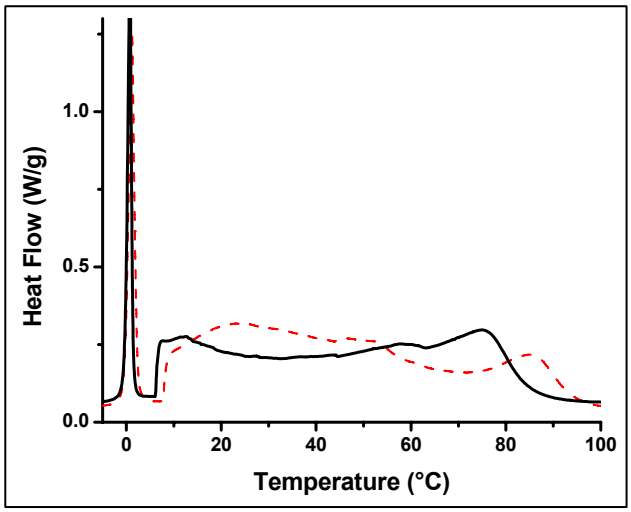

Fig. 3.69: Thermograms of washed samples.

All of these traces, however, exhibit a high extent of error; the fact that measurements of the same sample sometimes gave different results (not only differing by solvent signals), strongly suggests that DSC analysis, at least when performed on a device which could not be efficiently cooled, is unreliable for such low concentrations of the transient species – it suggests a different thermal behavior for systems containing NIPAAM but does not constitute an unambiguous proof for its presence and transition within the system. Also, the fact that in the nanocomposite system there are a number of components, some of them giving multiple signals, further complicates evaluation of the DSC graphs. CTAB, for example, produces several signals when its solution in water is heated (Fig. 3.70), as structural changes (phase transitions) occur in the liquid-crystalline system, and each of these transitions is an endothermic process (cf. Figure 1.4).[67] Theoretically, of course there should be no CTAB left in the nanostructure after washing, but it has been discussed in previous sections (cf.

Ch. 3.3.1) that washing of Petri dish samples was problematic due to their high film thickness, and that complete removal of CTAB was only achieved for samples prepared on Si wafers.

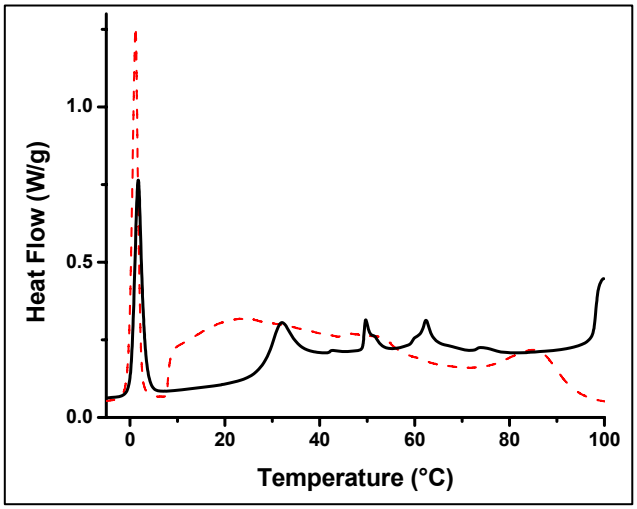

Fig. 3.70: Thermogram of an aqueous solution of CTAB.

Thus, we can infer that the composition of the samples is too diverse to allow the unambiguous detection of NIPAAM by methods of DSC analysis.

3.7 UV/Vis Spectroscopy

In order to find the optimum UV irradiation wavelength for photoinitiation, UV/Vis spectroscopy was performed. The spectra were recorded using a Perkin-Elmer Lambda 45 spectrometer. Solutions of BME and NIPAAM in methanol and ethanol were measured in various concentrations.

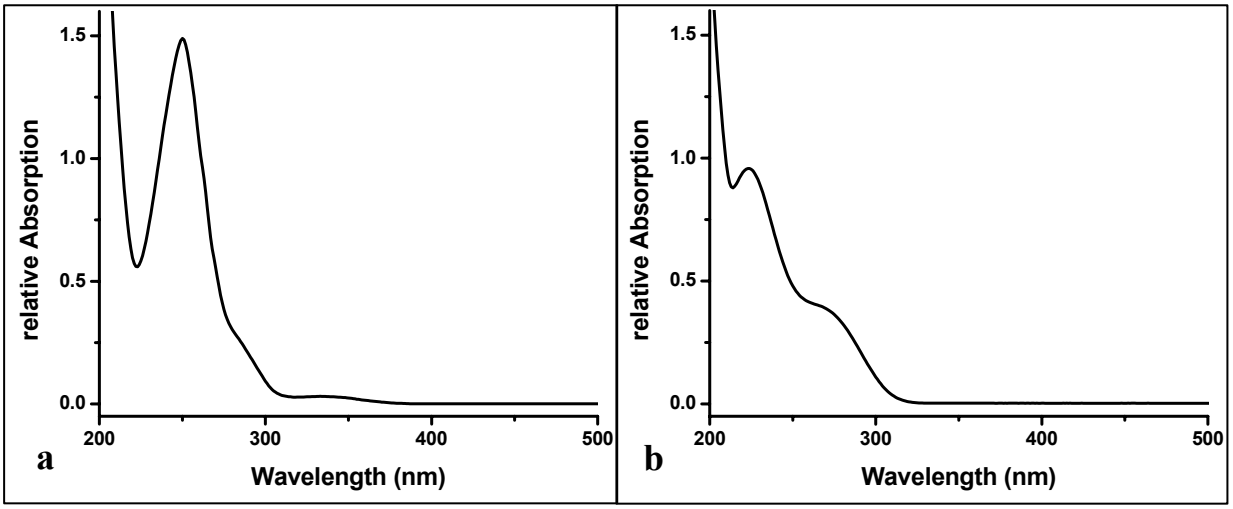

Fig. 3.71: UV/Vis spectra of **a**: benzoin dimethylether (BME), **b**: NIPAAM.

Fig. 3.71 **a** shows the spectrum of a BME (0.011%) solution in ethanol. There is a small absorbance maximum around 330-355 nm, and a very strong peak at 250 nm. The spectrum of NIPAAM (**b**, 0.02% in EtOH) shows a steady increase in absorbance below 300 nm; a local maximum is visible at ca. 225 nm.

These spectra suggest an optimum irradiation wavelength of about 250 nm. However, it must be taken into account that SiO_2 absorbs UV irradiation below ca. 275 nm. The UV lamp was equipped with a filter which could be set to three different maximum irradiation wavelengths: 254, 302 and 365 nm. The wavelength below 275 nm is not suitable, as the silica layers would block all irradiation and prevent reaction of the initiator. BME, on the other hand, shows a local minimum at about 305-310 nm, whilst NIPAAM still strongly absorbs in this range; it would be unwise to use this wavelength setting. Therefore, the chosen wavelength of 365 nm seems to be most suitable for the current system.

3.8 Spectroscopic Ellipsometry

A non-destructive method to determine the thickness of siliceous thin films is phase-modulated ellipsometry. Measuring a beam of ellipsometrically polarized light reflected by the sample, the wavelength dependence of the refractive index n(λ) of the film is determined.[68] In order to relate the ellipsometric data to the thickness and the refractive index, a theoretical model was used, which is based on the Cauchy relationship for n(λ). Because of the compositional complexity of the nanocomposite films, it was assumed, to a first approximation, that the films consist of SiO_2 only. The theoretical film thickness can be calculated (by fitting a theoretical function for n(λ), obtaining parameters such as the film thickness and the refractive index).

A very obvious problem, therefore, are the different optical characteristics of the polymer phase – certainly, the organic moieties differ greatly from the silica in e.g. the refractive index. No calculation models exist for these materials, especially for hybrid organic/inorganic nanophases. Hence, homogeneous optical properties throughout the film had to be assumed, which of course created a great error potential and, for some samples (e.g. as-prepared films), did not even lead to an acceptable model fit at all.

Table 3.1 shows the results of ellipsometrical measurements. The standard recipe films were prepared as usual, applying thermal treatment after dip-coating. The samples denoted as 'film without polymer' were prepared from a solution not containing any NIPAAM and DM but all other components (including 7-OTS).

Composition	Treatment	Film Thickness	Refractive Index
standard recipe	after thermal treatment	820 ± 15 nm	1.45 ± 0.02
	after washing	397 ± 4 nm	1.46 ± 0.01
film without polymer	after thermal treatment	704 ± 12 nm	1.52 ± 0.01
	after washing	320 ± 15 nm	1.37 ± 0.04

Table 3.1: Film Thickness and Refractive Index obtained from Ellipsometry Measurements.

Both samples show a dramatic decrease in thickness upon washing, by approx. 50%. The films containing polymer were about 15-25% thicker which is explained by the polymer widening the organic layers. Unfortunately, no useful results were obtained from the measurement of as-prepared films.

It was of course most interesting to investigate the film thickness of samples which are subject to swelling experiments. These data of these films, however, were difficult to fit because of the high water content of the samples. Only a few samples could be fitted; the obtained results however are most interesting, revealing a film thickness of 800 nm for a film in the swollen state (which exhibited a *d*-spacing of 5.2 nm), whereas the same film after de-swelling showed a thickness of ca. 400 nm (*d*-spacing: 3.3 nm). Using these figures, the nanocomposite film can be calculated to consist of 120-150 double layers of silica and hydrogel. It is fascinating to see that the film thickness almost doubles upon swelling of a sample.

3.9 Transmission-Electron Microscopy

An illustrative method to investigate the structure of a film is transmission electron microscopy (TEM). For lamellar structured samples, however, only a cross-sectional measurement reveals the true *d*-spacing. The preparation these samples is rather complicated and tedious. Samples not measured in cross-section may show too high *d*-spacing, or, if measured perpendicular to the lamellae, no structure at all, even though the sample is highly ordered. Therefore, SAXS Analysis (Chapter 3.4) was used as the routine technique to determine the degree of ordering in samples. Moreover, TEM measurements always only depict a very small part of the sample, whereas SAXS shows an average of the structure in the sample and allows to determine the homogeneity of a sample.

Several TEM measurements were performed, though, to be able to double-check the results obtained by SAXS. Figure 3.72 shows a standard-recipe sample measured before washing. This sample was not measured in cross-section: after preliminary drying at ambient conditions, the film was scratched with tweezers. The fragments were then transferred onto holey carbon copper grids. According to SAXS, this sample should be nicely ordered and lamellar.

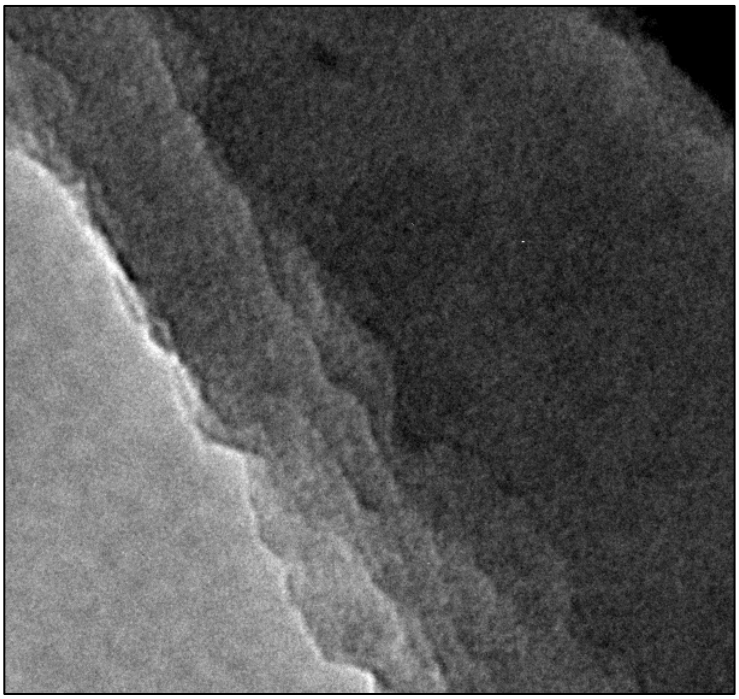

Fig. 3.72: Sample before washing, no cross-section.

In this picture, no ordered structure is visible. The edges of the broken layers of the sample indicate that the layers are oriented parallel to the image plane; hence, only one top layer is visible. Vice versa, the absence of any structure in this picture can be interpreted as indirect

proof: no 2-D or 3-D hexagonal or cubic structures are present, therefore the sample can only exhibit a lamellar structure or no structure at all.

The next picture (Fig. 3.73) was also taken from a sample measured as a powder scratched off the film. A standard-recipe film was used, again after thermal polymerization but before washing. This time, however, the layers are oriented (more or less) parallel to the electron beam, therefore, the layers are visible and an extended lamellar structure is revealed. The visible *d*-spacing equals about 3 nm; this is consistent with results obtained in SAXS measurements of thermally polymerized samples.

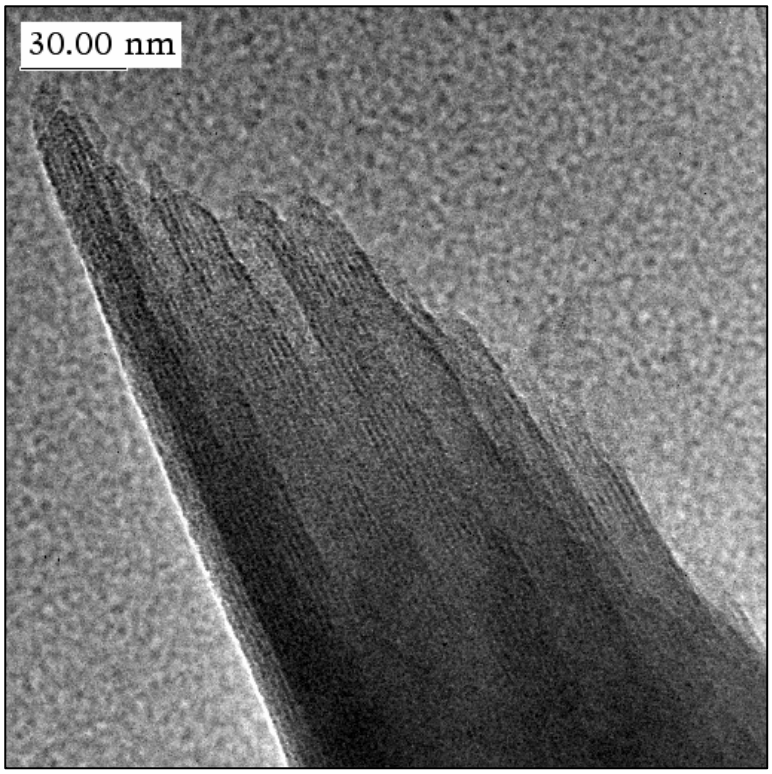

Fig. 3.73: Sample before washing, no cross-section.

As mentioned above, *cross-sectional* TEM pictures required a complicated preparation of samples. Several steps had to be performed in order to be able to achieve an accurate cut, including thermal treatment at relatively high temperatures (ca. 150°C) and thorough rinsing with acetone. It is clear that such treatments can also change the sample ordering itself; a compromise between performing a highly precise measurement or preserving a pristine sample structure had to be found. Certainly, the structural quality of a sample cannot increase during such treatments; therefore, the ordering in standard samples is likely to be higher than in the pictures shown.

In order to measure cross-sectional samples before washing, the normally performed treatment with acetone was left out. Nice pictures were obtained, though, clearly confirming the results obtained by SAXS. Figure 3.74 shows two of these samples.

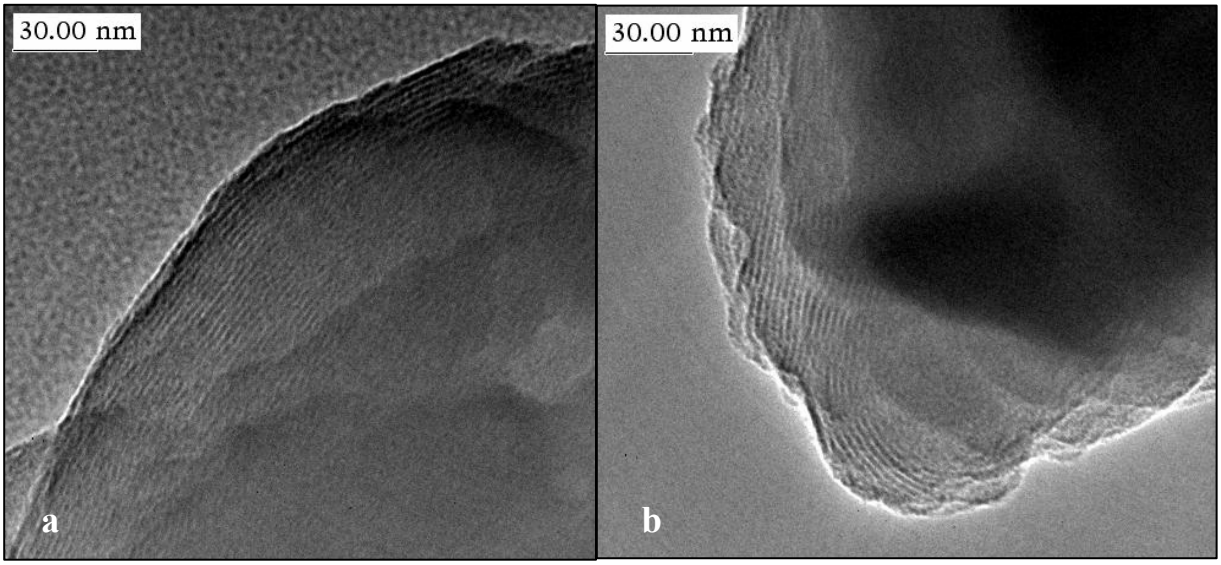

Fig. 3.74: TEM pictures of two non-washed samples measured in cross-section.

The high ordering of the sample is beautifully visible in both pictures, revealing a lamellar structure with a *d*-spacing of ca. 3 nm.

Thorough rinsing with acetone represents an analogous procedure as normally performed when washing a sample. This results in a substantial decrease in ordering, as the surfactant is removed. On the other hand, this truly tells the quality of the sample, regarding its stability and its polymer distribution (cf. Chapter 3.4). Two cross-sectional pictures of standard-recipe samples after washing are presented in Figure 3.75.

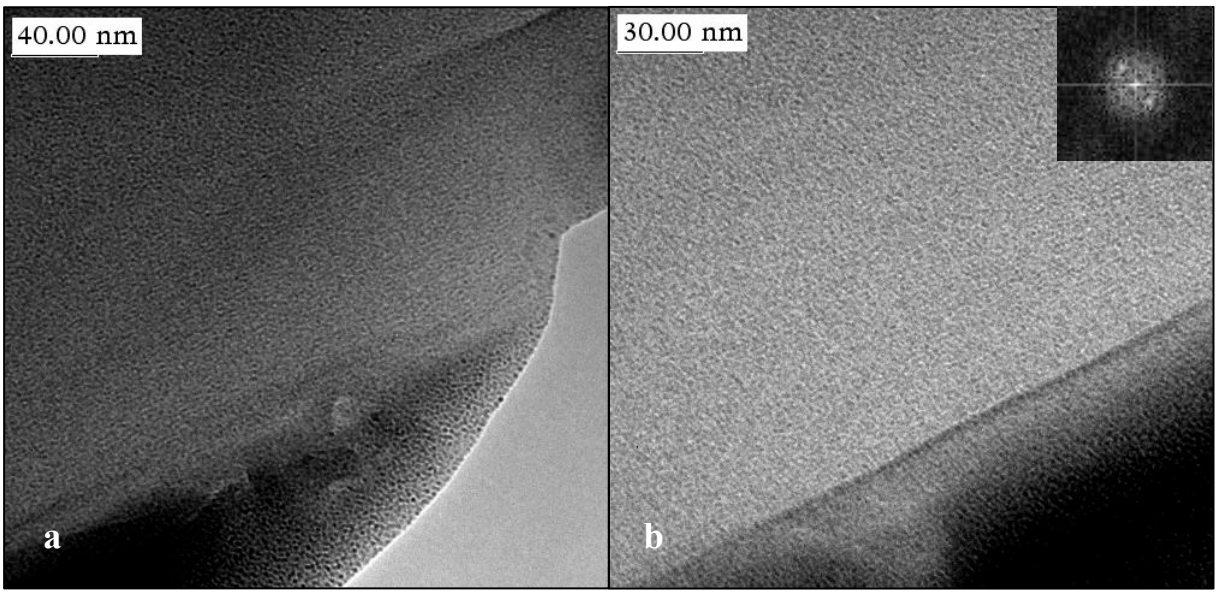

Fig. 3.75: TEM pictures of two washed standard-recipe samples measured in cross-section.

Indeed a significant decrease in ordering is visible; however the general orientation of the lamellae parallel to the surface remains, as is visible in **b**. The inset shows a Fourier transformation of the picture, which also proves that the structure of the sample is lamellar and still highly ordered. These results are consistent with the data obtained by SAXS measurements and confirms that the nanocomposite possesses lamellar structure and is highly ordered at all stages of processing.

4 Summary

The main goal of this work was to prepare nanocomposite thin films consisting of alternating layers of silica and an environmentally sensitive organic polymer, poly(NIPAAM-*co*-dodecyl methacrylate), showing unique swelling properties. The idea was to first create a structured film, employing evaporation-induced self-assembly (EISA). This was achieved by dip-coating Si wafers in a precursor solution, containing both a silica precursor (hydrolyzed TEOS, A2** sol), a structure-directing agent (surfactant), an initiator and the organic monomers. Other samples were prepared by spin-coating or casting of the sol onto silicon wafers or a Petri dish.

Evaporation of the solvent led to the formation of lamellar mesophases, initially consisting of layers of partially condensed silica alternating with organic phases containing the monomers, a coupling agent and an initiator. The samples then were polymerized, using free radical polymerization, and the silica matrix stabilized by condensation. Both photoinitiation and thermal initiation were employed and explored to optimize the sample preparation process, intending to obtain mechanically stable films but preserve a highly ordered mesostructure. Thermal treatment (usually at 120°C) also enhanced the condensation of the silica matrix, whereas photo-polymerization had to be followed by exposure to ammonia vapor to stabilize the inorganic layers. Finally, the surfactant was removed by washing with ethanol and acetone. As insufficient linkage between the layers caused the polymer to be washed out, a coupling agent was employed to establish a covalent connection between the silica matrix and the polymer. At all stages of processing, samples were analyzed by IR and NMR spectroscopy, small-angle X-ray scattering (SAXS), thermo-gravimetric analysis (TGA), differential scanning calorimetry (DSC), ellipsometry and transmission electron microscopy (TEM). Moreover, samples showing high ordering after washing were subject to swelling experiments in order to explore the functionality of the hydrogel within the nanocomposite film. The samples were immersed in water at different temperatures and then measured by SAXS to examine their ordering and changes in their structure.

FTIR and ^{13}C-NMR spectroscopy experiments were employed to explore the reactivity of the various components. Because of their structural complexity, and occurring superposition, many spectra were taken from samples only containing some of the components to facilitate the identification of peaks. Due to the relatively high amount of substance required for an

accurate measurement, the samples for IR and NMR Spectroscopy had to be prepared in a Petri dish by vertical draining. SAXS was performed with thin films on Si wafers (measuring in symmetric reflection) and was therefore used as the routine technique to analyze the structural quality of samples at all stages of processing. TEM experiments were carried out to confirm these results. Thermal analysis (TGA/DSC) was employed to explore the polymer content and functionality in the nanocomposite.

Very high ordering was found in SAXS diffractograms for films in the as-prepared state and after polymerization. The *d*-spacing (a measure for the cumulated thickness of an inorganic and an organic layer which can be obtained directly from a SAXS pattern) did not remain constant during the different stages of processing: it shrank during polymerization; however, the shrinkage was much more dramatic for thermal polymerization; this is due to a greatly increased rate of condensation of the silica species, and partial evaporation of monomers, which was also found in TGA and NMR experiments. The ammonia treatment caused a decrease in ordering. For both thermally and UV-polymerized samples, washing drastically diminished the ordering of the film. This appears logical, as it could be the consequence of an inhomogeneous distribution of the polymer: assuming a random distribution of the polymer chains, removing the surfactant as 'spacer' would create domains with a difference in distance between the silica sheets. In case the linkage between a polymer layer and the neighboring silica matrix is not good enough, either the polymer is washed out or even the whole film could delaminate. This was observed for a number of samples – either a typical, pronounced peak appeared at low *d*-spacing (ca. 2 nm), indicating a highly ordered structure but without incorporated polymer, or the structure was completely lost. Many samples, however, retained their ordering and the polymer species in the system, observed as a rather broad signal after washing corresponding to a *d*-spacing of about 3.8 nm, as the hydrogel underwent partial swelling under these conditions.

TEM images, measuring samples in cross-section, confirm the results obtained by SAXS, showing a high ordering of samples before and after washing. To unambiguously elucidate the structure type of the films, 2-D SAXS measurements were performed; the results clearly confirm the presence of a highly ordered, lamellar structure.

As the stability of films after washing was not fully reproducible, a variety of experiments was started to obtain further understanding about the complex processes happening in the

course of sample preparation. One of the crucial factors was the reactivity of the coupling agent. As mentioned above, the lack of a firm connection between the layers might result in their detachment and consequently the loss of film structure. Therefore, the coupling agent was employed to provide a covalent linkage between the layers, stabilizing the system. The reactivity of several coupling agents was investigated. 7-OTS, the coupling agent used for standard experiments, showed surprisingly low reactivity towards polymerization for thermal initiation as well as for photoinitiation. ^{29}Si-NMR experiments, on the other hand, revealed that the condensation degree of 7-OTS, in combination with the silica precursor, was very high for films after exposure to ammonia vapor but also for thermally treated samples. (Meth)acrylate silanes, which also seemed suitable as coupling agents, exhibited a substantially higher degree of polymerization after both UV irradiation and thermal treatment. The analysis by SAXS, however, showed that samples containing a (meth)acrylate coupling agent lost their structure upon condensation of the silica, which might be caused by the formation of hydrophobic oligomers already present in the primary solution, leading to an insufficient connection to the silica matrix, or too fast reaction, creating high mechanical stress within the system upon condensation of the silica. 7-OTS led to stable systems despite its low reactivity. It is possible that the connection between the layers at only some sites is the optimum for the system – providing enough linkage to prevent disassembly of the system, but on the other hand allowing flexibility for contraction and swelling processes.

A more general problem was the choice of the initiation method. As NIPAAM was the functional component of the system, and DM, the co-polymer, showed higher reactivity anyhow, the degree of polymerization of solely NIPAAM (which was easier to identify in IR and NMR spectra) was taken as measure for the efficiency of the initiation method. Photoinitiation resulted in a higher degree of polymerization but had the disadvantage of no concurrent silica condensation, so an additional ammonia treatment was necessary (films washed directly after UV polymerization lost their ordering). A detailed SAXS analysis revealed that this treatment was a critical preparation step; if not carried out thoroughly, insufficient silica condensation led to a loss of ordering upon washing, whereas a too intense treatment conceivably caused high mechanical stress within the film, bringing about a decrease in ordering as well. Therefore, thermal treatment was preferred. Also, the polymerization degree of the polymer (in the case of pure NIPAAM as well as for the co-polymer) in the nanocomposite was generally found to be reasonably high, and the

evaporation of monomers led to a decrease in polymer content but not to the loss of polymer functionality.

A ‘standard recipe’ was established and used to produce a number of films in order to explore the reproducibility upon variation of processing techniques. Due to a high number of parameters influencing the film quality (temperature at dip-coating, aging effects, polymerization time and temperature, washing conditions etc.), it appears impossible to achieve perfect reproducibility; however, by performing additional processing steps to ensure stable conditions, such as filtering the solution prior to dip-coating to remove dust and impurities, significantly improved results were obtained.

Washed samples were subject to swelling experiments in order to explore the functionality of the incorporated polymer. The wafers were immersed in de-ionized water at various temperatures (ranging from 5°C to 50°C), and the SAXS patterns were measured after each treatment. A significant response to changes in the external environment was found. At temperatures of 30°C and lower, the peaks were shifted towards higher *d*-spacing, indicating swelling of the polymer. Above 40°C, de-swelling of the polymer layers was observed – this is in good compliance to the LCST (critical solution temperature) of NIPAAM being at 32°C. Some samples exhibited swelling and de-swelling for 10 or more cycles, although the extent of swelling was very hard to control, as the swelling rate seemed to increase for each cycle. The observed *d*-spacing ranged from 2.8 nm in de-swollen states to more than 6.3 nm in swollen samples; this was the detection limit of the standard X-ray diffractometer used for routine measurements. The release of water incorporated in poly(NIPAAM) is an endothermic process, and must therefore be visible as a peak in DSC measurements. The poly(NIPAAM) content in the system studied in this work, however, is too low to unambiguously detect a transition and determine the critical temperature.

The SAXS data of the lamellar nanocomposite films were subject to detailed SAXS analyses. Longer scans of samples at various stages of swelling yielded diffractograms of outstanding quality, showing smooth peaks but not perfect ordering. A theoretical stacking model was applied to evaluate the SAXS data in terms of a limited number of structural parameters. Based on this approach, the SAXS curves could be reasonably fitted, providing invaluable structural parameters such as the thickness of the constituting silica/organic layers and their variances. The results strongly support the idea of one layer showing strong swelling and

de-swelling (the hydrogel layer), whereas the thickness of the other (the silica matrix) practically remains constant. Ellipsometry measurements allowed to determine the film thickness, which showed an increase from 400 nm to 800 nm upon swelling of a sample. Emanating from the measured *d*-spacing of 5.2 nm for the swollen sample, the number of layers was estimated to 120-150 (of each silica and polymer).

In order to get quantitative information about the polymer content of samples at different stages of processing, TGA experiments were performed. The thermograms of ordered samples show weight losses at lower temperatures than in non-structured films. Therefore, it can be inferred that in ordered samples, the polymer must be situated in a different chemical environment than in samples prepared without CTAB, where it is distributed within the silica matrix. This provides evidence that CTAB causes the polymer to be separated from the silica and sit in a distinct, organic nanophase. Finally, washed thin films prepared on Si wafers were investigated; it was found that the standard washing procedure is very efficient, leaving almost no surfactant in the system. The resulting polymer content in the sample was calculated to 22%.

5 Experimental Section

5.1 Chemicals

5.1.1 Surfactant

Cetyltrimethylammonium bromide (CTAB), $CH_3(CH_2)_{15}N^+(CH_3)_3\ Br^-$, a well-known cationic surfactant, was employed as structure-directing agent. The chemical (≥ 99.0%) was used as received from Aldrich, Inc.

5.1.2 Coupling Agents

Various silanes such as trimethoxy(7-octen-1-yl)silane $H_2C{=}CH(CH_2)_6Si(OCH_3)_3$ (7-OTS), 3-(trimethoxysilyl)propyl acrylate $H_2C{=}CHCOO(CH_2)_3Si(OCH_3)_3$ (PATMS) and 3-(trimethoxysilyl)propyl methacrylate $H_2C{=}C(CH_3)COO(CH_2)_3Si(OCH_3)_3$ (MPS) were used as coupling agents to provide a link between the polymer phase and the silica framework. The liquids were used as received from Fluka and Aldrich, Inc. Due to high reactivity, they were stored in a refrigerator and the containers not left open longer than necessary. PATMS contained 100 ppm BHT (butylated hydroxytoluene) as inhibitor which was not removed before usage of the chemical. MPS did not contain any inhibitor but was stored under nitrogen in a sealed bottle; the chemical was withdrawn using a syringe.

5.1.3 Monomers

Dodecyl methacrylate $H_2C{=}C(CH_3)COO(CH_2)_{11}CH_3$ (DM), also denoted as lauryl methacrylate, was ordered from Aldrich, Inc., and used as received (purum, 95.0%). The liquid was stored in a refrigerator because of its high reactivity. *N*-isopropylacrylamide $H_2C{=}CH\text{-}C(=O)\text{-}N(H)\text{-}CH(CH_3)_2$ (NIPAAM) is solid at room temperature, though rather volatile. The chemical (Aldrich Inc., 97%) was stored at room temperature in a closed bottle sealed with parafilm. NIPAAM is classified as toxic, so gloves were always used when handling the chemical and its solutions, and all procedures were carried out in a hood, if possible. In some experiments, BIS (*N*,*N'*-methylenebisacrylamide) or HDM (1,6-hexanediol dimethacrylate) were used as cross-linkers. These chemicals were stored at room temperature; HDM contained 100 ppm hydroquinone as inhibitor (as-received from Aldrich Inc.).

5.1.4 Initiators

BME (benzoin dimethyl ether, 2,2-dimethoxy-2-phenylacetophenone) was used as photoinitiator. Due to its sensitivity to UV irradiation, it was stored in a brown bottle additionally wrapped with aluminum foil (from Aldrich Inc.)

ACHN, 1,1'-azobis(1-cyclohexanecarbonitrile), was stored in a refrigerator and used as received from Aldrich Inc.

5.1.5 Further Chemicals

TEOS (tetraethyl orthosilicate, tetraethoxysilane), Aldrich Inc. (min. 99%), stored at room temperature.

TEMED (*N*,*N*,*N'*,*N'*-tetramethyl ethylenediamine), Aldrich Inc.

Ethanol abs. (200 proof) was used for the preparation of A2** stock solution and as solvent for precursor solutions.

5.2 Solution Assembly

Precursor solutions were prepared emanating from an acidic silica sol (A2**). This sol was made by mixing TEOS with ethanol, de-ionized water and 0.07 N hydrochloric acid in the molar ratios of 1 : 3.8 : 1 : 5×10^{-5}. The solution was homogenized using a magnetic stirrer bar and then heated to 60°C in a water bath. The temperature was kept constant for 90 min, whilst stirring was continued at 200 rpm. This procedure led to a partial hydrolysis of TEOS.[9] The pH value of the solution was set to equal the iso-electric point (IEP) of siloxane, therefore minimizing the siloxane condensation and stabilizing the system – this stock solution could be stored at -20°C for months without change (cf. Chapter 3.3.2). The solution was prepared in batches of usually ca. 250 mL, so up to 45 standard sample solutions could be assembled from one batch which in average was used within one month after preparation.

When assembling a sample solution, the desired amount of A2** stock solution (usually 5 mL) was pipetted into a scintillation vial previously cleaned by rinsing with acetone and then drying swiftly by spraying with nitrogen. The stock solution was not left at ambient conditions longer than necessary in order to prevent condensation reactions. Hence, the pipetted A2** solution still had a temperature below 0°C. Usually, this solution was left for 10 minutes to warm to near room temperature. 11.5 mL of additional ethanol or, for some experiments, another organic solvent such as tetrahydrofurane (THF) or n-butanol (n-BuOH) or their mixtures (1:1 or 1:2) with EtOH were added, followed by 0.2 mL de-ionized water (purified by a Fisher MilliPore system) and 0.6 mL dilute hydrochloric acid (0.07 N). To minimize evaporation of the volatile solvents, the vial was capped between addition of the individual components. Using an automated pipette, 0.44 mL of the coupling agent were added. Various functional silanes such as trimethoxy(7-octen-1-yl)silane (7-OTS), 3-(trimethoxysilyl)propyl acrylate (PATMS) and 3-(trimethoxysilyl)propyl methacrylate (MPS) were used as coupling agents. Next, 0.823 g of the structure-directing agent CTAB were weighed and added to the sol. After dissolution of CTAB in an ultrasonic bath, the organic monomers (dodecyl methacrylate and/or *N*-isopropylacrylamide) were subsequently added, followed by a photosensitive initiator (benzoin dimethylether, BME) or a thermal initiator (1,1'-azobis(1-cyclohexanecarbonitrile), ACHN). For some experiments, other initiators such as APS (ammonium peroxosulfate) or AIBN (azobisisobutyronitrile) were used. The standard molar ratio of reactants in the final solution was 1 TEOS : 22 EtOH : 5 H_2O : 0.004 HCl : 0.21 CTAB : 0.16 coupling agent : 0.32 DM : 0.14 NIPAAM : 0.02-0.04 initiator. In few experiments also TEMED (*N*,*N*,*N'*,*N'*-tetramethylethylene diamine) was

added as accelerator of the polymerization, or *N*,*N'*-methylenebisacrylamide (BIS) and 1,6-hexanediol dimethacrylate (HDM) as cross-linkers. The solution was homogenized in an ultrasonic bath for 5 minutes. Finally, it was filtered through a Gelman Acrodisc PTFE 0.2µm pore size filter.

5.3 Film Preparation

5.3.1 Dip-coating

(100)-silicon wafers were cut into pieces approx. 2x1 cm in size by scratching with a diamond head pen and then carefully breaking the wafer. The pieces were cleaned by washing with EtOH, rubbing with a rubber foam swab and rinsing with acetone. Next, they were placed in an oven which was heated up to 450°C at a rate of 1°C/minute. The maximum temperature was held constant for 6 h; afterwards the oven was cooled down at 1°C/min. In general, pure Si has a passive layer of SiO_2 adjacent to its surface. Yet, under ambient conditions, water molecules are adsorbed to the surface, creating $(RO)_3Si–OH$ groups. These groups cause the surface to be very hydrophilic. At high temperatures, the process is reversed and water is desorbed, leaving a less hydrophilic surface. As the wafers were instantly placed in a glove box under dry nitrogen, the re-adsorption of H_2O could be prevented. The effect was much less de-wetting of the newly-prepared films. The precursor solution, though still miscible with water, was highly hydrophobic, due to the high content of hydrophobic organic monomers, and caused difficulties upon dip-coating, producing films prone to develop spots or even de-wet on too hydrophilic substrates. No films at all could be obtained on non-calcined wafers. Even calcined wafers led to poor film quality if dirt or dust were present on the wafer surface or in the precursor solution – therefore, filtration of the solution before dip-coating was performed, which led to an improved quality of the film and reduced its tendency to develop spots. From the substrate, dust was removed by spraying the wafers with compressed N_2. Dip-coating was performed in a glove box under dried nitrogen (relative humidity of 2%). Usually, the wafer was dipped into the solution and then left for only 10-30 seconds before withdrawing it at a set standard speed of 50.9 $cm \cdot min^{-1}$. The solvent started to evaporate instantly, and within 10 seconds, the typical colorful interference pattern appeared, indicating formation of the thin film. Logically, the film formation started at the upper edge of the film, but as a drop of the solution remained on the lowest part of the wafer, the solvent evaporation process was disturbed in this area, and a typical strip was visible on all films next to the lower edge of the wafer. This “drop zone” showed less ordering and generally was not used for further analysis such as SAXS or TEM, but it was left on the wafer.

5.3.2 Spin-coating

Some wafers were not prepared by dip-coating but by spin-coating at 1000 or 2000 rpm. This was carried out in a hood under ambient conditions (no nitrogen atmosphere). One drop of solution was applied to the substrate before starting the rotation; as the excess solution was centrifuged over the edge of the wafer, the exact amount of solution applied did not have any effect on the film quality or thickness. Silicon wafers were used as substrates for spin-coating as well, but were cut into square pieces approximately 2-3 cm long. They were pre-treated as usual; also all further treatments were performed as with dip-coating samples.

5.3.3 Casting of Films

With respect to potential applications, both dip-coating and spin-coating seem processes which are hard to control. For example, large, non-plane substrates are unsuitable for both preparation techniques. The method of casting, where the film formation process only relies on the evaporation of the solvent, is a more straightforward approach, although the film thickness is practically uncontrollable, and much thicker films are obtained. Pre-treated Si wafers were used for these experiments; a small amount of precursor solution (ca. 20 μL) was applied with a syringe and then left to evaporate.

A larger amount of material needed for IR and NMR measurements was also obtained by casting: a few drops of the solution were applied onto a Petri dish. The dish was slued to all directions for a few seconds to get homogeneous covering of the whole bottom of the dish, and then placed in an upright position to obtain a thin layer by vertical draining. The polymerization was carried out as described above by either UV or thermal initiation. These samples were generally not subject to ammonia treatment, but some Petri dish samples were washed by applying a thin layer of EtOH onto the film and leaving it for 10 seconds before emptying the dish and washing analogously with acetone.

5.4 Polymerization

Both photoinitiation and thermal initiation were employed to polymerize the monomers within the organic moieties of the film. Thermal initiation had the advantage of a simultaneous condensation of the silica matrix during the heat treatment, whereas photoinitiation was performed at room temperature by placing the sample under UV irradiation, and had to be followed by a treatment with ammonia vapor to enhance condensation of the siliceous network. Prior to thermal polymerization, the samples were left inside the glove box for about 10-20 minutes for preliminary drying. A standard heat treatment was performed by putting the films in an oven pre-heated to 120°C and leaving them typically for 3 hours. ACHN was used as thermal initiator as it is reactive above 100°C and dissolves in EtOH but does not impede the self-assembly process. For polymerization by photoinitiation, the wafers were irradiated with UV light of 365 nm for 2 hours (using a UVP UVLM-26 6W Hg arc lamp source with filter). BME was used as initiator for these samples. The ammonia treatment was done by filling a jar with 15-20 mL of concentrated ammonia (30% solution in water) and taping the sample wafers to the wall, above the surface of the liquid. Then the jar was capped and left for 15-20 minutes. The alkaline NH_3 vapor acted as catalyst for silica condensation.

5.5 Washing

To remove the surfactant and any remaining monomers, the samples then were subsequently washed with ethanol and acetone. This washing treatment proved to be crucial; many films lost their ordering upon washing. First of all, is seems important that the mechanical stress caused by the solvent flux had to be minimized – several films rinsed with EtOH suddenly became detached from the substrate and were washed off. Of course this might be due to an already unstable linkage of the layers to the silicon wafer, but a gentler method such as dipping the wafers into a scintillation vial containing ethanol seemed to give much better results. Therefore, the standard washing method was dipping the samples into EtOH for 10 s and subsequently into acetone for 5 s. Yet some wafers were also additionally washed with water for 30 s or washed with EtOH for a second time.

Figure 5.1 **a** shows thin films prepared by dip-coating of Si wafers, after polymerization and washing, whereas a sample prepared by the 'Petri dish' method is presented in 5.1 **b**.

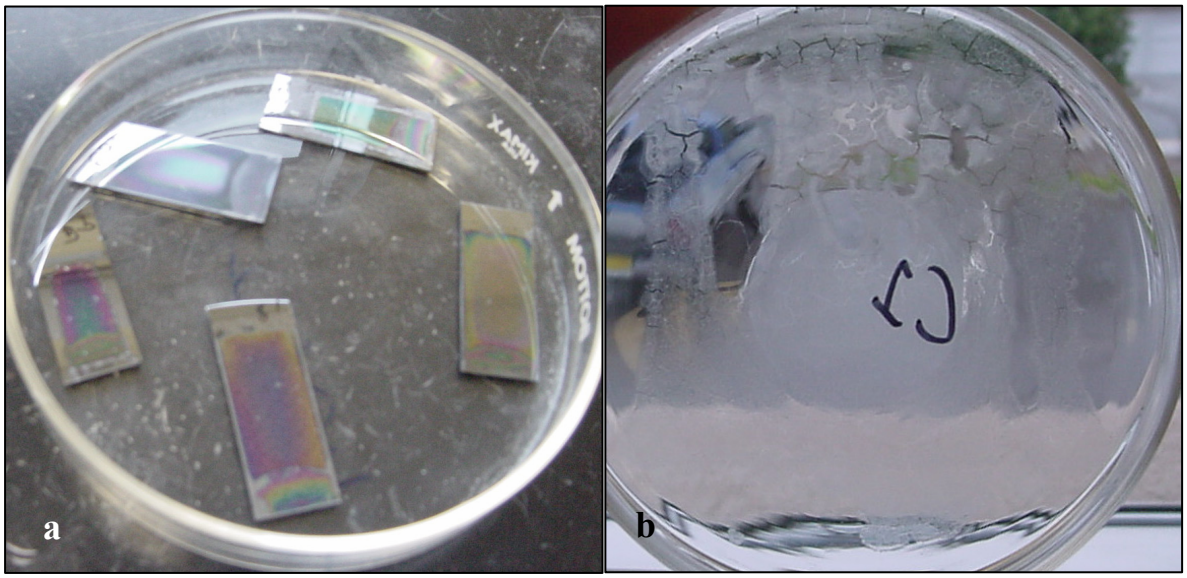

Fig. 5.1: **a**: Thin film samples prepared by dip-coating of Si wafers, **b**: 'Petri dish' sample.

5.6 Characterization

5.6.1 Small-Angle X-ray Scattering

The films were routinely analyzed by small-angle X-ray scattering (SAXS), using a standard Siemens D 500 diffractometer featuring Cu-Kα radiation filtered with Ni (λ = 1.5418 Å). The films were measured in symmetric reflection (θ - 2 θ geometry), using a typical 2 θ range of 1.2-10.0 degrees. For the measurement, the wafer was generally placed on the sample holder in such a way that the X-ray beam would hit the center of the film, neglecting the lowest section ("drop zone") of the wafer which was less ordered. A fast scan was performed for ca. 8 min, employing a step size of 0.04° and a dwelling time of 2 s. Longer measurements were performed for several hours or even overnight. Various slit openings were used for the measurements (as illustrated in figure 5.2), typically (in the order from the tube to the detector) 1.0°, 1.0°, 0.6°, 0.018°, 0.15° for the measurement of as-prepared and heat-treated samples, starting the measurement at 2 θ = 1.5°.

In the obtained SAXS patterns, the position of the main reflection corresponds to the *d*-spacing, the mean distance of repeating structure elements, e.g. the cumulated thickness of two alternating layers in a lamellar system. The correlation of position (2θ) and *d*-spacing is simple, as described in Bragg's equation

$$d = \frac{n \cdot \lambda}{2 \sin\theta} \qquad (5.1)$$

For the wavelength used, (5.1) simplifies to

$$d = \frac{0.7709}{\sin\theta} \text{ for (001) peaks.} \qquad (5.2)$$

In washed films, however, the *d*-spacing of reflections was (for swollen samples) often above 2.95 nm, meaning a 2 θ-position below 1.5°. Hence, the measurement had to be started at 1.2°, yet the primary beam reflection was very high up to 1.4° for the standard slit setup, causing intensities of 10^5 counts·s^{-1} or more. Therefore the setup had to be changed to apertures of 0.3°, 0.3°, 0.15°, no slit, 0.15°, reducing the intensity of irradiation reaching the sample and therefore decreasing the primary beam intensity. This also diminished the intensity of all reflections but was a reasonable compromise, getting an optimum ratio of signal to background intensity.

Fig. 5.3: Goniometer setup.

Swelling experiments were performed to investigate the properties of the hydrogel incorporated into the nanocomposite. They were carried out by immersing the sample in water at various temperatures and then measuring the diffractogram. Typically, the sample was put into a Petri dish filled with de-ionized water in a refrigerator at 5°C or in an oven at 30°C, 40°C or 50°C. Some experiments were performed at room temperature. The samples were left under water for minutes, hours or even days. After carefully removing the wafer from the Petri dish, it was blotted dry with a tissue and then instantly put onto a sample holder and measured.

5.6.2 IR Spectroscopy

Samples for IR measurements were prepared by the 'Petri dish method' described above. The analysis of samples in the as-prepared state was performed after leaving the film in a hood for 1-2 hours to obtain a completely dry film, whilst the polymerized samples could be used instantly after thermal or UV treatment. The film was scraped off the Petri dish, using a spatula or a razor blade, and transferred into a mortar. Then, it was mixed with a surplus of potassium bromide (KBr) with a pistil and pressed within a steel sample holder to get a clear pellet. A Bruker Vector 22 Fourier-transform infrared (FT-IR) spectrometer was used to obtain the IR spectra; the sample compartment was flushed with N_2 for 10 min before starting the measurement. The spectrum was calculated from 32 scans, obtaining a transmittance signal over wave numbers ranging from 400 to 4000 cm^{-1}, of which a background signal obtained from pure KBr was electronically subtracted.

5.6.3 NMR Spectroscopy

Solid-state ^{13}C and ^{29}Si magic-angle spinning (MAS) NMR measurements were performed on a 400 MHz Bruker AMX spectrometer using films prepared by casting onto a Petri dish. Due to the minimum amount of 50-100 mg of substance necessary for NMR analysis, one sample solution was sometimes used to create several Petri dish films which were then all combined for the measurement. For measurements in the as-prepared state, the films were dried overnight at room temperature before scraping them off into a scintillation vial previously flushed with nitrogen to remove any dust. Most polymerization treatments were carried out by placing the Petri dish in an oven or under UV irradiation and afterwards scraping the film off the Petri dish. Some samples, however, were first measured in the as-prepared state and then heat-treated within the NMR sample holder. All NMR measurements were carried out by Dr. Roger A. Assink at Sandia National Laboratories, Albuquerque. The ^{13}C experiments were performed at 100.6 MHz using direct polarization and high-powered ^{1}H decoupling, with a delay time of 8 seconds and 1024 scans; the samples were spun at 12 kHz in a 4 mm MAS probe. ^{29}Si experiments were performed at 79.5 MHz using direct polarization and high-powered ^{1}H decoupling, with a delay time of 240 s and 64 scans; the samples were spun at 6 kHz in a 7 mm MAS probe. Several different delay times were used for each sample in order to ensure that the recorded spectra were essentially quantitative. A few ^{1}H experiments were performed as well; they were carried out at 399.9 MHz using a 5 mm broadband probe and a sweep width of 50 ppm. Some experiments were performed at elevated temperatures (40°C); for these experiments, the sample holder containing the substance was brought to a defined temperature which was held overnight before starting the measurement.

5.6.4 UV/Vis Spectroscopy

In order to investigate the optimum UV irradiation wavelength for photoinitiation, UV/Vis spectra were recorded using a Perkin-Elmer Lambda 45 spectrometer. The samples were measured in a UV transparent cuvette against the pure solvent as a blank. The device recorded the absorbance over wavelength in the range of 200-600 nm.

5.6.5 Ellipsometry

The thickness of the films was measured by spectroscopical ellipsometry on a Multi-wavelength Ellipsometer by J. A. Woollam C., Inc. A xenon 75 W lamp and a mercury 100 W lamp were used as light source; the reflected beam was analyzed with a M44 Detector, recording the refractive index n over the wavelength λ. The film thickness was calculated using the Cauchy equation for mesoporous SiO_2 films. Films were measured at all steps of processing.

5.6.6 TGA Measurements

Thermo-gravimetric analysis (TGA) was performed on a TA Instruments Simultaneous Differential Techniques (SDT) 2960 device. This instrument heated up the sample at a steady rate whilst simultaneously measuring the decrease in its weight as well as the precise temperature difference to the set temperature (detecting exothermic and endothermic processes within the sample). It featured Pt-Pt/Rh thermocouples for both temperature control and measurement. The standard heating rate applied was 1°C/minute, starting at ambient temperature and ramping up to 600°C. Typically, 10-20 mg of sample were used for the measurement. Samples were usually prepared by the "Petri dish method", but in special measurements also films prepared on Si wafers were used. A standard-size wafer, however, only yielded ca. 0.5-1.0 mg of material upon scraping off the film. To facilitate preparation of films for TGA measurements, and to allow for enough material, precursor solutions for such measurements were prepared in batches three times the standard amount. The homogenized solution was transferred into a 50 mL graduated cylinder for dip-coating. Larger Si strips, ca. 2x6 cm in size, were used as substrates. Further treatment was carried out as usual. Afterwards, the film was scraped off the substrate and filled into a tared Al_2O_3 sample holder. The furnace was purged with argon or oxygen at 100 mL/min. As-prepared, thermally treated and washed samples as well as pure chemicals were studied. Some as-prepared samples were rapidly heated up to 120°C and kept at this temperature for 3 h before further heating to simulate a thermal treatment.

5.6.7 DSC Measurements

Some samples were investigated by differential scanning calorimetry (DSC). These measurements were carried out by heating the sample at a steady rate and measuring the heat flow to or from the sample in comparison to a reference. A TA Instruments DSC device was used. 5-15 mg of a Petri dish film were scraped off into an aluminum pan. Ca. 100 µL of de-ionized water were added to some samples to be able to see any water-release effects. Then the pan was non-hermetically sealed with an Al lid, weighed and placed onto the DSC sample holder. An empty Al pan was used as reference. The sample compartment was purged with argon at 50 mL/min. Unfortunately, the device did not have any means to control the temperature below ambient conditions, therefore, the only way to start a measurement below 25°C was to quench the sample compartment to temperatures of about -25°C using liquid nitrogen, then to quickly remove the quenching cup (replacing the lid to shield the compartment from air) and start ramping up the sample. Most samples were measured at heating rates of 5°C/minute, but for more exact measurements heating rates of 1°C/min were used. From the measured data, the heat flow per g of sample was calculated to get comparable graphs.

5.6.8 Transmission-Electron Microscopy

Transmission-Electron Microscopy (TEM) measurements were performed using a JEOL 2010 TEM at an acceleration voltage of 200 kV; the samples were prepared by scratching the film with tweezers and directly dispersing the film fragments onto holey carbon copper grids.

Bibliography

[1] C. Kresge, M. Leonowicz, W. Roth, C. Vartuli, J. Beck, *Nature* **359** (1992) 710-714.

[2] J. S. Beck, J. C. Vartuli, W. J. Roth, M. E. Leonowicz, C. T. Kresge, K. D. Schmitt, C. T. Chu, D. H. Olson, E. W. Sheppard, S. B. McCullen, J. B. Higgins, J. L. Schlenker, *J. Am. Chem. Soc.* **114** (1992) 10834-10843.

[3] I. Honma, H. S. Zhou, D. Kundu, A. Endo, *Adv. Mater.* **12** (2000) 1529-1533.

[4] R. D. Miller, *Science* **286** (1999) 421-423.

[5] C. J. Brinker, Y. Lu, A. Sellinger, H. Fan, *Adv. Mater.* **11** (1999) 579-585.

[6] A. J. Hurd, L. Steinberg, *Granular Matter* **3** (2001) 19-21.

[7] H. Yang, N. Coombs, I. Sokolov, G. A. Ozin, *Nature* **381** (1996) 589-592.

[8] L. Hench, J. K. West, *Chem. Rev.* **90** (1999) 33-72.

[9] Y. Lu, R. Ganguli, C. A. Drewien, M. T. Anderson, C. J. Brinker, W. Gong, Y. Guo, H. Soyez, B. Dunn, M. H. Huang, J. I. Zink, *Nature* **389** (1997) 364-368.

[10] J. Seddon, R. Templer: "Liquid Crystals and the Living Cell", *New Scientist* (1991) 45-49.

[11] A. Hozumi, Y. Yokogawa, T. Kameyama, K. Hiraku, H. Sugimura, O. Takai, M. Okido, *Adv. Mater.* **12** (2000) 985-987.

[12] S. H. Tolbert, T. E. Schäffer, J. Feng, P. K. Hansma, G. D. Stucky, *Chem. Mater.* **9** (1997) 1962-1967.

[13] M. Ogawa, H. Ishikawa, T. Kikuchi, *J. Mater. Chem.* **8** (1998) 1783-1786.

[14] P. Kipkemboi, A. Fogden, V. Alfredsson, K. Flodström, *Langmuir* **17** (2001) 5398-5402.

[15] J. M. Kim, Y. Sakamoto, Y. K. Hwang, Y. Kwon, O. Terasaki, S. Park, G. D. Stucky, *J. Phys. Chem.* **106** (2002) 2552-2558.

[16] K. Yu, A. J. Hurd, A. Eisenberg, C. J. Brinker, *Langmuir* **17** (2001) 7961-7965.

[17] D. Grosso, A. R. Balkenende, P. A. Albouy, M. Lavergne, L. Mazerolles, F. Babonneau, *J. Mater. Chem.* **10** (2000) 2085-2089.

[18] D. Grosso, F. Babonneau, P. A. Albouy, H. Amenitsch, A. R. Balkenende, A. Brunet-Bruneau, J. Rivory, *Chem. Mater.* **14** (2002) 931-939.

[19] S. Besson, T. Gacoin, C. Jacquiot, C. Ricolleau, D. Babonneau, J.-P. Boilot, *J. Mater. Chem.* **10** (2000) 1331-1336.

[20] M. Klotz, P.-A. Albouy, A. Ayral, C. Ménager, D. Grosso, A. Van der Lee, V. Cabuil, F. Babonneau, C. Guizard, *Chem. Mater.* **12** (2000) 1721-1728.

[21] S. A. Holt, J. L. Ruggles, J. W. White, R. F. Garrett, *J. Phys. Chem.* **106** (2002) 2330-2336.

[22] D. Grosso, F. Babonneau, G. J. de A. A. Soler-Illia, P. A. Albouy, H. Amenitsch, *Chem. Comm.* (2002) 748-749.

[23] K. Fontnell, A. Khan, B. Lindstrom, D. Maciejewska, S. Puang-Ngern, *Colloid Polym. Sci.* **269** (1991) 727-742.

[24] D. Kundu, H. S. Zhou, I. Honma, *J. Mater. Sci. Lett.* **17** (1998) 2089-2092.

[25] D. Grosso, A. R. Balkenende, P. A. Albouy, A. Ayral, H. Amenitsch, F. Babonneau, *Chem. Mater.* **13** (2001) 1848-1856.

[26] I. A. Aksay, M. Trau, S. Manne, I. Honma, N. Yao, L. Zhou, P. Fenter, P. M. Eisenberger, S. M. Gruner, *Science* **273** (1996) 892-898.

[27] F. Hua, Y. Lvov, T. H. Cui, *J. Nanosc. Nanotech.* **2** (2002) 357-361.

[28] R. A. Caruso, A. Susha, F. Caruso, *Chem. Mater.* **13** (2001) 400-409.

[29] O. Soppera, C. Croutxe-Barghorn, C. Carre, D. Blanc, *App. Surf. Sci.* **186** (2002) 91-94.

[30] Y. Lee, J. Kim, Y. Son, *Polymer-Korea* **23** (1999) 443-449.

[31] C. Sanchez, F. Ribot, L. Rozes, B. Alonso, *Mol. Cryst. and Liq. Cryst.* **354** (2000) 143-158.

[32] C. Leu, Z. Wu, K. Wei, *Chem. Mater.* **14** (2002) 3016-3021.

[33] Y. Lu, H. Fan, N. Doke, D. A. Loy, R. A. Assink, D. A. LaVan, C. J. Brinker, *J. Am. Chem. Soc.* **122** (2000) 5258-5261.

[34] T. Asefa, C. Yoshina-Ishii, M. J. MacLachlan, G. A. Ozin, *J. Mater. Chem.* **10** (2000) 1751-1755.

[35] Y. Lu, Y. Yang, A. Sellinger, M. Lu, J. Huang, H. Fan, R. Haddad, G. Lopez, A. R. Burns, D. Y. Sasaki, J. Shelnutt, C. J. Brinker, *Nature* **410** (2001) 913-917.

[36] A. Sellinger, P. M. Weiss, A. Nguyen, Y. Lu, R. A. Assink, W. Gong, C. J. Brinker, *Nature* **394** (1998) 256-260.

[37] M. E. Harmon, T. A. M. Jakob, W. Knoll, C. W. Frank, *Macromolecules* **35** (2002) 5999-6004.

[38] H. G. Schild, *Prog. Polym. Sci.* **17** (1992) 163-249.

[39] R. Gomes de Azevedo, L. P. N. Rebelo, A. M. Ramos, J. Szydlowski, H. C. de Sousa, J. Klein, *Fluid Phase Equ.* **185** (2001) 189-198.

[40] K. Otake, H. Inomata, M. Konno, S. Saito, *J. Chem. Phys.* **91** (1989) 1345-1350.

[41] S. Varghese, A. K. Lele, D. Srinivas, R. A. Mashelkar, *J. Phys. Chem.* **103** (1999) 9530-9532.

[42] M. Arotcaréna, B. Heise, S. Ishaya, A. Laschewsky, *J. Am. Chem. Soc.* **124** (2002) 3787-3793.

[43] D. Kuckling, M. E. Harmon, C. W. Frank, *Macromolecules* **35** (2002) 6377-6383.

[44] E. Diez-Pena, I. Quijada-Garrido, J. M. Barrales-Rienda, *Polymer* **43** (2002) 4341-4348.

[45] T. Serizawa, K. Wakita, M. Akashi, *Macromolecules* **35** (2002) 10-12.

[46] L. Liang, J. Liu, X. Gong, *Langmuir* **16** (2000) 9895-9899.

[47] K. Suzuki, T. Yumura, M. Mizuguchi, Y. Tanaka, C. Chen, M. Akashi, *App. Polym. Sci.* **77** (2000) 2678-2684.

[48] D. J. Beebe, J. S. Moore, J. M. Bauer, Q. Yu, R. H. Liu, C. Devadoss, B. Jo, *Nature* **404** (2000) 588-590.

[49] K. Kataoka, H. Miyazaki, M. Bunya, T. Okano, Y. Sakurai, *J. Am. Chem. Soc.* **120** (1998) 12694-12695.

[50] W. Zhang, I. Gaberman, M. Ciszkowska, *Anal.Chem.* **74** (2002), 1343-1348.

[51] M. Hesse, H. Meier, B. Zeeh: *"Spektroskopische Methoden in der organischen Chemie"*, Thieme, Stuttgart 1995, 40-54.

[52] S. Thomas, Institute of Chemistry, University Potsdam: *Spectroscopy Online Spectroscopic Tools*, Internet: http://www.spec-online.de.

[53] J. Gasteiger, Center for Computational Chemistry and Institute of Organic Chemistry, University of Erlangen: *Telespec – IR Spectra Simulation on the WorldWideWeb*, Internet: http://www2.chemie.uni-erlangen.de/services/telespec/index.html.

[54] M. Hesse, H. Meier, B. Zeeh: *"Spektroskopische Methoden in der organischen Chemie"*, Thieme, Stuttgart 1995, 157-162.

[55] K. Hayamizu, M. Yanagisawa, O. Yamamoto, Japanese National Institute of Advanced Industrial Science and Technology: *Integrated Spectral Data Base System for Organic Compounds*, Internet: http://www.aist.go.jp/RIODB/SDBS/menu-e.html.

[56] U.S. National Institute for Science and Technology, *NIST Online Spectroscopic Data Base*, Internet: http://webbook.nist.gov/chemistry.

[57] Sigma-Aldrich Co.: *Product Information/Structural Data Base*, Sigma-Aldrich Website, Internet: www.aldrich.com.

[58] E. Diez-Pena, I. Quijada-Garrido, J. Barrales-Rienda, M. Wilhelm, H. Spiess, *Macromol. Chem. Phys.* **203** (2002), 491-502.

[59] F. Zeng, Z. Tong, H. Feng, *Polymer* **38**, (1997), 5539-5544.

[60] T. Serizawa, K. Wakita, M. Akashi, *Macromolecules* **35** (2002), 10-12.

[61] T. Wolff, C. Burger, W. Ruland, *Macromolecules* **27** (1994), 3301-3309.

[62] E. Diez-Pena, I. Quijada-Garrido, P. Frutos, J. M. Barrales-Rienda, *Macromolecules* **35** (2002), 2667-2675.

[63] E. Diez-Pena, I. Quijada-Garrido, J. M. Barrales-Rienda, *Polymer Bulletin* **48** (2002), 83-91.

[64] M. Lazzari, T. Kitayama, K. Hatada, O. Chiantore, *Macromolecules* **31** (1998), 8075-8082.

[65] J. Falbe, M. Regitz: Römpp Lexikon Chemie, Vol. 5, Thieme, Stuttgart 1998, 3447-3448.

[66] H. Gausepohl, R. Gellert: Kunststoff-Handbuch Vol. 4: Polystyrol, C. Hanser, München 1996, 524.

[67] K. Fontnell, A. Khan, B. Lindstrom, D. Maciejewska, S. Puang-Ngern, *Colloid Polym. Sci.* **269** (1991), 727-742.

[68] "Phase Modulated Ellipsometry", © Beaglehole Instruments 1999, Internet: http://www.beaglehole.com.